

Lipids, lipid droplets and lipoproteins in their cellular context; an ultrastructural approach

Lipiden, lipid druppels en lipoproteïnen in hun cellulaire kontekst;
een ultrastructurele aanpak
(met een samenvatting in het Nederlands)

Proefschrift

ter verkrijging van de graad van doctor aan de Universiteit Utrecht
op gezag van de rector magnificus, prof.dr. G.J. van der Zwaan,
ingevolge het besluit van het college voor promoties in het openbaar
te verdedigen op woensdag 13 februari 2013 des ochtends te 10.30 uur

door

Robertus Jacobus Mesman
geboren op 2 januari 1982 te Gouda

Promotoren:

Prof.dr. G. Van Meer

Prof.dr. J.C.M. Holthuis

Co-promotor:

Dr. J.A. Post

Paranymphs:

Elly van Donselaar

Joep van den Dikkenberg

Correspondence: RobMesman@gmail.com

ISBN: 978-90-393-5911-2

The research described in this thesis was performed at the divisions of Membrane Enzymology and BioMolecular Imaging, Institute of Biomembranes, Utrecht University, The Netherlands, with financial support from the European Union Framework VII Program LipidomicNet (proposal 202272).

The printing of this thesis was financially supported by:
De Stichting tot bevordering van de Electronenmicroscopie in Nederland (SEN),
Leiden, The Netherlands.

Table of contents

Scope of this thesis		7
Chapter 1	Preservation of cellular lipids in EM sample preparation	9
Chapter 2	Lipid droplets: biogenesis and interactions with other organelles	23
Chapter 3	Immuno-gold labeling efficiency of Apolipoprotein B depends on its lipidation state	41
Chapter 4	Tracing cellular lipid flows at the ultrastructural level using a clickable fatty acid	55
Chapter 5	High-pressure freezing of adherent cells for frozen hydrated sectioning; a novel method	69
Chapter 6	Summarizing Discussion	79
Samenvatting		89
Acknowledgements / Dankwoord		91
Curriculum Vitae		93

Abbreviations

ApoB	Apo-lipoprotein B	LDL	Low density lipoprotein
BFA	Brefeldin A	MAG	Monoacylglycerol
BSA	Bovine serum albumin	MC	Membrane carrier
BSA-c	Acetylated bovine serum albumin	MTP	Microsomal transfer protein
CEMOVIS	Cryo-electron microscopy of vitreous sections	MVB	Multivesicular body
cFA	Clickable fatty acid	OsO ₄	Osmium tetroxide
CFG	Cold water fish skin gelatin	PA	Phosphatidic acid
cPLA2 α	Cytosolic phospholipase A2 alpha	PC	Phosphatidylcholine
DAG	Diacylglycerol	PE	Phosphatidyl-ethanolamine
DGAT	Diacylglycerol-acyl-transferase	PFA	Formaldehyde, derived from paraformaldehyde
EM	Electron Microscopy	PHEM	Pipes-hepes-EGTA-MgCl buffer
ER	Endoplasmic reticulum	PS	Phosphatidylserine
FA	Fatty acid	TAG	Triacylglycerol
FS	Freeze-substitution	TAMOI	Tannic acid mediated osmium impregnation
GA	Glutaraldehyde	TEM	Transmission electron microscopy
HDL	High density lipoprotein	TLC	Thin layer chromatography
HPF	High-pressure freezing	UA	Uranyl acetate
IgG	Immunoglobulin G	VLDL	Very low density lipoprotein
LD	Lipid droplet		

Scope of this thesis

Lipids are key to cellular life. They form the building blocks of membranes by which cells compartmentalize the chemical reactions that sustain the living state. Furthermore, lipids can act as messengers in signal transduction pathways and provide a means to store metabolic energy. Our current knowledge on the composition of cellular membranes and the processes of cellular lipid homeostasis (polar lipid synthesis, fatty acid transport and storage of neutral lipids) is mostly based on biochemical data. These data are obtained by lipid analysis of subcellular fractions and studies using fluorescent lipid analogs. While the molecular analysis of cellular fractions can shed light on the lipid composition of subcellular organelles and the mechanisms by which cells control membrane lipid homeostasis, a major shortcoming of this approach is that pure organelles are hard to obtain. Moreover, cell lysis and subsequent processing of membranes may cause substantial changes in lipid organization and turnover. Fluorescent lipid analogs have been used to monitor inter-organellar trafficking and distribution of lipids in living cells, but these fluorescent probes provide limited spatial resolution and have been reported to behave differently from the lipids they are supposed to mimic.

Since transmission electron microscopy uses electrons instead of photons, it has a much higher spatial resolution compared to light or fluorescence microscopy. Furthermore, the magnification range of a transmission electron microscope is sufficient to image individual membrane leaflets within cells. In this thesis, cellular lipids, lipid droplets and lipoproteins were studied, exploring the use of transmission electron microscopy as a tool to gain insight in the subcellular distribution and processes involved in cellular lipid homeostasis at the ultrastructural level. In order to do this, many electron microscopical technique challenges had to be dealt with, since the existing experimental approaches were often not suitable for this kind of research.

Biological specimens must be fixed and processed first in order to allow their visualization in an electron microscope. In **Chapter 1**, we discuss several sample preparation methods for transmission electron microscopy. We discuss the level of lipid preservation for these sample preparation procedures, based on the information available in the literature. From this we derive those parameters that drive lipid extraction, which allows us to better assess the lipid retention in a given sample preparation procedure. This information is used to select those sample preparation procedures which have the highest level of lipid preservation.

The knowledge obtained in chapter 1 serves as a basis for the studies reported in **Chapter 2**. Here approaches to visualize the biogenesis of lipid droplets and the interactions of these neutral lipid storing organelles with other cellular organelles are studied. By combining several sample preparation and imaging techniques we find indications that the biogenesis of lipid droplets takes place in the mitochondria-associated ER membranes, thereby making critical progress in visualizing the initial stages of lipid droplet formation. The interaction between lipid droplets and other cellular organelles is assessed using electron tomography. By reconstructing the 3d volumes from recorded tilt-series we could reveal membrane contacts between organelles within the section, which would be missed using conventional transmission electron

microscopy. This allows us to show direct membrane contacts between LDs and ER membrane and between an LD and a lysosome.

In **Chapter 3** we investigated the formation of very low density lipoproteins, the main carriers of neutral lipid in the blood circulation and an important risk factor in cardiovascular disease. Immuno-gold labeling on ApoB, the main apo-protein on VLDL, could in principle be used to determine where in the synthesis route of VLDL the second lipidation step takes place. However, initial experiments were faced with a loss of antigenicity of ApoB. We show that this loss is most likely due to the lipid scavenging action of bovine serum albumin, used as a blocking agent during the labeling procedure. This shows that lipid loss does not only occur during sample preparation but can also take place during the subsequent processing steps. By reducing de-lipidation of ApoB within the sections by albumin we are able to successfully localize ApoB by immuno-gold labeling.

In **Chapter 4** we study an alternative to fluorescent lipid analogs. The use of a clickable fatty acid, combined with an optimized specimen preparation procedure, allows us to trace the flow of de-novo synthesized cellular lipid at the ultrastructural level. Using specific inhibitors against the triacylglycerol synthase DGAT2 and the Golgi stabilizing protein Arf1p we are able to change and re-direct this lipid flow. We visualized these changes within the cell by immuno-gold labeling, validating the use of clickable fatty acids as a suitable tool for imaging lipid flows on the nanometer scale.

In **Chapter 5** we explore a novel method that allows cryo-immobilization and frozen hydrated sectioning of adherent growing cells. Using this method, cells can be high-pressure frozen and sectioned while still being attached to the substrate they were grown on. This provides a faster and less artifact-prone method for freezing samples for frozen hydrated sectioning, cryo-electron microscopy of vitreous sections (CEMOVIS) and VIS2FIX. The method described reduces sample preparation time, making the use of shorter incubation times possible. Next to this, the method it brings CEMOVIS one step closer to the ultimate goal: visualizing cells in their native state at high resolution.

In **Chapter 6** the findings presented in this thesis are discussed in a broader context. We consider the significance of technical advances for future studies. Furthermore, we elaborate on the relationship between lipid droplets and lipoproteins and the possible connections and similarities in the biogenesis mechanisms of these neutral lipid inclusions.

Chapter 1

Preservation of cellular lipids in EM sample preparation

R.J. Mesman^{1,2,3,*}, G. Van Meer^{2,3}

¹Membrane Enzymology, Department of Chemistry, Utrecht University, Padualaan 8, 3584 CH Utrecht, the Netherlands

²Biomolecular Imaging, Department of Biology, Utrecht University, Padualaan 8, 3584 CH Utrecht, the Netherlands

³Institute of Biomembranes, Utrecht University, Padualaan 8, 3584 CH Utrecht, the Netherlands

Abstract

Using transmission electron microscopy cells and tissues can be studied at the ultrastructural level. However during sample preparation lipids, which provide an essential part in the cell's ultrastructure, can be extracted. In the literature the data on lipid extraction during EM sample preparation is limited. Here we provide an overview on what is known in terms of lipid extraction for a number of commonly used sample preparation techniques. Furthermore we analyze the underlying processes within the preparation techniques to identify the mechanisms causing lipid extraction. Using the dielectric constant as a measurement for polarity, we show that this parameter can to a large extent explain the differences in lipid retention between the preparation processes.

Introduction

Transmission electron microscopy allows samples to be studied at the nanometer scale. However, for biological specimens this is not straightforward. First of all, transmission electron microscopes (TEMs) operate at a high vacuum, in which water inside a specimen would rapidly evaporate and thereby destroy the sample. Secondly, the resolution obtained by transmission electron microscopy decreases with increasing sample thickness and most cells and tissues are too thick to be directly analyzed in the TEM. Therefore, preparation of biological samples for electron microscopy is aimed at either immobilizing or removing water within the sample while retaining the ultrastructural organization of the cell, and providing the specimen with enough rigidity to be sectioned into electron translucent slices without compromising the internal structures. Although the ultimate goal is to observe a sample at high resolution in the native state, the preceding preparation procedure could introduce artifacts, or as stated in one of the textbooks on EM sample preparation; "An electron micrograph is an image of an altered specimen compared with its living state. The degree of alteration shown by a specimen apparently varies depending on the preparatory procedure used. Because one examines an altered specimen out of necessity, it is important to understand the process that causes the alterations." [1]

Lipids together with membrane proteins form the basic structure of cellular membranes, which in turn provide a boundary between the cellular compartments that characterize the ultrastructural architecture of the cell. As one can imagine, extraction of these lipids can seriously disturb the structural integrity and appearance of membranes and of other lipid-rich structures. So in terms of obtaining high resolution images that closely represent the native ultrastructure using transmission electron microscopy, it pays to put effort in finding the optimal sample preparation procedure with regard to lipid extraction. Especially when one is interested in the ultrastructural localization of lipids, the issue is not only prevention of lipid extraction but also retention of the spatial distribution of lipids within the sample [2]. The literature offers only a few comprehensive articles dealing with the preservation of lipids during sample preparation for transmission electron microscopy. Most of these are from the early seventies and discuss chemical fixation and resin embedding protocols. Data about lipid loss in more recently established preparation procedures is scarce and often incomplete. Here we provide an overview on what is known about lipid retention in commonly used sample preparation techniques and, by comparing these, try to find those parameters that allow us to explain the level of lipid extraction in a given sample preparation procedure.

Reported lipid extraction in TEM sample preparation methods

Chemical fixation, dehydration and resin embedding

In the earliest application of electron microscopy on biological specimens, osmium tetroxide was used to stabilize the specimen and increase its resistance to the potential damaging effect of the electron beam [3]. Osmium remained the primary fixative for electron microscopy [4] until the introduction of aldehydes as fixatives by Sabatini *et al.* [5] in 1963. While osmium provided adequate ultrastructural preservation, it is incompatible with cytochemistry due to its oxidative nature [5]. Since then, chemical fixation for resin embedded samples is mostly carried out using an aldehyde as primary fixative and post-fixation with osmium tetroxide. This is followed by dehydration in an organic solvent (mostly ethanol or acetone) and infiltration with the resin of choice. There appear to be as many chemical fixation protocols as electron-microscopists, each of the protocols having slight changes in fixatives, buffers and additives which all could influence lipid retention. Most published papers about lipid extraction provide data for only one approach, either by comparing which lipids can be extracted before and after fixation using chloroform/methanol extraction [6,7] or by examining the loss of radiolabeled lipid during sample processing [8–10]. The first method gives some insights in the degree of cross-linking of lipids while the latter provides more practical data: which lipids are actually lost during every step of the sample preparation procedure. The extensive work of Cope and Williams is a good example of the latter category and compares a number of fixation and embedding protocols on the retention of the polar [11,12] and neutral lipids [13].

For the most commonly used fixation procedure (fixation by glutaraldehyde followed by osmium tetroxide, dehydration and embedding in epoxy resin), Cope and Williams reported a loss of 1% phosphatidylethanolamine (PE), 11% phosphatidylcholine (PC) and 57% of the neutral lipids, most of which is extracted during dehydration and the first resin infiltration steps [11,13]. Omission of the osmium post fixation increased the lipid loss to 47% for PE, 100% for PC and 70% for neutral lipids. In contrast, after fixation with only osmium, 2.6% PE and 2.5% PC was lost, indicating that aldehyde fixation has only little effect on the retention of both polar and neutral lipids. In fact, only a few polar lipids are considered to be fixed by aldehydes [6]. Phosphatidylserine (PS) and PE contain an amino-group that reacts with aldehydes but the product of this reaction would run differently on a thin layer chromatography plate and can therefore not be recognized as PS or PE using this method.

Lipid retention observed with these methods does not necessarily mean retention *in-situ*; lipids could be displaced within the sample without being extracted into the processing fluids. When observing the ultrastructure of chemically fixed and resin embedded samples, lipid droplets often appear extracted or deformed. A simultaneous fixation with glutaraldehyde and osmium [14,15] provides better ultrastructural preservation of lipid droplets, suggesting an increase in neutral lipid retention. However there are no data on lipid retention for this method.

Tokuyasu cryo-sections

After the invention of the cryo-ultramicrotome, which allows samples to be sectioned at sub-zero temperatures, a completely different sample preparation procedure was developed by Tokuyasu [16]. Instead of dehydration and resin embedding, chemically fixed cells are embedded in gelatin, infiltrated with sucrose and snap-frozen in liquid nitrogen. These blocks are sectioned in a cryo-ultramicrotome and sections are picked up and transferred to grids using either a drop of sucrose or methylcellulose / sucrose [17]. Sections can subsequently be immuno-labeled, and are stabilized in methylcellulose containing uranyl acetate.

There are no direct data on lipid retention for this technique though some estimation on the level of lipid retention can be made. Roozmond [18] measured the release of lipids from cryostat sections of unfixed rat brain into water or 4% PFA with or without 1% CaCl_2 (Table 1). In water, phospholipid extraction was measured to be about 7.1%, with the different phospholipid classes extracted in ratio to their abundance. In 4% PFA the extraction was reduced to 2.7% and since this fixative reacts mainly with PS and PE, it changed the ratio in which the phospholipids were extracted. Addition of 1% CaCl_2 to the fixative further decreased the lipid extraction to 1.3% but also changed the ratio of extraction. For Tokuyasu cryo-sections, the lipid extraction is most likely comparable or lower than the amount of lipid extracted in PFA + CaCl_2 observed by Roozmond. In the Tokuyasu method, the sample is fixed and cryo-protected before freezing. Therefore, the membrane will not be damaged by the formation of ice crystals, which could cause extraction. There are no data on lipid losses during further processing of these sections for immuno-labeling. Although this method was not found to be suited for efficient labeling of glycolipids [19], Tokuyasu cryo-sections have been used to study the localization of cholesterol [20]. Because of the amphipathic nature of cholesterol the procedure had to be optimized by either addition of uranyl acetate to the fixative or by omitting gelatin infiltration and keeping sections at 4°C during the labeling procedure and thereby minimizing cholesterol loss.

Table 1 Phospholipid released from Cryostat sections of rat hypothalamus.

Values derived from Roozmond (1969) for the release of phospholipids from cryostat sections into water or 4% formaldehyde with or without 1% CaCl_2 . Values for individual phospholipids represent percentages of total extracted lipid phosphorus.

Lipid	H_2O	$\text{H}_2\text{O} + 1\% \text{CaCl}_2$	4% PFA	4% PFA + 1% CaCl_2
% extracted	7.1 ± 0.6	2.0 ± 0.3	2.7 ± 0.3	1.3 ± 0.3
PS	11.2 ± 1.5	14.8	4.4	11.4
SM + PI	17.5 ± 2.1	10.7	21.9	15.4
PC	45.5 ± 1.5	23.8	37.0	42.5
PE	25.5 ± 3.3	15.4	7.6	3.9

Cryo-immobilization and freeze-substitution

The main drawback of chemical fixation is that cellular processes are not stopped instantaneously. It takes time for fixatives to penetrate into the specimen and fix the

cellular content. Using cryo-immobilization, samples are immobilized within milliseconds, fast enough to capture transient processes such as the formation and docking of membrane vesicles. The main requirement is that samples are frozen in a vitreous state, without ice-crystals which disturb the cellular ultrastructure. Plunge-freezing, jet freezing and metal mirror (slam) freezing allow for vitrification of samples up to 10-20 μm , which is not enough for most mammalian cell types. Using high-pressure freezing [21], it is possible to vitrify samples up to 200 μm in thickness. However, for observation in the transmission electron microscope these samples need to be processed first. Freeze-substitution is often the method of choice. Here water is replaced by an organic solvent, usually containing fixatives, at sub-zero temperatures (-90°C). Effectively, the sample is dehydrated and fixed at the same time, while the lipids and proteins are still immobilized. After substitution, samples are most often embedded in resin, either at low temperature (down to -80°C) using Lowicryl resins or at ambient temperature using epoxy resins.

At present there are only four studies dealing with lipid extraction during freeze-substitution of cryo-immobilized specimens; Humbel (1984) using erythrocyte ghosts substituted in methanol [22], Weibull (1984) using pre-fixed *A. Laidlawii* cells and ghosts substituted in methanol or acetone [23], van Genderen (1991) measuring the loss of Forssman glycolipid from pre-fixed Madin-Darby Canine Kidney (MDCK) cells substituted in methanol containing 0.5% uranyl acetate [19] and Maneta-Peyret (1999) using rat brain and liver either fixed or unfixed, substituted in ethanol [24]. Humbel reported a loss of 9% of total phospholipids when embedding at -70°C and 15% when embedding at -30°C . The extraction was reduced to 2% and 4% respectively when 0.5% uranyl acetate was added to the methanol. Weibull showed an extraction of 5% of cellular lipid for substitution with acetone and embedding at -70°C and 15-45% extraction when using methanol as substitution medium. For substitution of pre-fixed cells in methanol containing uranyl acetate and embedding at -45°C van Genderen observed 100% retention of Forssman glycolipid. Maneta-Peyret reported lipid losses of 55-60% for substitution in ethanol and embedding at -80°C , which was reduced to 24% if 0.5% uranyl acetate was added to the substitution medium. For pre-fixed tissue, lipid extraction was close to 80% with little effect of uranyl acetate.

CEMOVIS

Cryo-Electron Microscopy Of Vitreous Sections (CEMOVIS)[25] can be considered to be the holy grail in sample preparation. In short, a sample is high-pressure frozen, cryo-sectioned and observed in the transmission electron microscope at liquid nitrogen temperatures. The only artifacts in this method are those introduced during sectioning (compression, knife marks, crevasses and chatter) and specimen handling (ice contamination)[26]. Since there is no additional specimen preparation, there is no lipid extraction. Though this method allows the observation of the native ultrastructure, at the moment cellular components can only be identified by their morphology.

VIS2FIX

Recently a new specimen preparation procedure for high-pressure frozen samples was developed, combining frozen hydrated sectioning, on-section fixation and freeze-substitution - rehydration. This method, called VIS2FIX[27], comes in two flavors; one in which frozen hydrated sections are freeze-substituted, rehydrated and stabilized with

methycellulose / uranyl acetate (VIS2FIX_{FS}) and a hydrated method in which frozen hydrated sections are placed on frozen fixative (containing uranyl acetate) at -90°C, thawed to 0°C, fixed and stabilized with methycellulose / uranyl acetate (VIS2FIX_H). Since VIS2FIX_{FS} is essentially a rapid freeze-substitution, the level of lipid extraction is most likely comparable to that found for freeze-substitution of whole cells. For VIS2FIX_H the level of lipid extraction will depend on the fixative used. A combination of glutaraldehyde and uranyl acetate resulted in well preserved membranes. Addition of osmium tetroxide to this mixture allowed the preservation of the hydrophobic core of lipid droplets [27] indicating an increased level of neutral lipid retention using this technique.

Table 2 Lipid extraction in commonly used sample preparation procedures

Percentages of lipid extracted in commonly used EM sample preparation procedures. Values derived from the studies of Cope and Williams (1968, 1969) (a); based on Roozmond (1969) (b); Weibull (1984)(c); Maneta-Peyret (1999)(d); Humbel (1984)(e).

Sample preparation method	tissue	temperature	Percentage of lipid extracted					neutral lipids
			total	PE	PC	PS	SM + PI	
Chemical fixation								
Glutaraldehyde	rat liver	RT	-	47%	100%	nd	nd	70%
Glutaraldehyde; Osmium	rat liver	RT	-	1%	11%	nd	nd	57%
Osmium	rat liver	RT	-	2.6%	2.5%	nd	nd	nd
Tokuyasu cryo-sections								
	rat brain	RT	1.3%	0.05%	0.55%	0.14%	0.2%	nd
Freeze-substitution								
Acetone	A.Laidlawii	-90→-70°C	5.1%	nd	nd	nd	nd	nd
Ethanol	rat brain	-80°C	55%	nd	nd	nd	nd	nd
	rat liver	-80°C	58%	nd	nd	nd	nd	nd
Ethanol + UA	rat brain	-80°C	24%	nd	nd	nd	nd	nd
	rat liver	-80°C	23%	nd	nd	nd	nd	nd
Methanol	A.Laidlawii	-90→-70°C	15-45%	nd	nd	nd	nd	nd
	erythrocyte	-90→-70°C	7%	nd	nd	nd	nd	nd
	erythrocyte	-90→-30°C	15%	nd	nd	nd	nd	nd
Methanol + UA	erythrocyte	-90→-70°C	2%	nd	nd	nd	nd	nd
	erythrocyte	-90→-30°C	4%	nd	nd	nd	nd	nd

Discussion

The sample preparation procedures discussed here each have different levels of lipid retention (Table 2), but by taking a closer look at the processes within these preparation methods we may be able to identify the underlying mechanisms determining the level of lipid retention.

In the sample preparation procedures where a resin is used to embed the samples (chemical fixation and freeze-substitution), water is replaced by an organic solvent to improve resin infiltration and polymerization. Most of the lipid extraction takes place during this dehydration step and the choice of solvent has a profound impact on the level of lipid retention. The main difference between the solvents used for dehydration is their polarity. As formulated by Reichardt [28]; “The ‘polarity’ of a solvent is determined by its solvation behavior which in turn depends on the action of intermolecular forces (Coulomb, directional, inductive, dispersion, and charge-transfer forces, as well as hydrogen-bonding forces) between the solvent and the solute.” Currently there are many approaches to measure polarity. Here we will use the dielectric constant to represent

polarity. Although this measurement represents only one of the aspects of polarity [28], it is the one for which most data are available.

As mentioned before, during dehydration water is replaced by an organic solvent. But like all other cellular components, polar lipid head-groups are able to bind water. Above 0°C the water molecules in this so called hydration shell are exchanged rapidly with the surrounding bulk water [29]. Thus during dehydration at room temperature when water mixes with the solvent, the solvent can directly interact with the membranes, allowing the extraction of lipids to take place (in practice extraction increases from 70 - 100% solvent).

Since with membrane lipids the head-group is first in contact with the solvent, it is likely to be the main determinant for extraction. As known from biochemistry, the rate of extraction depends on polarity; polar solvents preferably extract polar lipids, while non-polar solvents preferably extract non-polar lipids. If the polarity of the head-group is close to that of the solvent it will have a higher affinity for the solvent than for the lipid bilayer. The polarity of the various lipid head-groups can be derived from their relative migration on thin layer chromatography (TLC), though this is a measure of lipid polarity in the particular solvent system used for the TLC. A more reliable value for the polarity of membrane lipids can be obtained from direct measurements on liposomes and lipid micelles. The dielectric constant of PC and PS liposomes has been calculated to be 34, using the Stokes shift of DPE fluorescence [30]. This value stayed constant when the liposomes were above their phase transition temperature. Others have calculated the values of the dielectric constant for the polar region of model membranes to be between 27 and 30 [31].

Table 3 Solubility of fatty acids in dehydration solvents (g FA/100g solvent)

Values derived from Ralston & Hoerr (1942, 1944), Kolb (1954)* and Hoerr & Harwood (1952)** for the solubility of fatty acids in ethanol, methanol and acetone at 0 to 20°C. Solubility depends on the level of unsaturation and the length of the acyl chains.

Fatty Acid	Ethanol 95%			Ethanol 100%		
	0°C	10°C	20°C	0°C	10°C	20°C
Myristic (C14)	3.86	7.64	18.9	7.07	9.77	23.9
Palmitic (C16)	0.85	2.10	4.93	1.89	3.20	7.21
Stearic (C18)	0.24	0.65	1.13	0.42	1.09	2.25
Oleic (C18:1)	235**	1470**	∞**	nd	nd	nd
Linoleic (C18:2)	∞**	∞**	∞**	nd	nd	nd
	Methanol			Acetone		
	0°C	10°C	20°C	0°C	10°C	20°C
Myristic (C14)	2.8	5.8	17.3	2.75	6.50	13.8
Palmitic (C16)	0.8 / 0.46*	1.3	3.7	0.60 / 0.66*	1.94 / 1.6*	4.28
Stearic (C18)	0 / 0.09*	0 / 0.26*	0.1	0.21 / 0.11*	0.80 / 0.54*	1.54
Oleic (C18:1)	250**	1820**	∞**	159**	870**	∞**
Linoleic (C18:2)	∞**	∞**	∞**	∞**	∞**	∞**

If the lipid head-group has an affinity for the solvent, the composition of the acyl chains determines whether the lipid will go in solution or stay within the membrane. There are a few reports on the solubility of a number of fatty acids in organic solvents [32–35]. Although the actual values might not be of use here, there are certain trends in the solubility data that can be extrapolated to our case: shorter acyl-chains are extracted more easily than longer chains, while the presence of unsaturated bonds makes fatty acids even more extractable (Table 3). Experimental data show that for dehydration at room temperature the level of lipid extraction appears to be correlated to the polarity of the solvent used for dehydration. Dehydration by ethanol, with a dielectric constant of 25.3 at 20°C, extracted more phospholipids from liver than dehydration using acetone with a dielectric constant of 21.0 at 20°C [8].

Table 4 Polarity of commonly used organic solvents compared to water

Temperature dependency of the dielectric constant of organic solvents and water derived from the handbook of chemistry and physics 92th edition, section 6.

Solvent	Polarity (dielectric constant) $\epsilon_r(T)$					
	20 °C	0°C	-30°C	-50°C	-70°C	-90°C
H ₂ O	80.1	87.7	--	--	--	--
Methanol	33.0	37.3	45.1	51.6	59.1	67.6
Ethanol	25.3	28.2	33.3	37.5	42.5	48.2
Acetone	21.0	23.5	27.8	31.0	34.6	38.4

The polarity of organic solvents is temperature dependent (Table 4): with decreasing temperature the dielectric constant of the solvent rises. This is reflected by the decrease in solubility of fatty acids in solvents with decreasing temperature [34] (Table 5). This increase in solvent polarity is likely to affect the rate of lipid extraction during freeze-substitution. At the low temperatures employed during freeze-substitution not much is known about the dielectric constant of lipids. For pure PC and PE liposomes the dielectric constant of the head-group drops to 4, the estimated value for the acyl chains, when these lipids are brought below their phase transition temperature [30]. For cellular membranes such a transition temperature is difficult to establish since these membranes contain many lipid species with different acyl-chain compositions. Also the question remains whether this drop in dielectric constant occurs when samples are cryo-immobilized by high-pressure freezing. One of the main contributing factors to the dielectric constant of membrane lipids is the head-group rotation [31]. After cryo-immobilization it can be expected that this rotation is limited therefore suggesting a decrease in the dielectric constant. If this is the case, the acyl chain composition will have more influence on the extraction of lipids during freeze-substitution than during room temperature dehydration.

Table 5 Solubility of fatty acids in substitution solvents (g FA/100g solvent)

Values derived from Kolb (1954) for the solubility of fatty acids in acetone or methanol, at sub-zero temperatures. Solubility of fatty acids decreases with lower temperatures. The level of unsaturation and the length of the acyl chains still determine the solubility.

Fatty Acid	Methanol					
	-10°C	-20°C	-30°C	-40°C	-50°C	-60°C
Palmitic (C16)	0.16	0.050	--	--	--	--
Stearic (C18)	0.031	0.011	--	--	--	--
Oleic (C18:1)	nd	4.02	0.86	0.29	0.10	0.03
Linoleic (C18:2)	nd	nd	nd	nd	3.10	0.90
	Acetone					
	-10°C	-20°C	-30°C	-40°C	-50°C	-60°C
Palmitic (C16)	0.27	0.10	0.038	--	--	--
Stearic (C18)	0.023	0.005	--	--	--	--
Oleic (C18:1)	nd	5.20	1.68	0.53	0.17	0.055
Linoleic (C18:2)	nd	nd	nd	nd	4.10	1.20

Another difference between dehydration at room temperature and freeze-substitution is that in the latter, water is in a solid phase. During freeze-substitution the ice has to be substituted first before the solvent can interact with the membrane. Methanol has a high polarity at -90°C (Table 3) and is able to remove most water (bulk water and water in the hydration shells of proteins, lipids and glycans) at this temperature. This would explain the increase in lipid extraction during substitution to higher temperatures observed by Humbel [22]. Acetone, on the contrary, has a much lower polarity at -90°C and can only accommodate 1% water at that temperature. Therefore substitution of bulk and bound water takes much longer and lipid extraction will start later. Humbel also observed that during freeze-substitution of erythrocyte ghosts mainly PE was extracted [22]. Erythrocytes contain about 27% PE and 30% PC [36], and during room temperature preparation PC is extracted more easily than PE [6,11]. This effect can be explained if one assumes that the water shell around the phospholipid head-groups needs to be substituted before the lipid can be extracted. PE has been calculated to bind about 8 whereas PC is able to bind about 32 water molecules [37]. This is strengthened by the 100% retention of Forssman glycolipid as found by van Genderen, since glycolipids are capable of binding many more water molecules due to the presence of the sugar chains [37,38]. The lower polarity of acetone compared to methanol at substitution temperatures would also imply a slight increase in the extraction of unsaturated lipids when acetone is used as the substitution medium (Table 5). The only conflicting data are those found by Maneta-Peyret; since the polarity of ethanol is between those of methanol and acetone one would expect the lipid extraction to be between the values found for those solvents, however the rates of extraction reported are much higher. This discrepancy could be due to the preparation procedure used in the study of Maneta-Peyret. Samples were slam-frozen, thus only well frozen up to 20 µm within the sample. Furthermore freeze-substitution started at -80°C, the temperature at which cubic ice recrystallizes to hexagonal ice. Therefore the

increased levels of lipid extraction could also be due to ice-crystal damage within the samples and loss of cellular material in the substitution medium.

Since both the Tokuyasu technique and the VIS2FIX_H method lack a dehydration step, lipid retention in these samples is expected to be much higher compared to resin embedded samples. The small loss of lipid during fixation can be negated by the addition of CaCl₂ to the fixative. The effect of CaCl₂ on the retention of polar lipids during fixation [18] also depends on polarity. Ca²⁺ binds to negatively charged (PS, PI) and zwitterionic phospholipids [39] and alters their polarity [30]. During the pickup of Tokuyasu cryo-sections using methylcellulose/sucrose the sections are slightly stretched [17]. This can cause loss of weakly fixed material, such as lipids. For both Tokuyasu cryo-sections and VIS2FIX_H processed sections, further lipid loss may still occur during further processing of the sections for immuno-labeling. Especially after thawing of the sections, when in Tokuyasu cryo-sections polar lipids might re-organize to cover the exposed hydrophobic surface [20].

The use of uranyl acetate, either during freeze-substitution or as a secondary fixative, was observed to increase lipid retention [10,20,22,24]. Uranyl ions have been shown to bind to the phosphorus groups of phospholipids [40,41] with the exception of phosphatidic acid (PA)[40]. One uranyl ion can bind up to four lipid phosphorus groups [42], effectively cross-linking membrane phospholipids and inhibiting lateral lipid diffusion. Additionally, binding of the positively charged uranyl ions to the membrane affects the polarity of the lipids and thereby their extractability. Although uranyl acetate has been reported not to react with glycosphingolipids or cholesterol [40], the use of uranyl acetate did improve cholesterol retention [20], though this could be a synergistic effect of increased sphingomyelin retention. The binding of uranyl ions to lipids is an electrostatic interaction and completely reversible. Also it has been reported not to alter the migration of lipids on TLC [10].

Conclusion

Both for chemical fixation and freeze-substitution, lipid retention depends heavily on the fixation procedure and the solvent used for dehydration [11–13]. The differences in lipid loss between these methods can be explained by considering the polarity of both the solvent and the lipids. Reactions with fixatives can either cross-link lipids or alter the head-group polarity (aldehydes and uranyl acetate) or the degree of unsaturation of the lipids (osmium tetroxide) and thereby influence lipid retention. It appears that besides fixing cellular content, reaction of aldehydes or osmium tetroxide with lipids can also make them more prone to extraction [13,18,23,24], this again is most likely caused by changes in the polarity of these lipids. For PFA fixation, this effect can be countered to a certain extent by addition of 1% CaCl₂ to the fixative [6,18]. In the case of freeze-substitution, lipid retention is increased by the presence of uranyl acetate [22,24] and a lower embedding temperature [22]. Here, also polarity appears to be the main determinant of lipid extraction, with the difference that not the polarity of lipid head-groups but the amount of bound water determines whether a lipid is prone to extraction. The use of uranyl acetate as a fixative should be considered essential for the preservation of lateral lipid distribution since it can bind up to four phospholipids per uranyl molecule [42]. Methods that

do not rely on dehydration have increased lipid retention during sample preparation but might not be able to preserve the lateral organization of lipids after sectioning. Once again, the addition of uranyl acetate to the fixative (as is the case for VIS2FIX) could alleviate this problem.

Combining the information on lipid retention with the level of ultrastructural preservation, cryo-immobilization by high-pressure freezing followed either by VIS2FIX or freeze-substitution and low temperature embedding are currently the methods of choice to study lipids and lipid-rich structures by transmission electron microscopy.

Acknowledgments

We thank Laura van Niftrik for useful comments and critically reading the manuscript. Thanks to Jacques Dubochet for the interesting discussion regarding hydration shells in high-pressure frozen biological specimens.

References

- Hayat MA. Principles and techniques of electron microscopy: biological applications. 4th edition. Cambridge University Press; 2000.
- Hoetzel S, Sprong H, van Meer G. The way we view cellular (glyco)sphingolipids. *J Neurochem* 2007;103 Suppl 1:3–13.
- Marton L. Electron microscopy of biological objects. *Nature* 1934;133:911.
- Palade GE. A study of fixation for electron microscopy. *J Exp Med* 1952;95:285–298.
- Sabatini DD, Bensch K, Barnett RJ. Cytochemistry and Electron Microscopy The preservation of cellular ultrastructure and enzymatic activity by aldehyde fixation. *J Cell Biol* 1963;17:19–58.
- Roosmond RC. The effect of fixation with formaldehyde and glutaraldehyde on the composition of phospholipids extractable from rat hypothalamus. *J Histochem Cytochem* 1969;17:482–486.
- Gigg R, Payne S. The reaction of glutaraldehyde with tissue lipids. *Chem Phys Lipids* 1969;3:292–295.
- Ashworth CT, Leonard JS, Eigenbrodt EH, Wrightsman FJ. Hepatic intracellular osmiophilic droplets: effect of lipid solvents during tissue preparation. *J Cell Biol* 1966;31:301–318.
- Ward BJ, Gloster JA. Lipid losses during processing of cardiac muscle for electron microscopy. *J Microsc* 1976;108:41–50.
- Weibull C, Christiansson A, Carlemalm E. Extraction of membrane lipids during fixation, dehydration and embedding of *Acholeplasma laidlawii*-cells for electron microscopy. *J Microsc* 1983;129:201–207.
- Cope GH, Williams MA. Quantitative studies on the preservation of choline and ethanolamine phosphatides during tissue preparation for electron microscopy. *J Microsc* 1969;90:31–46.
- Cope GH, Williams MA. Quantitative studies on the preservation of choline and ethanolamine phosphatides during tissue preparation for electron microscopy. *J Microsc* 1969;90:47–60.
- Cope GH, Williams MA. Quantitative studies on neutral lipid preservation in electron microscopy. *J Microsc* 1968;88:259–277.
- Hirsch JG, Fedorko ME. Ultrastructure of human leukocytes after simultaneous fixation with glutaraldehyde and osmium tetroxide and “postfixation” in uranyl acetate. *J Cell Biol* 1968;38:615–627.
- Franke WW, Krien S, Brown RM. Simultaneous glutaraldehyde-osmium tetroxide fixation with postosmication. An improved fixation procedure for electron microscopy of plant and animal cells. *Histochemie* 1969;19:162–164.
- Tokuyasu KT. A technique for ultracryotomy of cell suspensions and tissues. *J Cell Biol* 1973;57:551–565.
- Liou W, Geuze HJ, Slot JW. Improving structural integrity of cryosections for immunogold labeling. *Histochem Cell Biol* 1996;106:41–58.
- Roosmond RC. The effect of calcium chloride and formaldehyde on the release and composition of phospholipids from cryostat sections of rat hypothalamus. *J Histochem Cytochem* 1969;17:273–279.
- van Genderen IL, van Meer G, Slot JW, Geuze HJ, Voorhout WF. Subcellular localization of Forssman glycolipid in epithelial MDCK cells by immuno-electronmicroscopy after freeze-substitution. *J Cell Biol* 1991;115:1009–1019.
- Möbius W, Ohno-Iwashita Y, van Donselaar EG, Oorschot VMJ, Shimada Y, Fujimoto T, Heijnen HFG, Geuze HJ, Slot JW. Immunoelectron microscopic localization of cholesterol using biotinylated and non-cytolytic Perfringolysin O. *J Histochem Cytochem* 2002;50:43–55.
- Moor H, Riehle U. Snap freezing under high pressure: a new fixation technique for freeze-etching. In: *Proc. 4th Eur. Reg. Conf. Electron Microsc.* 1968. p. 33–34.
- Humbel BM. Gefriersubstitution ein weg zur verbesserung der morphologischen und zytochemischen untersuchung biologischer proben im elektronenmikroskop. Diss. Naturwiss. ETH Zürich, Nr. 7609. 1984;
- Weibull C, Villiger W, Carlemalm E. Extraction of lipids during freeze-substitution of *Acholeplasma laidlawii*-cells for electron microscopy. *J Microsc* 1984;134:213–216.
- Maneta-Peyret L, Compère P, Moreau P, Goffinet G, Cassagne C. Immunocytochemistry of lipids: chemical fixatives have dramatic effects on the preservation of tissue lipids. *Histochem J* 1999;31:541–547.
- Al-Amoudi A, Chang J-J, Leforestier A, McDowall A, Salamin LM, Norlén LPO, Richter

- K, Blanc NS, Studer D, Dubochet J. Cryo-electron microscopy of vitreous sections. *EMBO J* 2004;23:3583–3588.
26. Al-Amoudi A, Studer D, Dubochet J. Cutting artefacts and cutting process in vitreous sections for cryo-electron microscopy. *J Struct Biol* 2005;150:109–121.
27. Karreman MA, van Donselaar EG, Gerritsen HC, Verrips CT, Verkleij AJ. VIS2FIX: a high-speed fixation method for immuno-electron microscopy. *Traffic* 2011;12:806–814.
28. Reichardt C. Empirical parameters of the polarity of solvents. *Angew Chem Int Ed* 1965;4:29–40.
29. Borle F, Seelig J. Hydration of Escherichia coli lipids: Deuterium T1 relaxation time studies of phosphatidylglycerol, phosphatidylethanolamine and phosphatidylcholine. *BBA-Biomembranes* 1983;735:131–136.
30. Kimura Y, Ikegami A. Local dielectric properties around polar region of lipid bilayer membranes. *J Membr Biol* 1985;85:225–231.
31. Raudino A, Mauzerall D. Dielectric properties of the polar head group region of zwitterionic lipid bilayers. *Biophys J* 1986;50:441–449.
32. Ralston AW, Hoerr CW. The solubilities of the normal saturated fatty acids. *J Org Chem* 1942;7:546–555.
33. Hoerr CW, Ralston AW. The solubilities of the normal saturated fatty acids. II. *J Org Chem* 1944;9:329–337.
34. Kolb D, Brown J. Low temperature solubilities of fatty acids in selected organic solvents. *J Am Oil Chem Soc* 1955;32:357–361.
35. Hoerr CW, Harwood HJ. The solubilities of oleic and linoleic acids in common organic solvents. *J Phys Chem* 1952;56:1068–1073.
36. Dodge JT, Phillips GB. Composition of phospholipids and of phospholipid fatty acids and aldehydes in human red cells. *J Lipid Res* 1967;8:667–675.
37. Sen A, Hui S-W. Direct measurement of headgroup hydration of polar lipids in inverted micelles. *Chem Phys Lipids* 1988;49:179–184.
38. Arnulphi C, Levstein PR, Ramia ME, Martin CA, Fidelio GD. Ganglioside hydration study by 2H-NMR: dependence on temperature and water/lipid ratio. *J Lipid Res* 1997;38:1412–1420.
39. Hutton WC, Yeagle PL, Martin RB. The interaction of lanthanide and calcium salts with phospholipid bilayer vesicles: The validity of the nuclear magnetic resonance method for determination of vesicle bilayer phospholipid surface ratios. *Chem Phys Lipids* 1977;19:255–265.
40. Shah DO. Interaction of uranyl ions with phospholipid and cholesterol monolayers. *J Colloid Interface Sci* 1969;29:210–215.
41. Ginsburg H, Wolosin JM. Effects of uranyl ions on lipid bilayer membranes. *Chem Phys Lipids* 1979;23:125–131.
42. Huang TH, Blume A, Das Gupta SK, Griffin RG. Nuclear magnetic resonance and calorimetric study of the structure, dynamics, and phase behavior of uranyl ion / dipalmitoylphosphatidylcholine complexes. *Biophys J* 1988;54:173–179.

Chapter 2

Lipid droplets: biogenesis and interactions with other organelles

R.J. Mesman^{1,2,3,*}, E.G. van Donselaar², K.N.J. Burger^{3,4}, J.C.M. Holthuis^{1,3,5}

¹Membrane Enzymology, Department of Chemistry, Utrecht University, Padualaan 8, 3584 CH Utrecht, the Netherlands

²Biomolecular Imaging, Department of Biology, Utrecht University, Padualaan 8, 3584 CH Utrecht, the Netherlands

³Institute of Biomembranes, Utrecht University, Padualaan 8, 3584 CH Utrecht, the Netherlands

⁴Endocrinology and Metabolism, Department of Biology, Utrecht University, Padualaan 8, 3584 CH Utrecht, the Netherlands

⁵Molecular Cell Biology, Fachbereich Biologie/Chemie, Universität Osnabrück, Barbarastraße 13, 49076 Osnabrück, Germany

*Corresponding author:

Abstract

Lipid droplets (LDs) play an important role in cellular lipid homeostasis. These storage organelles for neutral lipids are surrounded by a phospholipid monolayer and have been suggested to function in various other cellular processes. LDs have been found in close association with a number of other cellular organelles, but the nature of these interactions has not been well studied. How lipid droplets are formed also remains an enigma, though it is a widely held view that their biogenesis occurs in the endoplasmic reticulum (ER). Here we explore the use of transmission electron microscopy and tomography to investigate the early stages of LD formation and gain insight into the association of LDs with other organelles. Taking advantage of an experimental cell system in which nascent LDs can be accumulated, we found the first indications that LD formation is initiated in ER membranes preferentially those associated to mitochondria.

Introduction

Fatty acids (FAs) are used for the synthesis of polar lipids but also provide a potent source of energy in all cells. As an excessive amount of free FAs and sterols can seriously disturb cellular homeostasis, these molecules are stored in an esterified form as neutral triacylglycerol (TAG) or sterol-esters in specialized storage organelles, called lipid droplets (LDs). LDs contain a neutral lipid core surrounded by a phospholipid monolayer with a specific lipid composition [1], which is stabilized by a number of amphipathic helix-containing proteins, called PAT proteins [2] or perilipins [3]. The amount and composition of PAT proteins on a lipid droplet is not constant (see also the review by Wolins *et al.* (2006) [4]. Of the PAT proteins, only perilipin (perilipin 1) and adipophilin (perilipin 2) are tightly bound to the LD surface. TIP47 (perilipin 3), S3-12 (perilipin 4) and Oxpap (perilipin 5) can also exist in a cytosolic form. In adipocytes, the composition of PAT proteins also regulates the release of fatty acid from lipid droplets by lipases [5].

The presence of a phospholipid monolayer instead of a lipid bilayer makes the lipid droplet a unique organelle within the cell. Lipid droplets are thought to have other functions besides the storage of neutral lipids, such as assisting in the breakdown of hydrophobic proteins [6,7] and in cellular trafficking [8,9]. LDs have been implicated in the pathogenesis of several cardiovascular and muscle diseases. Furthermore, ectopic lipid storage has been linked to reduced insulin sensitivity and Diabetes type 2.

Lipid droplets within a cell can differ in lipid composition and even within a single lipid droplet the neutral lipid appears to be organized, with unsaturated lipids and cholesterol in the periphery and the most saturated lipids in the center [10]. This packing could account for the appearance of 'layers' within lipid droplets in freeze-fracture replicas [11]. Though these differences in lipid composition between lipid droplets have been observed for 3T3-L1 cells and adipocytes, newly synthesized TAG appears to be uniformly incorporated into existing lipid droplets in other cell types [12].

LDs are by no means static storage organelles. Even in the earliest studies using electron microscopy, LDs have been shown to interact with the cytoskeleton and other

cellular organelles such as ER, mitochondria, peroxisomes, endosomes and lysosomes [13,14]. Although some of these interactions could be based on artifacts from the sample preparation, as is the case for the so-called ER inclusions in LDs reported by McGookey [15], which upon close inspection appear to be exactly like myelin figures caused by dehydration. Whether the LD organelle interactions are just close associations or actual membrane contacts is difficult to assess using standard TEM analysis of thin sections and ask for other approaches such as Electron Tomography.

Until now the precise mechanism by which LDs are formed is still unknown. A widely-held view is that the endoplasmic reticulum (ER), which contains the TAG-synthesizing diacylglycerol acyltransferases (DGATs) [16,17] (Figure 1), plays a crucial role in LD biogenesis. DGAT1 is an ER-resident transmembrane protein with a broad acyl-CoA-transferase activity that besides TAG can also synthesize monoacylglycerol (MAG) and diacylglycerol (DAG) [22]. DGAT2 belongs to an entirely different family of acyl-transferases and is dedicated to the synthesis of TAG. DGAT2 has two predicted isoforms. The main difference between these is the absence of a transmembrane region in isoform 2. DGAT2 has been shown to localize to lipid droplets (LDs) after stimulation with fatty acid [17], suggesting that this enzyme can mediate the synthesis of TAG on the surface of pre-existing LDs.

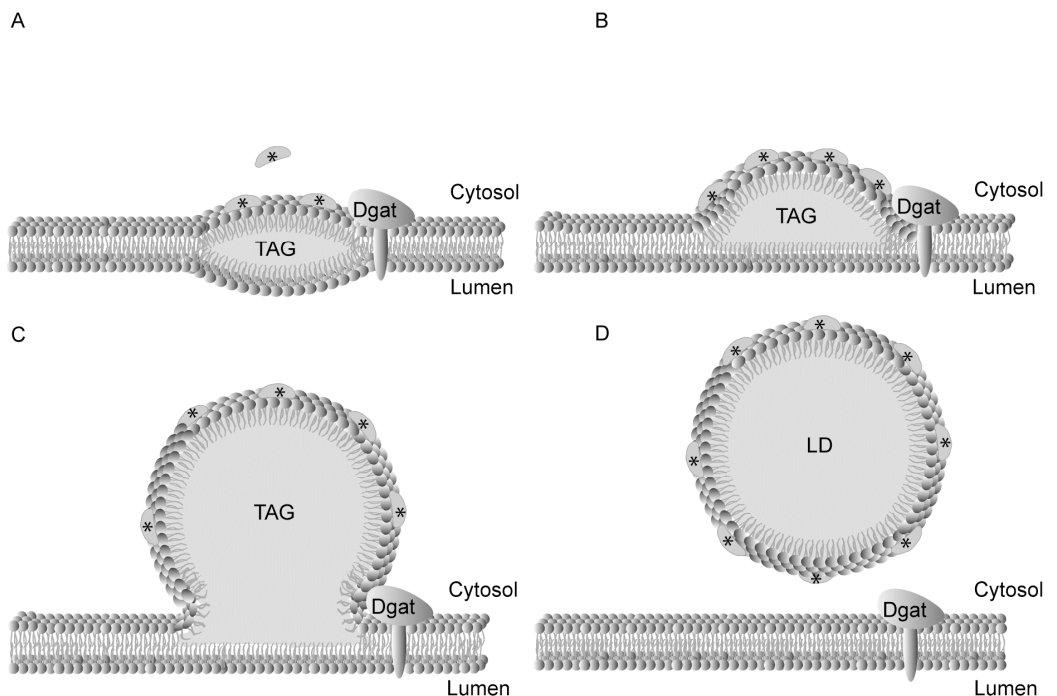


Figure 1. Lipid droplet formation according to the budding model The budding model is the most widely accepted model for lipid droplet biogenesis. (A) Triacylglycerol (TAG) synthesized by DGAT accumulates between the membrane leaflets and causes a change in the membrane curvature. This curvature is stabilized by PAT proteins(*) like TIP47. (B) Stabilization of the lipid lens by the PAT proteins facilitates expansion of the lens towards the cytosol. (C) The lipid lens approaches its critical size and a neck region starts to form. (D) The nascent lipid droplet buds out of the ER and becomes a cytosolic lipid droplet.

There are a number of theories on lipid droplet formation. The most widely accepted theory is the budding model [18,19] (Figure 1). This model postulates that newly synthesized TAG accumulates between the two leaflets of the ER membrane, forming a lens like structure which, when it has reached a critical size, buds off from the ER membrane [20]. This process is thought to be assisted by proteins that help stabilize membrane curvature. One of these proteins is the PAT protein TIP47 or perilipin 3. Consistent with a role in an early stage of LD formation, TIP47 has been reported to localize to DAG rich areas in the ER membrane [21] whereas a reduction of TIP47 protein levels by RNA interference was shown to abolish formation of mature LDs without changing the level of TAG synthesis [22].

The polar lipid composition of membrane leaflets surrounding the lipid lens could also contribute to the budding of the lipid droplet. Recently, cytosolic phospholipase A2 alpha (cPLA2 α) has been implicated to be essential for the formation of lipid droplets [23] and inhibition of this lipase resulted in a 60-70% decrease of LD formation after arachidonic acid stimulation [24]. After activation, cPLA2 α hydrolyzes phospholipids to lysophospholipids [25] and could thereby assist in inducing the membrane curvature required for transforming the lipid lens into a lipid droplet. These lipid lenses or nascent LDs have been calculated to be about 12 nm in diameter [26] though this model did not take into account the stabilizing effect of PAT proteins. Nascent LDs are most likely very small in size, making it difficult to detect these structures even with an electron microscope. This could be overcome by either labeling these structures or by increasing their abundance.

An alternative model for lipid droplet formation is based on the similarity between lipid droplets and lipoproteins. Like the formation of lipoproteins, which will be discussed in Chapter 3, the formation of LDs could take place outside the membrane bilayer. First, polar lipids are bound to a lipid binding protein, after which neutral lipids are loaded within the micelle formed by the polar lipids. However, there is little experimental evidence for this model.

To visualize the early stages of LD formation at the ultrastructural level, we applied a combination of electron microscopy techniques on a cell system in which this process can be manipulated. To this end, we used human HeLa cells in which expression of the PAT protein TIP47 is knocked down by \pm 70% by stable expression of a short interfering hairpin RNA [22]. The TIP47kd cell line converts oleic acid into TAG without forming LDs, most likely because the budding of nascent LDs from the ER membrane is blocked. Feeding TIP47kd cells with oleic acid would thus provide a means to accumulate nascent LDs. To visualize these structures, TIP47kd and control cells were subjected to transmission electron tomography, staining of lipid inclusions by imidazole/osmium-tetroxide, and immuno-localization of remaining TIP47. Transmission electron tomography creates a three-dimensional reconstruction of a sample by back-projection of transmission images taken at different tilt angles [27,28]. The resolution of this technique allows determining membrane contacts and continuities and thereby provides important information on the organization of structures within a sample. For this reason it was used to study the association of LDs with other cellular organelles.

Results and Discussion

Setting the time-frame for LD biogenesis

Inclusions of TAG can be stained by lipid specific dyes, though some of these have been shown to induce LD fusion [29]. We used the fluorescent stain Nile Red, which does not induce fusion, [30] to monitor LD formation and pick an optimal time point for chemical fixation and EM analysis. The emission spectrum of Nile Red depends on the polarity of its surrounding medium [31]. When exposed to neutral lipid, the dye emits gold-yellow light that can best be observed in the green channel (excitation, 450-500 nm; emission, greater than 528 nm). After staining with Nile Red, numerous LDs could be observed in human HeLa cells grown in medium supplemented with 10% FCS (Figure 2A). To stimulate formation of new LDs rather than expanding pre-existing LDs, we decided to pre-incubate the cells in medium supplemented with delipidated FCS. After overnight incubation in lipid-free medium, the number of lipid droplets within the cell was drastically reduced (Figure 2B). When 100 μ M oleic-acid complexed to albumin was added to these cells, large lipid droplets could be observed after 20 min of incubation (Figure 2C). This time period was used in all subsequent experiments with control and TIP47kd HeLa cells.

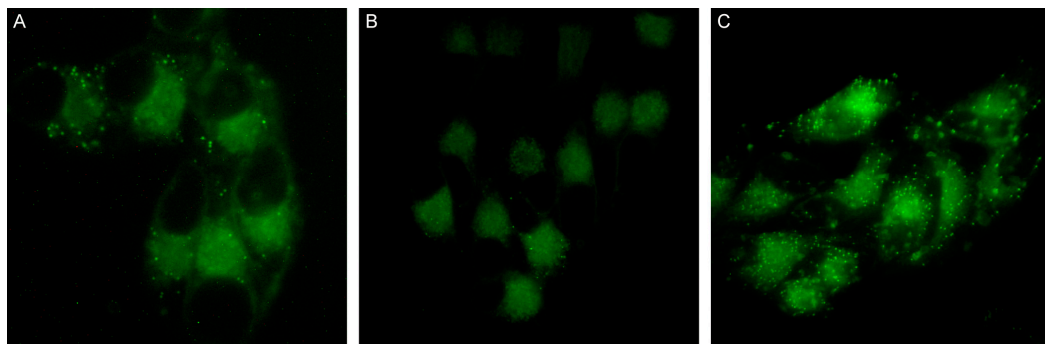


Figure 2. Setting a rough time-scale for LD formation HeLa cells were grown on coverslips and incubated overnight in delipidated culture medium. The next day cells were incubated with 100 μ M oleic acid bound to albumin. At specific time points cells were fixed with 4% formaldehyde and stained with Nile-red before being imaged by fluorescence microscopy. (A) HeLa cells grown on culture medium containing 10% fetal calf serum. Using the green channel, lipid droplets can be visualized. (B) After overnight incubation in culture medium containing 10% delipidated serum the amount of lipid droplets is drastically decreased. (C) 20 min after addition of 100 μ M oleic acid, newly formed lipid droplets can be observed throughout the cells. All images were taken at 40x magnification.

TEM tomography on HeLa TIP47kd cells

As a pilot experiment, HeLa TIP47kd cells were loaded for 20 min with oleic-acid before chemical fixation. To obtain an optimal ultrastructural preservation of LDs, cells were fixed with glutaraldehyde and osmium tetroxide (OsO_4) simultaneously [32,33] as discussed in Chapter 1. Before dehydration and embedding in Epon, the intrinsic contrast of the samples was enhanced by post-fixation with tannic-acid followed by osmium tetroxide (TAMOI) [34]. This provides optimal contrast throughout the sample, which is a prerequisite for tomographic reconstruction. 500 nm sections were first analyzed by conventional TEM to identify regions containing ER membranes, the site where LD formation is thought to occur. Of these regions dual axis tilt series were

recorded and reconstructed. Interestingly, in several tomograms (3 out of 5), lens like structures could be observed in the ER membrane (Figure 3, dashed circles). These structures were not observed in HeLa TIP47kd cells that had not been incubated with oleic acid (3 tomograms analyzed). The lenses typically measured up to 15 nm in thickness and 17 nm in length. These dimensions are slightly larger than the calculated critical size for spontaneously budding LDs [26].

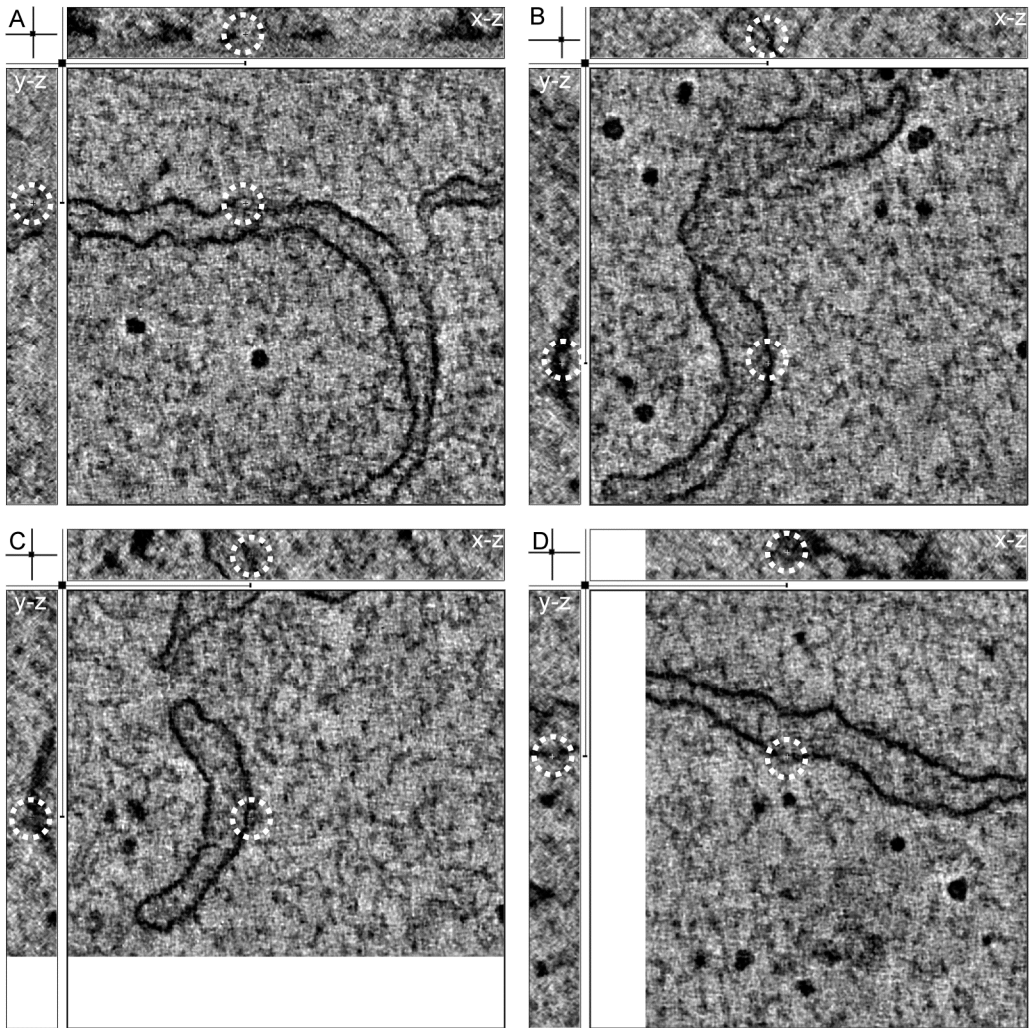


Figure 3. Lens like structures in the ER in tomograms of chemically fixed TIP47kd HeLa cells

HeLa TIP47kd cells grown on aclar were incubated for 20 min with 100 μ m oleic acid before chemical fixation with 2% glutaraldehyde and 2% osmium tetroxide in 0.1M cacodylate buffer, followed by contrast enhancement using the TAMOI method. Samples were dehydrated in ethanol and embedded in Epon. (A-D) Electron tomography on 350 nm sections revealed lens like structures in the ER membrane (dashed white circles) which were also visible in the X-Z, Y-Z view.

To rule out that these lens-like structures are artifacts caused by chemical fixation, we avoided this step and physically fixed the oleic acid-treated HeLa TIP47kd cells by high-pressure freezing followed by freeze-substitution, TAMOI and embedding in Epon. In tomographic reconstructions from these samples (3 tomograms analyzed), we were unable to find lens-like structures in the ER. This result raised the possibility that the lens-like structures observed previously are induced by chemical fixation and may not correspond to initial stages of LD formation. However, at this point we cannot exclude two alternative possibilities. First, we may have not analyzed sufficient tomograms of high-pressure frozen, freeze-substituted cells to detect the lipid lenses. Second, lipid lenses may be less apparent in freeze-substituted samples compared to chemically fixed material, since freeze-substitution preserves the cellular ultrastructure to such an extent that the lens-like structures could be easily obscured by nearby cellular components. As an alternative approach to visualize early stages of LD formation at the ultrastructural level, we next explored the use of imidazole as a specific stain for lipid inclusions.

Staining of lipid inclusions

A combination of osmium tetroxide with imidazole has previously been shown to intensify the staining of lipid droplets [35]. Since a transmission electron micrograph is in essence the sum of all the information in the z-direction of the section, it is often difficult to assess the identity of individual structures in a micrograph of a thick section. The increase in contrast of lipid inclusions provided by the imidazole-osmium stain might aid us in the detection of nascent LDs in thick sections intended for electron tomography. We first tested this method in combination with our optimized chemical fixation protocol (see above) before exploring the suitability of this method in freeze-substitution. In thin sections of control HeLa cells, lipid droplets were indeed stained after using imidazole as a mordant (Figure 4A). However, also lipid inclusions in lysosomes appeared to be intensely stained (Figure 4B). Attempts to use this technique as a tool to pin-point the location of early lipid droplets within thick resin sections resulted in too many false-positives during the identification of the regions of interest for electron tomography. Therefore, we decided to try to identify the site of lipid droplet biogenesis by immunolocalization of one of the proteins involved in this process.

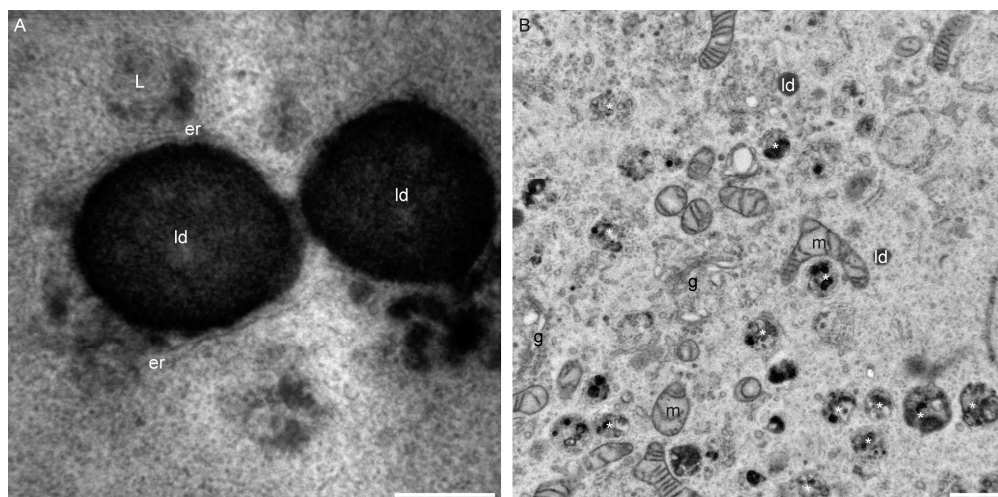


Figure 4. Staining of neutral lipid inclusions using imidazole-osmium

HeLa cells grown on aclar were incubated for 20 min with 100 μ m oleic acid before chemical fixation with 2% glutaraldehyde and 2% osmium tetroxide in 0.1 M cacodylate buffer, followed by imidazole-osmium staining, dehydration in ethanol and embedding in Epon. (A) After imidazole-osmium treatment lipid droplets appear intensely stained. ER membranes can be identified in close association with the LDs. (B) At lower magnification however it becomes clear that not only LDs but also lipid inclusions in multivesicular bodies are intensely stained. *: multivesicular body, er: endoplasmic reticulum, g: Golgi, ld: lipid droplet, m: mitochondria. All scale bars represent 500 nm.

Immuno-localization of TIP47

A complementary method to localize early LDs at the ultrastructural level would be the immuno-localization of TIP47. This protein is required for efficient LD formation [22]. TIP47 localizes to ER membranes enriched in DAG [21], which is the precursor for TAG. Immuno-gold labeling of TIP47 may thus help pinpoint sites of LD formation. We tested antibodies against TIP47 on Tokuyasu cryo-sections [36] of oleic acid-treated HeLa cells. Immuno-gold labeling of TIP47 showed the presence of TIP47 on the periphery of LDs (Figure 5A). As discussed in Chapter 1, the hydrated VIS2FIX method [37] allows for efficient immuno-labeling and combines rapid cryo-immobilization with good lipid retention. Therefore, we tried to localize TIP47 on sections processed via the VIS2FIX_H method. While the labeling of TIP47 on the periphery of LDs was reproducible, at first there was still considerable background label on the nucleus, mitochondria and the formvar film. Changing the block buffer from 1% BSA to 0.5% acetylated BSA (BSA-c) reduced most of this background (Figure 5B). In oleic acid-treated TIP47kd cells, we expected the remaining TIP47 to localize primarily to the site of TAG synthesis to stabilize newly formed lipid lenses. When immuno-labeling VIS2FIX_H sections of these cells, hardly any TIP47 could be detected (Figure 5C), as expected. However, we did observe sparse gold label on the periphery LDs as well as on small electron translucent structures in mitochondria-associated regions of the ER membrane (Figure 5D, dashed white circles). Since the TAG synthase DGAT2 has been reported to reside in these membranes [17], the structures observed here may well correspond to early LDs. More quantitative experiments are needed to validate these preliminary results. For example, in TIP47kd HeLa cells grown in delipidated medium, TIP47 should be absent from the

mitochondria-associated ER membranes. Furthermore, TEM tomography may be used to provide more insight in the TIP47 positive structures present in the mitochondria-associated ER after oleic acid stimulation.

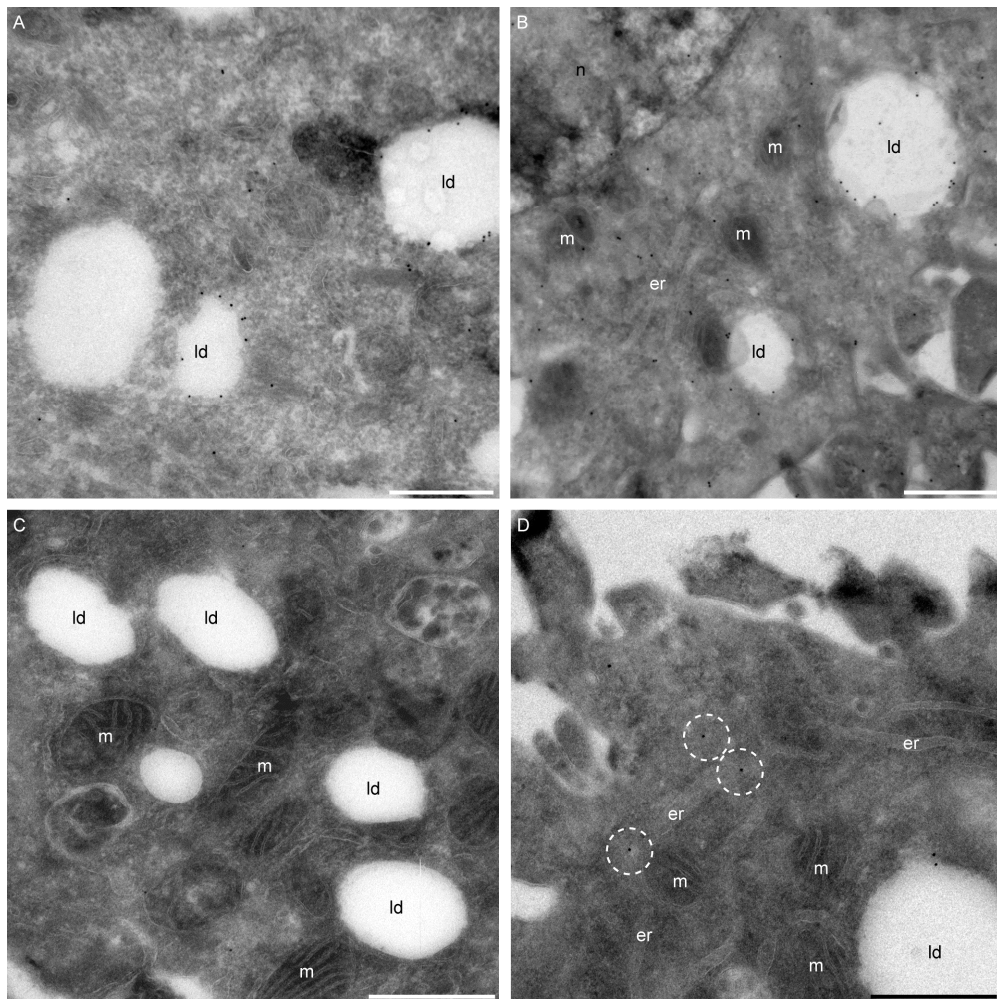


Figure 5. Immuno-localization of TIP47 on control and TIP47kd HeLa cells

Tokuyasu cryo-sections and VIS2FIX_H sections of HeLa cells (A,B) and TIP47kd HeLa cells (C,D) were labeled for TIP47 using specific antibodies. (A) Tokuyasu cryo-section of HeLa cells incubated with oleic acid and labeled for TIP47. Gold label can be detected in the cytosol and on the periphery of lipid droplets. (B) This result was reproducible on VIS2FIX_H sections, though these required a more stringent blocking step to reduce background label. (C) Hardly any TIP47 could be detected on VIS2FIX_H sections of TIP47kd cells. (D) In some sections specific label could be detected on small electron translucent structures in the mitochondria associated ER membrane (dashed white circles). er: endoplasmic reticulum, ld: lipid droplet, m: mitochondria, n: nucleus. All scale bars represent 500 nm.

Validation of LD-organelle interactions using TEM tomography

TEM tomography provides a tool to validate the interactions between LDs and other organelles previously observed in transmission electron micrographs of thin sections. Tilt-series were recorded from 500 nm sections of high-pressure frozen, freeze-substituted and Epon embedded HeLa cells, loaded for 60 min with oleic acid to assure the presence of large LDs. In the reconstructions of these tilt-series we observed close association of LDs with mitochondria, ER membranes, lysosomes and multivesicular bodies. For ER membranes, membrane contact sites between ER and LD could be observed. (Figure 6A, B). The LDs themselves appeared electron translucent, as if most of the neutral lipid content had been extracted during substitution and embedding. As discussed in Chapter 1, when freeze-substitution is combined with low temperature embedding using Lowicryl resin instead of Epon embedding, the extraction of neutral lipids should be reduced. Additionally, immuno-labeling can be performed on Lowicryl sections. This would allow us to identify organelles based on specific immuno-labeling rather than on ultrastructure alone. Therefore, we decided to apply freeze-substitution and low temperature embedding with Lowicryl HM20 at -50°C. We first analyzed thin sections of these samples and found that part of the neutral lipids in the core of the LD was retained during substitution, while those more to the periphery were still extracted in the process (Figure 6C). The partial extraction of the neutral lipid content made it difficult to define the LD's phospholipid monolayer in tomographic reconstructions, thus limiting the suitability of this method to define LD-organelle interactions.

The latter problem might be circumvented by the use of the VIS2FIX_H method [37]. While this method combines a well-preserved ultrastructure with efficient immuno-labeling, the section thickness is limited to a maximum of about 100 nm due to the sectioning properties of the vitreous ice. Furthermore, it is unknown whether sections obtained with this technique could withstand the extended exposure to the electron beam during the recording of the tilt-series. To test this, we used a section of THP-1 monocytes immuno-labeled for the lysosomal protein LAMP2. In this section, a LAMP2 positive lysosome was observed in close association with a lipid droplet (Figure 6D). A tilt-series was recorded and re-constructed using the gold-label as fiducial marker. In the reconstructed tilt-series, the interface between the LD and the lysosome resembled a phospholipid monolayer, suggesting that the lysosome had partially fused with the LD's phospholipid monolayer (Figure 6E, F). This type of hemi-fusion has also been proposed for peroxisome-LD interactions in yeast [38]. The direct contact shown here between the lysosome and the LD closely resembles the mechanism for micro-autophagy reported in the literature [39,40]. This suggests that the involvement of autophagy in LD metabolism [41] might also be mediated via micro-autophagy.

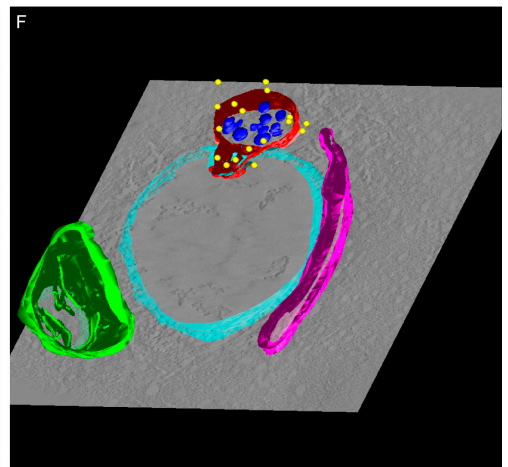
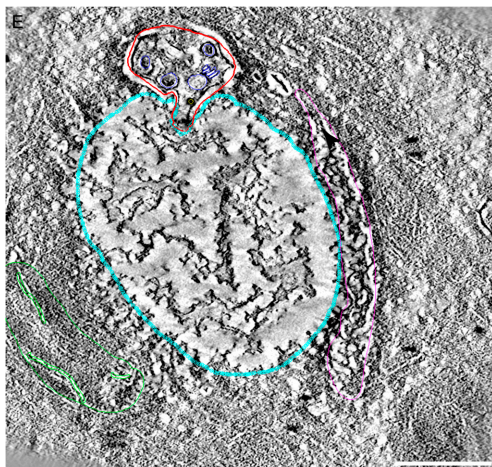
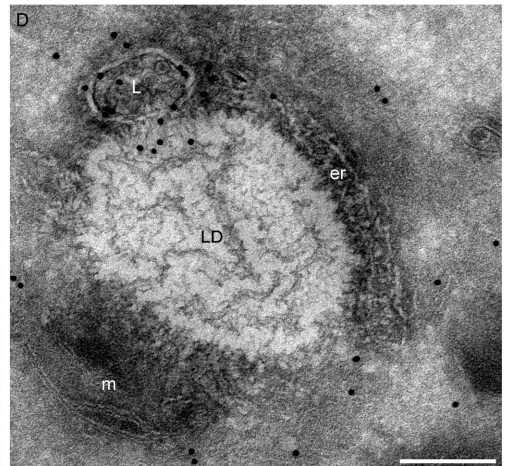
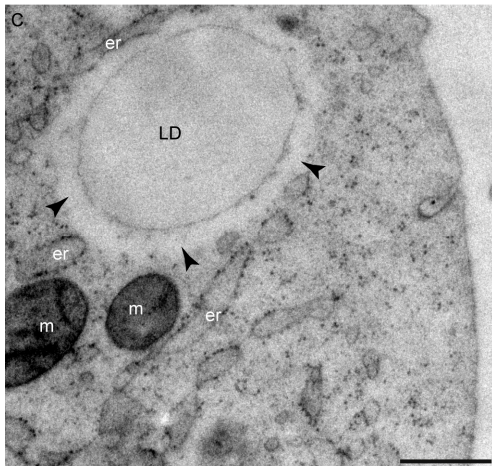
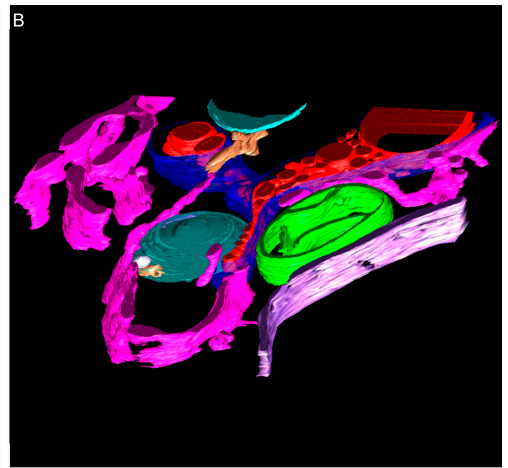
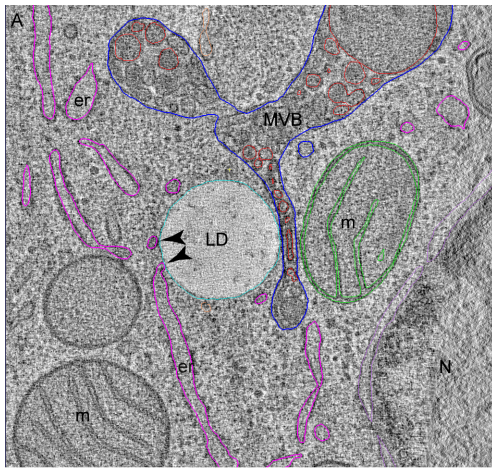


Figure 6. Validation of LD - organelle interactions using electron tomography

(A) Direct membrane contact between ER and LD could be observed in reconstructed tilt-series from high-pressure frozen, freeze-substituted and Epon embedded HeLa cells (arrowheads). (B) Model of the reconstructed tomogram showing LDs (light blue), ER membranes (pink), MVB (blue) with internal vesicles (red), mitochondria (green) and the nuclear envelope (purple). While membrane contrast was sufficient to allow for efficient reconstruction of the tilt series, LDs appeared extracted. (C) Using low temperature embedding with Lowicryl HM20 extraction of the LD content was reduced, though the rim of the LD still appeared extracted (arrowheads). (D) In a hydrated VIS2FIX section of THP-1 cells labeled for LAMP2 a LAMP2 positive lysosome appeared in close association with an LD. (E) Tomographic reconstruction revealed that the interface between LD and lysosome resembles a phospholipid monolayer, suggesting a hemi-fusion between LD and lysosome (arrowhead). (F) Model of the reconstructed tomogram showing the LD (light blue), ER membrane (pink), lysosome (red) with internal vesicles (blue), mitochondria (green) and the gold label for LAMP2 (yellow). er: endoplasmic reticulum, g: Golgi, L: lysosome, ld: lipid droplet, m: mitochondria, MVB: multivesicular body, n: nucleus. All scale bars represent 500 nm.

Concluding remarks

Since all enzymes involved in the synthesis of TAG are located in the ER membrane, it is generally believed that the biogenesis of lipid droplets takes place in this organelle. Inclusions of TAG between the membrane leaflets would bud out, stabilized by PAT proteins such as TIP47, to form a lipid droplet. The goal of the present study was to explore new approaches to visualize this process at the ultrastructural level, in order to gain further insight in the underlying mechanism. Initial experiments with chemically fixed samples indeed revealed the presence of small lens-like structures in the ER of oleic acid-stimulated TIP47kd HeLa cells, which were absent in untreated cells. However, the presence of these structures could not be verified in high-pressure frozen freeze-substituted samples. Immunogold labeling of a potential marker of nascent LDs, TIP47, on hydrated VIS2FIX sections of oleic acid-stimulated TIP47kd HeLa cells showed gold label in ER membranes, especially those associated with mitochondria. Addressing whether LD biogenesis indeed occurs preferentially in these mitochondria-associated ER membranes will require a more detailed and quantitative analysis. If mitochondria-associated ER membranes are indeed the site of LD biogenesis, TIP47 should no longer present on these membranes when TIP47kd HeLa cells are grown in delipidated medium. In addition, electron tomography on oleic acid stimulated TIP47kd HeLa cells labeled for TIP47 should be used to visualize neutral lipid inclusions in these ER subdomains. Ultimately, in control HeLa cells, TIP47 should also localize to the mitochondria-associated ER membranes shortly after oleic acid treatment. Finally, a method that would allow the labeling of individual lipid molecules (see chapter 4) might be used to directly demonstrate the presence of neutral lipid in the lens-like structures.

Using electron tomography, we were able to better characterize the nature of LD-organelle interactions. For most organelles these were mainly close appositions to the LD without involving direct membrane contact. For both ER and lysosomes however, direct membrane contacts could be observed. The mechanism for micro-autophagy, as reported in the literature, bears a close resemblance to the contact between the lysosome and the LD observed here. This suggests that the reported role for autophagy in LD metabolism may also be micro-autophagy mediated.

Materials and methods

Reagents

Oleic acid (Sigma-Aldrich, St. Louis, MO) was bound to bovine albumin in a 6:1 molar ratio, as described in Van Greevenbroek et al. (1995)[42] Briefly; 20% w/v bovine serum albumin (essentially fatty acid free, Sigma-Aldrich) was dissolved in culture medium at RT and subsequently cooled down to 4°C. Fatty acid in 96% ethanol was added to 100 mM NaOH in 96% ethanol to a final concentration of 12 mM FA. The ethanol was evaporated under N₂ flow, the resulting FA/NaOH pellet dissolved in 0.5 ml AD at 55°C, followed by the addition of 0.5 ml 20% BSA in culture medium. The FA/Albumin solution was stored at -20°C until used at a final concentration of 100 µM FA, in FA free medium.

FA-free medium was prepared by supplementing low glucose DMEM with 10% FCS delipidated by chemical extraction with (2:1) di-isopropylether (Sigma-Aldrich) : 1-butanol (Sigma-Aldrich) as described by Cham & Knowles (1976)[29]. After extraction, FCS was subjected to nitrogen flow for 2 hours before dialyzing three times overnight against PBS.

Cell culture

Control HeLa and HeLa TIP47kd cells (a kind gift of Dr. Stephan Höning, Köln University) were cultured in low glucose DMEM (PAA, Pasching, Austria) with 10% fetal bovine serum (PPA). All experiments were carried out between passage 5 to 7.

Chemical fixation and imidazole-osmium staining

HeLa cells grown on aclar pieces were incubated for 20 minutes with 100 µM oleic acid complexed to albumin (6:1 molar ratio) before chemical fixation with 2% glutaraldehyde and 2% osmium tetroxide in 0.1 M cacodylate buffer for 2 hours before dehydration in ethanol and stepwise infiltration and embedding in Epon. For samples intended for TEM tomography, contrast was enhanced using the TAMOI method [34] before dehydration. In case of imidazole-osmium staining the fixative was replaced after 15 min with 0.1M imidazole in 0.1 M cacodylate buffer and incubated for 15 min. Next the imidazole was replaced with fresh fixative and the cells were fixed for 1¾ hours before dehydration in ethanol and embedding in Epon.

Tokuyasu cryo-sections

HeLa cells at 80% confluence were incubated with 100 µM oleic acid complexed to albumin (6:1 molar ratio) for 20 minutes to stimulate LD formation. Cells were fixed for 24 hours with 2% PFA + 0.5% GA in phosphate buffer (pH7.4), scraped and pelleted in 12% gelatin. After solidifying at 4°C the pellet was cut in small blocks, infiltrated overnight with 2.3 M sucrose, mounted on aluminum pins and snap-frozen in liquid nitrogen. 90 nm sections were cut on a cryo-ultramicrotome (UC6/FC6, Leica microsystems, Vienna, Austria) at -120°C. The sections were picked up with a drop of 1.15 M methylcellulose / 1% sucrose and mounted on a grid.

High-pressure freezing

Samples for freeze-substitution

HeLa cells were grown to 80% confluence on Aclar discs glued to the bottom of a Petri dish using matrigel [43]. Cells were incubated overnight with FA free medium and challenged the next day with 100 μ M oleic acid complexed to albumin (6:1 molar ratio) for 20 minutes to stimulate LD formation. Aclar discs were placed in the 100 μ m deep recess of a type A platelet (Engineering office M.Wohlwend, Senwald, Switzerland) filled with culture medium and covered with a type B platelet (Engineering office M.Wohlwend), flat side down. The specimen sandwich was placed in the standard holder and high-pressure frozen in an EMHPF (Leica Microsystems) operating at 2100 bar.

Samples for VIS2FIX

HeLa cells at 80% confluence were incubated overnight with FA free medium and challenged the next day with 100 μ M oleic acid complexed to albumin (6:1 molar ratio) for 20 minutes to stimulate LD formation. Cells were gently trypsinized and pelleted (154 rcf, 37°C). Part of the cell pellet was re-suspended in medium containing dextran at a final concentration of 15%. The resulting cell suspension was high-pressure frozen in copper tubes in an EMHPF (Leica Microsystems) operating at 2100 bar, using a modified specimen holder. All samples were frozen within 8 minutes after re-suspension to prevent possible endocytosis of dextran.

Freeze-substitution and Epon embedding

Samples were freeze substituted from -90 to 0°C in an AFS2 (Leica Microsystems) using anhydrous acetone (Seccosolv, Merck) containing 2% osmium tetroxide (EMS, Hatfield, PA) and 3% H₂O. At 0°C, samples were washed in pure anhydrous acetone, contrast was enhanced using the TAMOI method [34]. Samples were gradually infiltrated with increasing concentrations of Epon (EMS) in anhydrous acetone and subsequently embedded in pure Epon. Samples were polymerized 60°C for 3 days. 50 nm sections were cut on an ultramicrotome (Ultracut E, Reichert-Jung, now Leica microsystems) using a diamond knife (Diatome, Biel/Bienne, Switzerland) and placed on a grid.

Freeze-substitution and low temperature Lowicryl embedding

Samples were freeze substituted from -90 to -50°C in an AFS2 (Leica Microsystems) using anhydrous acetone (Seccosolv, Merck) containing 0.2% uranyl acetate (Merck). At -50°C, samples were washed in pure anhydrous acetone and gradually infiltrated with increasing concentrations of Lowicryl HM20 (EMS) in anhydrous acetone and subsequently embedded in pure Lowicryl. Samples were polymerized by UV irradiation at -50°C for 5 days. 50 nm sections were cut on an ultramicrotome (Ultracut E, Reichert-Jung, now Leica microsystems) using a diamond knife (Diatome, Biel/Bienne, Switzerland) and placed on a grid.

VIS2FIXH

Tubes were transferred from liquid nitrogen to a cryo-ultramicrotome (UC6/FC6, Leica micro-systems) set to -150°C, and subsequently trimmed to a pyramidal block face. 80 nm frozen-hydrated sections were cut and directly attached to the grid by

electrostatic force using the Crion system (Leica microsystems). Grids were processed according to the VIS2FIXH method [24] using 0.2% uranyl acetate and 0.2% glutaraldehyde in 0.1MPhem (pH6.9) as fixative.

Immuno-labeling

Sections were blocked using either 1% lipid free BSA (#A7906, Sigma-Aldrich, St. Louis, MO), 0.5% BSA-c (Aurion, Wageningen, NL) diluted in 0.1 M Phem. Grids containing Tokuyasu cryo-sections were blocked for 5 min, grids with VIS2FIX_H sections were blocked for 20 min. Sections were subsequently labeled for TIP47 using Rabbit anti-full length TIP47 (a kind gift of Dr. Stephan Höning, Köln university) followed by 10 nm protein-A gold (CMC UMCUtrecht). Antibodies were diluted in block buffer. Sections were contrasted with uranyl oxalate (pH 7) and stabilized in 1.8% methylcellulose / 0.4% uranyl acetate.

Imaging

TEM micrographs were recorded on a Tecnai 12 120 kV transmission electron microscope (FEI Company) at 80 kV equipped with a sidemounted Megaview II CCD camera (SIS, Münster, Germany). When needed, the TEM images were scaled for optimal contrast by employing linear adjustments of the levels for the entire image.

For electron tomography, tilt series were automatically recorded at 200 kV using a Tecnai-20 equipped with a bottom-mounted slow-scan CCD camera (Tem-Cam F214;TVIPS GmbH, Gauting, Germany) and a motorized goniometer. Specimens were tilted about two orthogonal axes at 1° intervals from -65° to +65°, resulting in two datasets of 131 high-resolution images (1×1 K). Images were aligned, tomograms computed and the two single-axes tomograms merged into one using the program package IMOD [44].

Acknowledgements

We would like to thank Jan Andries Post for critically reading the manuscript and Willie Geerts for the introduction into the use of the IMOD software package.

References

1. Tauchi-Sato K, Ozeki S, Houjou T, Taguchi R, Fujimoto T. The surface of lipid droplets is a phospholipid monolayer with a unique fatty acid composition. *J Biol Chem* 2002;277:44507–44512.
2. Brasaemle DL. Thematic review series: adipocyte biology. The perilipin family of structural lipid droplet proteins: stabilization of lipid droplets and control of lipolysis. *J Lipid Res* 2007;48:2547–2559.
3. Kimmel AR, Brasaemle DL, McAndrews-Hill M, Sztalryd C, Londos C. Adoption of PERILIPIN as a unifying nomenclature for the mammalian PAT-family of intracellular lipid storage droplet proteins. *J Lipid Res* 2010;51:468–471.
4. Wolins NE, Brasaemle DL, Bickel PE. A proposed model of fat packaging by exchangeable lipid droplet proteins. *FEBS Lett* 2006;580:5484–5491.
5. Wang H, Hu L, Dalen K, Dorward H, Marcinkiewicz A, Russell D, Gong D, Londos C, Yamaguchi T, Holm C, Rizzo MA, Brasaemle D, Sztalryd C. Activation of Hormone-sensitive Lipase Requires Two Steps, Protein Phosphorylation and Binding to the PAT-1 Domain of Lipid Droplet Coat Proteins. *J Biol Chem* 2009;284:32116–32125.
6. Fujimoto T, Ohsaki Y. Proteasomal and autophagic pathways converge on lipid droplets. *Autophagy* 2006;2:299–301.
7. Ohsaki O, Jinglei C, Fujita A, Fujimoto T. Lipid droplets are a site of ubiquitin-dependent degradation of apolipoprotein B. *Cell Struct Funct* 2005;30:74–74.
8. Welte MA. Proteins under new management: lipid droplets deliver. *Trends Cell Biol* 2007;17:363–369.
9. Zehmer JK, Huang Y, Peng G, Pu J, Anderson RGW, Liu P. A role for lipid droplets in inter-membrane lipid traffic. *Proteomics* 2009;9:914–921.
10. Rinia HA, Burger KNJ, Bonn M, Müller M. Quantitative label-free imaging of lipid composition and packing of individual cellular lipid droplets using multiplex CARS microscopy. *Biophys J* 2008;95:4908–4914.
11. Robenek H, Hofnagel O, Buers I, Robenek M, Troyer D, Severs N. Adipophilin-enriched domains in the ER membrane are sites of lipid droplet biogenesis. *J Cell Sci* 2006;119:4215–4224.
12. Cheng J, Fujita A, Ohsaki Y, Suzuki M, Shinohara Y, Fujimoto T. Quantitative electron microscopy shows uniform incorporation of triglycerides into existing lipid droplets. *Histochem Cell Biol* 2009;132:281–291.
13. Cushman SW. Structure-function relationships in the adipose cell. I. Ultrastructure of the isolated adipose cell. *J Cell Biol* 1970;46:326–341.
14. Novikoff AB, Novikoff PM, Rosen OM, Rubin CS. Organelle relationships in cultured 3T3-L1 preadipocytes. *J Cell Biol* 1980;87:180–196.
15. McGookey DJ, Anderson RG. Morphological characterization of the cholesteryl ester cycle in cultured mouse macrophage foam cells. *J Cell Biol* 1983;97:1156–1168.
16. Van Golde LMG, Fleischer B, Fleischer S. Some studies on the metabolism of phospholipids in Golgi complex from bovine and rat liver in comparison to other subcellular fractions. *BBA-Biomembranes* 1971;249:318–330.
17. Stone SJ, Levin MC, Zhou P, Han J, Walther TC, Farese RV Jr. The endoplasmic reticulum enzyme DGAT2 is found in mitochondria-associated membranes and has a mitochondrial targeting signal that promotes its association with mitochondria. *J Biol Chem* 2009;284:5352–5361.
18. Murphy DJ, Vance J. Mechanisms of lipid-body formation. *Trends Biochem Sci* 1999;24:109–115.
19. Murphy DJ. The biogenesis and functions of lipid bodies in animals, plants and microorganisms. *Prog Lipid Res* 2001;40:325–438.
20. Wanner G, Theimer RR. Membranous appendices of spherosomes (oleosomes). *Planta* 1978;140:163–169.
21. Skinner JR, Shew TM, Schwartz DM, Tzekov A, Lepus CM, Abumrad NA, Wolins NE. Diacylglycerol enrichment of endoplasmic reticulum or lipid droplets recruits perilipin 3/TIP47 during lipid storage and mobilization. *J Biol Chem* 2009;284:30941–30948.
22. Bulankina AV, Deggerich A, Wenzel D, Mutenda

- K, Wittmann JG, Rudolph MG, Burger KNJ, Höning S. TIP47 functions in the biogenesis of lipid droplets. *J Cell Biol* 2009;185:641–655.
23. Gubern A, Barceló-Torns M, Barneda D, López JM, Masgrau R, Picatoste F, Chalfant CE, Balsinde J, Balboa MA, Claro E. JNK and ceramide kinase govern the biogenesis of lipid droplets through activation of group IVA phospholipase A2. *J Biol Chem* 2009;284:32359–32369.
24. Guijas C, Perez-Chacon G, Astudillo AM, Rubio JM, Gil-de-Gomez L, Balboa MA, Balsinde J. Simultaneous Activation of p38 and JNK by Arachidonic Acid Stimulates the Cytosolic Phospholipase A2-dependent Synthesis of Lipid Droplets in Human Monocytes. *J Lipid Res* 2012
25. Cai B, Caplan S, Naslavsky N. cPLA2 α and EHD1 interact and regulate the vesiculation of cholesterol-rich, GPI-anchored, protein-containing endosomes. *Mol Biol Cell* 2012;23:1874–1888.
26. Zanghellini J, Wodlei F, Von Grünberg HH. Phospholipid demixing and the birth of a lipid droplet. *J Theor Biol* 2010;264:952–961.
27. Penczek P, Marko M, Buttle K, Frank J. Double-tilt electron tomography. *Ultramicroscopy* 1995;60:393–410.
28. Frank J. Approaches to large-scale structures. *Curr Opin Struc Biol* 1995;5:194–201.
29. Fukumoto S, Fujimoto T. Deformation of lipid droplets in fixed samples. *Histochem Cell Biol* 2002;118:423–428.
30. Greenspan P, Mayer EP, Fowler SD. Nile red: a selective fluorescent stain for intracellular lipid droplets. *J Cell Biol* 1985;100:965–973.
31. Greenspan P, Fowler SD. Spectrofluorometric studies of the lipid probe, nile red. *J Lipid Res* 1985;26:781–789.
32. Hirsch JG, Fedorko ME. Ultrastructure of human leukocytes after simultaneous fixation with glutaraldehyde and osmium tetroxide and “postfixation” in uranyl acetate. *J Cell Biol* 1968;38:615–627.
33. Franke WW, Krien S, Brown RM. Simultaneous glutaraldehyde-osmium tetroxide fixation with postosmication. An improved fixation procedure for electron microscopy of plant and animal cells. *Histochemie* 1969;19:162–164.
34. Jiménez N, Vocking K, Van Donselaar E, Humbel B, Post J, Verkleij A. Tannic acid-mediated osmium impregnation after freeze-substitution: A strategy to enhance membrane contrast for electron tomography. *J Struct Biol* 2009;166:103–106.
35. Angermüller S, Fahimi HD. Imidazole-buffered osmium tetroxide: an excellent stain for visualization of lipids in transmission electron microscopy. *Histochem J* 1982;14:823–835.
36. Tokuyasu KT. A technique for ultracyotomy of cell suspensions and tissues. *J Cell Biol* 1973;57:551–565.
37. Karreman MA, Van Donselaar EG, Gerritsen HC, Verrips CT, Verkleij AJ. VIS2FIX: a high-speed fixation method for immuno-electron microscopy. *Traffic* 2011;12:806–814.
38. Binns D, Januszewski T, Chen Y, Hill J, Markin VS, Zhao Y, Gilpin C, Chapman KD, Anderson RGW, Goodman JM. An intimate collaboration between peroxisomes and lipid bodies. *J Cell Biol* 2006;173:719–731.
39. De Duve C, Wattiaux R. Functions of Lysosomes. *Annu Rev Physiol* 1966;28:435–492.
40. Mijaljica D, Prescott M, Devenish RJ. Microautophagy in mammalian cells: revisiting a 40-year-old conundrum. *Autophagy* 2011;7:673–682.
41. Singh R, Kaushik S, Wang Y, Xiang Y, Novak I, Komatsu M, Tanaka K, Cuervo AM, Czaja MJ. Autophagy regulates lipid metabolism. *Nature* 2009;458:1131–1135.
42. Van Greevenbroek MM, Voorhout WF, Erkelens DW, Van Meer G, De Bruin TW. Palmitic acid and linoleic acid metabolism in Caco-2 cells: different triglyceride synthesis and lipoprotein secretion. *J Lipid Res* 1995;36:13–24.
43. Jiménez N, Van Donselaar EG, De Winter DAM, Vocking K, Verkleij AJ, Post JA. Gridded Aclar: preparation methods and use for correlative light and electron microscopy of cell monolayers, by TEM and FIB–SEM. *J Microsc* 2010;237:208–220.
44. Kremer JR, Mastronarde DN, McIntosh JR. Computer Visualization of Three-Dimensional Image Data Using IMOD. *J Struct Biol* 1996;116:71–76.

Chapter 3

Immuno-gold labeling efficiency of Apolipoprotein B depends on its lipidation state

R.J. Mesman^{1,2,3,*}, E.G. van Donselaar², J.A.Post^{2,3}

¹Membrane Enzymology, Department of Chemistry, Utrecht University, Padualaan 8, 3584 CH Utrecht, the Netherlands

²Biomolecular Imaging, Department of Biology, Utrecht University, Padualaan 8, 3584 CH Utrecht, the Netherlands

³Institute of Biomembranes, Utrecht University, Padualaan 8, 3584 CH Utrecht, the Netherlands

*Corresponding author

Abstract

High levels of very low density lipoprotein (VLDL) in the blood circulation are considered to be a risk factor for cardiovascular disease. Insights in the assembly of VLDL could aid in the development of new intervention strategies to lower the VLDL level. These insights could be provided by immuno-transmission electron microscopy. However, the current 'on-section'-labeling strategies often suffer from a loss of antigenicity of ApoB, the main apo-lipoprotein of VLDL. By using Tokuyasu cryo-sections of HepG2 Hepatoma cells, we show that this loss of antigenicity is most likely due to delipidation of ApoB during the labeling procedure. On sections blocked with lipid free BSA, the amount of specific label was marginally higher than the background. The use of non delipidating blocking agents; CFG, lipidated BSA or BSA-c greatly improved the labeling efficiency. For improved ultrastructural preservation, cryo-immobilization is preferred over chemical fixation. Therefore we compared two other sample preparation procedures using cryo-immobilized samples for immuno-transmission electron microscopy. Both methods provided samples with a well preserved ultrastructure. After immuno-labeling, sections of high-pressure frozen, freeze-substituted and Lowicryl HM20 embedded HepG2 cells hardly showed any specific label for ApoB. Labeling on frozen hydrated sections processed according to the hydrated VIS2FIX method showed efficient labeling.

Introduction

In chapter 2 we discussed the storage of lipids within the cell in cytosolic lipid droplets. In the blood circulation lipids are transported either as fatty acids bound to albumin or in the form of lipid globules called lipoproteins. Like lipid droplets, these lipoproteins consist of a combination of neutral lipids surrounded by a polar lipid monolayer, which is stabilized by apo-proteins. The different classes of lipoproteins each have specific functions and can be distinguished by differences in apo-proteins, lipid composition and their relative density. The following lipoproteins can be distinguished, in increasing density and decreasing triacylglycerol content: chylomicrons, very low density lipoprotein (VLDL), low density lipoprotein (LDL) and high density lipoprotein (HDL) (for a review see Olson (1997) [1]. VLDL is synthesized postprandially by the liver and transports triacylglycerol from the liver to the peripheral tissues. VLDL can be identified by its main apo-protein ApoB100. Being a precursor for the low density lipoprotein (LDL), a high level of VLDL is considered to be a risk factor for atherosclerosis and cardiovascular disease [1–3].

VLDL formation is assumed to be a two-step process [4,5]. First, ApoB is co-translationally lipidated in the ER by the microsomal triglyceride transfer protein (MTP) [6,7] (figure 1A). This lipidation step is essential for correct folding of ApoB and inhibition of lipidation leads to ubiquitination and degradation of ApoB [8,9]. The neutral lipids (triacylglycerol and sterol-esters) used in this lipidation step are either synthesised de-novo in the ER by DGAT1 [10] or, alternatively, might be derived from cytosolic lipid droplets (LDs) (figure 1B), which function as storage sites for neutral lipids. Blocking ER to Golgi transport with Brefeldin A induces aggregation of ApoB in ER membranes around lipid droplets [11,12] indicating a tight connection between LDs and ApoB

lipidation.

Lipidated ApoB assembles to form VLDL2 particles which travel through the Golgi. The formation of triglyceride-rich VLDL1 particles, which are excreted, requires a second lipidation step (figure 1C). However, where this lipidation step takes place and whether the required triglycerides are synthesised de-novo or transferred from LDs to the VLDL2 particle is still under debate.

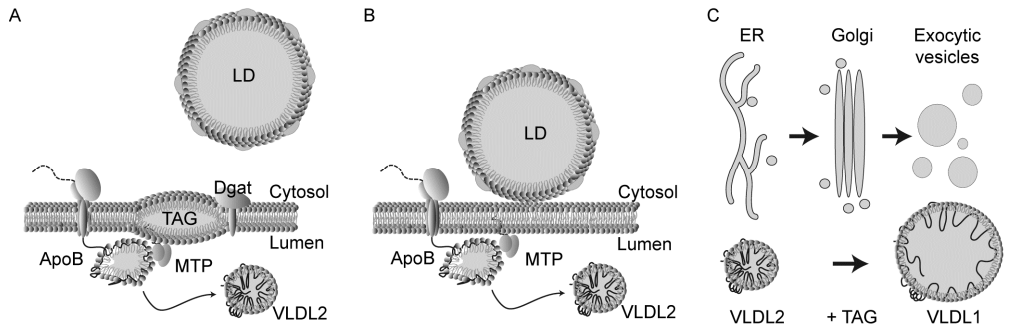


Figure 1. Co-translational lipidation of ApoB and VLDL Assembly

ApoB is Co-translationally lipidated by the action of the Microsomal Transfer Protein (MTP). First polar lipids are added, followed by the addition of a hydrophobic core of neutral lipids. (A) These neutral lipids are either directly synthesized by DGAT1 or (B) could be transferred from a cytosolic lipid droplet to the partially lipidated ApoB, thereby forming a VLDL2 particle. (C) The formation of triglyceride rich VLDL1 from VLDL2 requires an additional lipidation step, however it remains unclear where or how this lipidation step takes place.

Since ApoB is the main protein component of VLDL, immuno-localization of ApoB using transmission electron microscopy can provide valuable insights on the molecular and ultrastructural details of VLDL synthesis. This knowledge could subsequently aid in the development of new intervention strategies in cardiovascular disease.

Immuno-localization for electron microscopy is usually performed using either 'pre-embedding'- or 'on-section'-labeling methods. In 'pre-embedding'-labeling the antibody binding takes place between fixation and dehydration of the sample. Therefore, only changes in the epitope due to the fixation process can interfere with or inhibit antibody binding. However, this technique relies on membrane permeabilisation, which has detrimental effects on the preservation of ultrastructural details. In 'on-section'-labeling the entire sample is first processed, embedded and sectioned before the immuno-labeling takes place, ensuring optimal ultrastructural preservation but with a higher risk of losing antigenicity during one of the processing steps. The method of labeling on thawed cryo-sections (Tokuyasu cryo-sections)[13–15], allows for labeling 'on-section' before the sample is embedded and without any dehydration steps reducing the chance of losing antigenicity. However, despite of this, attempts to use thawed cryo-sections for immuno-localization of ApoB were hampered by the loss of antigenicity of ApoB or displacement of entire VLDL particles on the section surface during sectioning [16]. Immuno-labeling on sections of chemically fixed, snap frozen, freeze-substituted and Lowicryl HM20 embedded specimens, has been used as an alternative [16]. Although the authors report efficient labeling in ER, and Golgi membranes using this technique, their results also show abundant gold label for ApoB within the hydrophobic core of lipid

droplets.

Because of the need for proper labeling of ApoB, we wondered what could be the cause of the reported loss of antigenicity of ApoB in Tokuyasu cryo-sections. In most cases the loss of antigenicity of proteins is caused by strong fixation, steric hindrance or protein denaturation, all of which are generally avoided using the Tokuyasu technique. Since lipidation of ApoB is essential for correct folding of the protein, as discussed above, we hypothesized that potential extraction of lipid from ApoB during sample preparation might destabilize the structure of the protein and thereby altering its 3D conformation. This in turn would result in loss of the epitopes recognized by antibodies and thereby causing a loss in antigenicity of ApoB. We identified two potentially delipidating steps in the protocol for immuno-labeling on Tokuyasu cryo-sections. The first one is when the grids containing sections are placed on buffer at 37°C to melt away the gelatin, used to prepare the specimen block, and the methylcellulose, used in the pickup process. This process is potentially delipidating since 37°C is well above the phase transition temperature of most lipids in mammalian cells. Due to the open structure of the cryo-sections, lipids could be washed out during the melting process. This has been shown to be the case for cholesterol when labeling on Tokuyasu cryo-sections [17] and we suspect this could also be the case for other lipids.

The second potentially lipid removing step is during the blocking step, which is used to reduce non-specific antibody binding [18]. This is often carried out using a solution of lipid-free bovine serum albumin (BSA). Albumin is also known to function as a lipid scavenger and one molecule of albumin can bind up to 11 lipid molecules [19]. We suspected that by using lipid free BSA for the blocking step, ApoB is effectively delipidated by the lipid scavenging action of BSA, thereby changing the conformation of the protein causing loss of antigenicity.

To test these hypotheses we performed immuno-labeling for ApoB on Tokuyasu cryo-sections of HepG2 cells. To test the effect of melting at 37°C, Tokuyasu cryo-sections were picked up in a drop of methylcellulose/sucrose or directly adhered to a grid using electrostatic charge and placed on frozen buffer (0.1M PBS), thawed and labeled for ApoB. The effect of blocking on labeling efficiency was tested by using the following blocking agents; 1% lipid-free BSA, 1% lipidated BSA (BSA-L), 1% cold-fish-skin gelatin (CFG), and 1% poly-acetylated BSA (BSA-c).

As mentioned earlier, chemical fixation followed by snap-freezing and freeze-substitution has been used as an alternative for Tokuyasu cryo-sections. A more ideal approach would be cryo-immobilization by high-pressure freezing followed by freeze-substitution. With high-pressure freezing, samples can be almost instantaneously immobilized, providing improved ultrastructural preservation compared to chemical fixation [20,21]. After freeze-substitution and resin embedding, sections can be immuno-labeled. This is often carried out using Lowicryl resins [22], since antigens tend to be more exposed on the section surface using Lowicryl compared to epoxy resins [23]. In our personal experience though, only a few antibodies work on sections from freeze substituted and Lowicryl embedded samples. Recently a new method called VIS2FIX [24] has been introduced which provides samples that are well suited for immuno-labeling. With VIS2FIX, samples are cryo-immobilized by high-pressure freezing,

subsequently sectioned and the sections are fixed either by freeze-substitution and rehydration (VIS2FIX_{FS}) or by thawing the sections on frozen fixative (VIS2FIX_H or hydrated VIS2FIX). This method has been successfully used to label for various proteins and even lipids and could provide a good alternative for freeze-substitution to Lowicryl. To test both methods, we processed high-pressure frozen HepG2 cells either by freeze-substitution to Lowicryl HM20 or according to the hydrated VIS2FIX method [24] and subsequently performed 'on-section'-labeling for ApoB.

Results and Discussion

For the immuno-localization of ApoB we used the HepG2 hepatoma cell line. The rate of VLDL synthesis and ApoB protein levels varies between cells, depending on the cell cycle and/or the availability of triacylglycerol. Therefore we incubated HepG2 cells for 90 minutes with oleic-acid complexed to albumin to stimulate VLDL assembly [25]. Secreted VLDL is also taken up again by the cells, so for studying the labeling efficiency we analysed both the exocytic pathway (ER, Golgi) and the endo/lysosomal system. Results were obtained from three independent immuno-labeling experiments on sections from the same sample block.

As expected, after stimulation with oleic-acid/albumin a large percentage of the cells showed a clear expansion of the Golgi system, indicative of an active excretion pathway. For immuno-labeling of ApoB we first applied our standard protocol for labeling on Tokuyasu cryo-sections, using 1% lipid free BSA as blocking buffer [15]. After immuno-labeling for ApoB hardly any gold label could be detected using 1% lipid free BSA as block buffer (figure 2A) despite the morphological indication of an active excretion pathway. This is consistent with the results reported in the literature [16].

Next we changed the blocking solution from 1% lipid free BSA to 0.5% cold water fish skin gelatin (CFG). Gelatin molecules do not contain hydrophobic pockets; therefore CFG is incapable of extracting lipids. After immuno-labeling for ApoB (using the same cells and the same antibody) a clear increase in the amount of labeled organelles and the quantity of specific label could be detected for the ER membranes, the Golgi system (figure 2B) and in multivesicular bodies either belonging to the secretory or the endosomal pathway (figure 2C).

To prove that the effect of changing the block buffer on the amount of specific label is due to a decrease in lipid extraction and not due to other differing properties between BSA and gelatin, we performed the labeling procedure using either 1% (partially) lipidated BSA (BSA-l) or 1% BSA-c as block buffer. In BSA-c the poly-acetylation prevents protein folding, thereby abolishing the capacity of BSA to bind lipids.

Both the use of 1% BSA-l and 1% BSA-c as blocking agent clearly increased the amount of labeled organelles and the quantity of specific label for ApoB in the ER, Golgi and endo/lysosomal system, compared to the BSA blocking protocol (figure 2D). These results were also reproducible when using a primary antibody against ApoB from a different host species (data not shown). When comparing the density of specific label per organelle between the different block reagents, blocking with either 0.5% CFG or 1% BSA-c was found to give the best ratio of specific label to background (figure 2D).

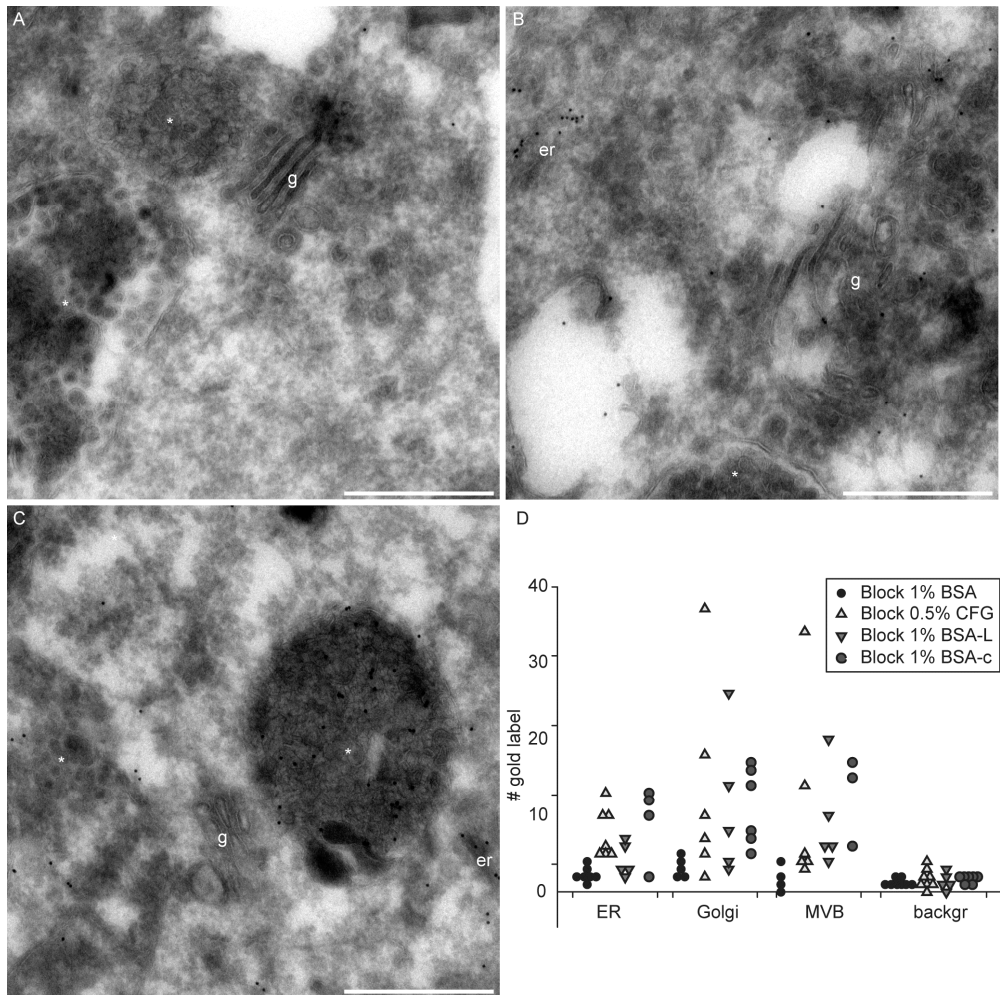


Figure 2. Loss of antigenicity of ApoB is due to lipid scavenging by Albumin

Ultra-thin cryo-sections of HepG2 cells fixed with 4% PFA were immuno-labeled for ApoB using either 1% lipid free BSA, 0.5% CFG, 1% lipidated BSA or 1% BSA-c as blocking agent. (A) After blocking with 1% lipid free BSA hardly any gold label could be detected, in Golgi membranes and multivesicular bodies. (B,C) Using 0.5% CFG as blocking agent resulted in a clear increase in labeling efficiency of ApoB. Almost all cells were labeled and label could be detected throughout the entire exocytic pathway. (D) Scatterplot of the amount of gold label for each blocking agent in the different cellular compartments, counted from the results of three independent experiments using sections from the same sample block. Gold label on the nucleus, mitochondria and cytosol was counted as background. The amount of specific label on sections blocked with lipid free BSA was marginally higher than the background within the same micrograph. The use of CFG, lipidated BSA or BSA-c greatly improved the labeling efficiency, in some cases up to 3 fold. *: multivesicular body, er: endoplasmic reticulum, g: Golgi, m: mitochondria. All scale bars represent 500 nm.

As mentioned earlier, the melting step at 37°C can in theory contribute to the loss of lipid from the sections, leading to reduced labeling efficiency of ApoB. We avoided this melting step by directly adhering the cryo-sections to a grid using electro-static charge instead of the methylcellulose/sucrose pickup. Sections were labeled for ApoB using 0.5% CFG as block buffer. Omission of the melting step did not further increase labeling efficiency. However the washout of cellular contents, a known feature of Tokuyasu cryo-sections from cells fixed with paraformaldehyde (PFA) only, was greatly reduced (Figure 3A). Overall the ultrastructure more resembled that of samples fixed with a combination of glutaraldehyde and PFA.

For labeling on sections from Lowicryl embedded samples and VIS2FIXh processed samples we used the best blocking buffers as identified on the Tokuyasu sections; 0.5% CFG or 1% BSA-c. Sections were blocked for 20 minutes to prevent background labeling on the Lowicryl and the formvar film. Lowicryl sections were not post-stained after labeling, allowing better visualization of the gold label on the micrographs. Since the cells were trypsinized before freezing, which could interfere with cellular trafficking, we only analysed those cells that still had intact cell-cell contact areas (about 75% of all cells present in the section). Lowicryl embedded samples showed a well preserved ultrastructure and the nuclei showed no signs of ice-crystal damage, indicative of a well frozen sample. The labeling efficiency however was only marginally better compared to the Tokuyasu sections blocked with lipid free BSA (figure 4B). Also background label could still be detected on mitochondria and the resin itself.

Sections processed according to the hydrated VIS2FIX method (figure 4C, D) had a level of ultrastructural preservation which was at the least comparable to that of the freeze substituted and Lowicryl embedded samples. Some cellular compartments, such as the trans-Golgi network, were much more apparent in VIS2FIX_H processed cells than in Lowicryl sections. In terms of labeling efficiency the VIS2FIX_H sections were comparable to and sometimes even better than Tokuyasu sections blocked with either CFG or BSA-c. This combination of excellent ultrastructural preservation and labeling efficiency may be used, in future research, to provide valuable insights in the mechanisms underlying VLDL synthesis and maturation.

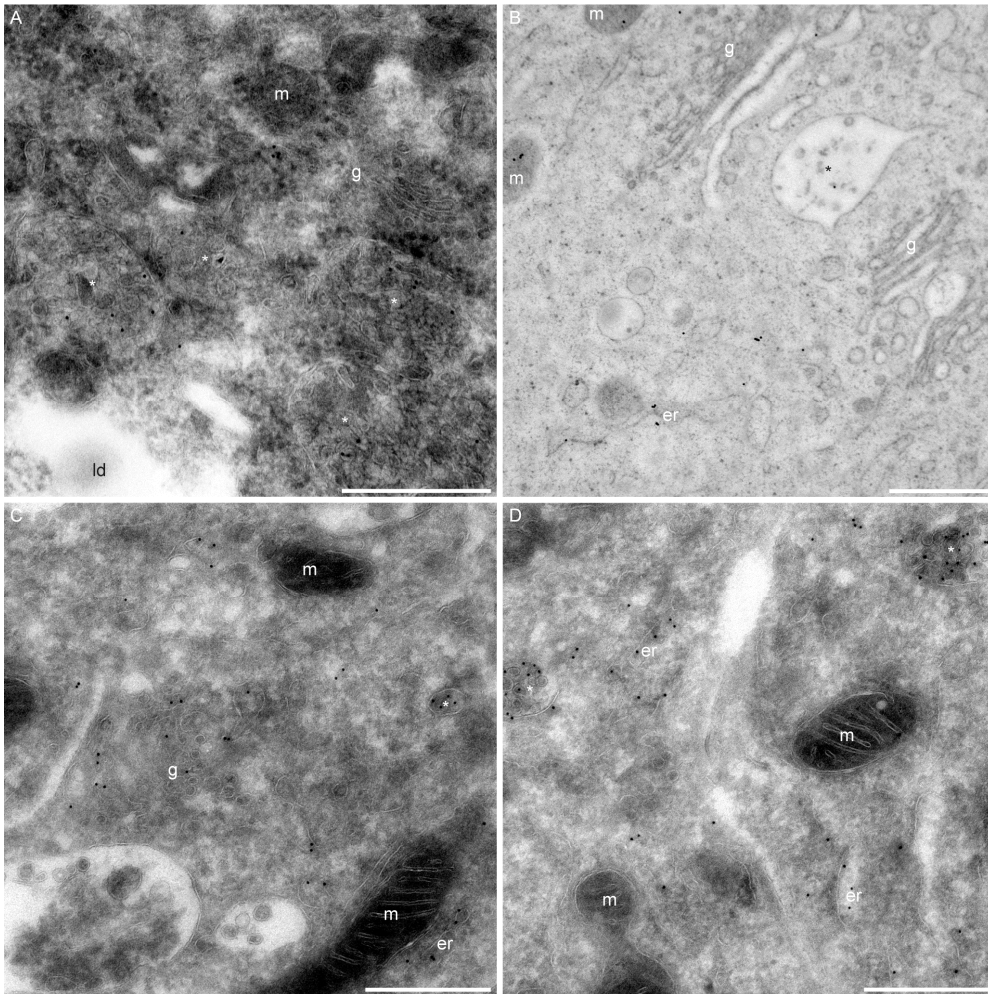


Figure 3. Improving ultrastructural preservation

(A) Ultra-thin cryo-sections of HepG2 cells fixed with 4% PFA were transferred to a grid using the Crion system, subsequently placed on frozen buffer and thawed to room temperature. Sections were labeled for ApoB using 0.5% CFG as blocking agent. No difference in labeling efficiency could be observed between the sections processed in this way and those picked up using methylcellulose/sucrose. However the loss of cellular content is much reduced. Golgi areas do not show empty spaces often seen in Tokuyasu cryo-sections. (B) High-pressure frozen and freeze-substituted HepG2 cells were embedded in Lowicryl HM20. 50 nm sections were cut and subsequently labeled for ApoB using 1% BSA-c as blocking agent. Sections were imaged without post-staining. The labeling efficiency is lower than on Tokuyasu sections using a non-delipidating blocking agent. The expanded Golgi is devoid of label and some background label can be seen on the mitochondria. (C,D) Frozen hydrated sections from high-pressure frozen HepG2 cells processed according to the hydrated VIS2FIX method. Sections were labeled for ApoB using 1% BSA-c as blocking agent. The labeling efficiency is comparable to Tokuyasu cryo-sections blocked with BSA-c or CFG, but the ultrastructure is much better preserved. *: multivesicular body, er: endoplasmic reticulum, G: Golgi, ld: lipid droplet, m: mitochondria. All scale bars represent 500 nm.

Conclusion

Here we have shown that loss of antigenicity of ApoB in Tokuyasu cryo-sections is caused by the lipid scavenging action of Albumin during the blocking step. This could be counteracted by using cold water fish skin gelatin or acetylated BSA as blocking agent. Avoiding thawing of the sections at 37°C by directly adhering the sections to the grid has no effect on labeling efficiency but greatly improves the retention of cellular components, otherwise washed out. This allows the use of mildly fixed samples, which often have better labeling efficiency, without the reduction in morphological details that is often associated with mild fixation. Freeze-substitution and embedding in Lowicryl HM20, suggested in the literature to have better labeling properties, was shown not to label efficiently. The recently developed hydrated VIS2FIX method [24] combined with a non-delipidating block buffer provided a good alternative, combining both efficient labeling with good ultrastructural preservation. The use of these improved methods may provide valuable insights in the ultrastructural details of VLDL synthesis, thereby increasing our understanding of this process and possibly allow the development of new intervention strategies to lower the risk of cardiovascular disease associated with high VLDL levels. Additionally the reduction or prevention of delipidation during labeling procedures is of interest for any protein whose 3D conformation depends on binding of lipids.

Materials and Methods

Cell culture

HepG2 cells (ATCC, passage 3)(kind gift from CMC, UMCUtrecht, NL) were cultured in low glucose DMEM (#E15-891, PAA, Pasching, Austria) with 10% fetal bovine serum (#A15-151, PPA). All experiments were carried out between passage 5 to 7.

Tokuyasu cryo-sections

HepG2 cells at 80% confluence were incubated with 100 μ M oleic acid complexed to albumin (6:1 molar ratio) for 90 min to stimulate VLDL production. Cells were fixed for 24 hours with 4% PFA in phosphate buffer (pH7.4) containing 1% CaCl_2 , scraped and pelleted in 12% gelatin. After solidifying at 4°C the pellet was cut in small blocks, infiltrated overnight with 2.3M sucrose, mounted on Aluminium pins and snap-frozen in liquid nitrogen. 100 nm sections were cut on a cryo-ultramicrotome (UC6/FC6, Leica microsystems, Vienna, Austria) at -120°C. The sections were picked up with a drop of 1.15 M methylcellulose / 1% sucrose and mounted on a grid. Alternatively sections were directly attached to the grid by electrostatic force using the Crion system (Leica microsystems), placed on frozen buffer and warmed up to room temperature.

High-pressure freezing

HepG2 cells at 80% confluence were incubated with 100 μ M Oleic acid complexed to albumin (6:1 molar ratio) for 90 min to stimulate VLDL production. Cells were gently trypsinized and pelleted (154 rcf, 37°C). For samples intended for freeze-substitution, part of the cell pellet was re-suspended in medium containing type IX ultra-low gelling temperature agarose (#A5030, Sigma-Aldrich, St. Louis, MO) at a final concentration of 0.5%. The resulting cell suspension was high-pressure frozen in 100 μ m deep aluminium platelets (M.Wohlwend, Sennwald, Switzerland) in an EMHPF (Leica Microsystems) operating at 2100 bar. For samples intended for VIS2FIX, part of the cell pellet was re-suspended in medium containing dextran at a final concentration of 15%. The resulting cell suspension was high-pressure frozen in copper tubes. All samples were frozen within 8 min after re-suspension to prevent possible endocytosis of dextran.

Freeze-substitution

Samples were freeze substituted from -90 to -50°C in an AFS2 (Leica Microsystems) using anhydrous acetone (Seccosolv, Merck) containing 0.2% uranyl acetate (Merck). At -50°C, samples were gradually infiltrated with increasing concentrations of Lowicryl HM20 (#14340, EMS, Hatfield, PA) in anhydrous acetone subsequently embedded in pure HM20. Samples were polymerized by UV irradiation at -50°C for 5 days. 50 nm sections were cut on an ultramicrotome (Ultracut E, Reichert-Jung, now Leica microsystems) using a diamond knife (Diatome, Biel/Bienne, Switzerland) and placed on a grid.

VIS2FIX_H

Tubes were transferred from liquid nitrogen to a cryo-ultramicrotome (UC6/FC6, Leica micro-systems) set to -150°C, and subsequently trimmed to a pyramidal block face. 80 nm frozen-hydrated sections were cut and directly attached to the grid by

electrostatic force using the Crion system (Leica microsystems). Grids were processed according to the VIS2FIXH method [24] using 0.2% uranyl acetate and 0.2% glutaraldehyde in 0.1 M Phem (pH6.9) as fixative.

Immuno-labeling

Sections were blocked using either 1% lipid free BSA (#A7906, Sigma-Aldrich, St. Louis, MO), 1% lipidated BSA (#05482, Fluka, Buchs, Switzerland), 0.5% CFG (#G7765, Sigma-Aldrich) or 1% BSA-c (Aurion, Wageningen, NL) diluted in 0.1 M Phem. Grids containing Tokuyasu cryo-sections were blocked for 5 min, grids with VIS2FIXH and Lowicryl sections were blocked for 20 minutes. Sections were subsequently labeled for ApoB using either Goat anti-ApoB (#600.100.101, Rockland Immunochemicals, Gilbertsville, PA) followed by Rabbit anti-Goat IgG (Nordic Immunological Laboratories, Eindhoven, NL) or Sheep anti-ApoB (#PC086 The binding site, Birmingham, UK) followed by Rabbit anti-Sheep IgG (Nordic Immunological Laboratories, Eindhoven, NL). Both were visualized using 10 nm protein-A gold (CMC UMCUtrecht). Antibodies were diluted in block buffer. Sections were contrasted with uranyl oxalate (pH7) and stabilized in 1.8% methylcellulose / 0.4% uranyl acetate.

Imaging

TEM micrographs were recorded on a Tecnai 12 120 kV transmission electron microscope (FEI Company) at 80 kV with a bottom mount TEMCam-F214 (Tietz Video and Image processing systems) CCD camera. When needed, the TEM images were scaled for optimal contrast by employing linear adjustments of the levels for the entire image. The gold label density was assessed by counting the number of gold particles on labeled organelles in micrographs from three independent labeling experiments. Within the micrograph, labeled organelles of comparable size were selected (10 of each type per condition) and the number of gold particles counted using Fiji (ImageJ).

Acknowledgements

We would like to thank Laura van Niftrik for critically reading the manuscript. We thank Matthia Winter-Karreman for the useful discussions.

References

1. Olson RE. Discovery of the Lipoproteins, Their Role in Fat Transport and Their Significance as Risk Factors. *J Nutr* 1998;128:439S–443S.
2. Walldius G, Jungner I. The apoB/apoA-I ratio: a strong, new risk factor for cardiovascular disease and a target for lipid-lowering therapy--a review of the evidence. *J Intern Med* 2006;259:493–519.
3. Olofsson S-O, Wiklund O, Borén J. Apolipoproteins A-I and B: biosynthesis, role in the development of atherosclerosis and targets for intervention against cardiovascular disease. *Vasc Health Risk Manag* 2007;3:491–502.
4. Boström K, Borén J, Wettsten M, Sjöberg A, Bondjers G, Wiklund O, Carlsson P, Olofsson SO. Studies on the assembly of apo B-100-containing lipoproteins in HepG2 cells. *J Biol Chem* 1988;263:4434–4442.
5. Rustaeus S, Lindberg K, Stillemark P, Claesson C, Asp L, Larsson T, Borén J, Olofsson SO. Assembly of very low density lipoprotein: a two-step process of apolipoprotein B core lipidation. *J Nutr* 1999;129:463S–466S.
6. Gordon DA, Wetterau JR, Gregg RE. Microsomal triglyceride transfer protein: a protein complex required for the assembly of lipoprotein particles. *Trends Cell Biol* 1995;5:317–321.
7. Gordon DA, Jamil H, Gregg RE, Olofsson S-O, Borén J. Inhibition of the Microsomal Triglyceride Transfer Protein Blocks the First Step of Apolipoprotein B Lipoprotein Assembly but Not the Addition of Bulk Core Lipids in the Second Step. *J Biol Chem* 1996;271:33047 – 33053.
8. Gordon DA, Jamil H. Progress towards understanding the role of microsomal triglyceride transfer protein in apolipoprotein-B lipoprotein assembly. *Biochim Biophys Acta* 2000;1486:72–83.
9. Rutledge AC, Su Q, Adeli K. Apolipoprotein B100 biogenesis: a complex array of intracellular mechanisms regulating folding, stability, and lipoprotein assembly. *Biochem Cell Biol* 2010;88:251–267.
10. Yamazaki T, Sasaki E, Kakinuma C, Yano T, Miura S, Ezaki O. Increased Very Low Density Lipoprotein Secretion and Gonadal Fat Mass in Mice Overexpressing Liver DGAT1. *J Biol Chem* 2005;280:21506–21514.
11. Ohsaki O, Jinglei C, Fujita A, Fujimoto T. Lipid droplets are a site of ubiquitin-dependent degradation of apolipoprotein B. *Cell Struct Funct* 2005;30:74–74.
12. Ohsaki Y, Cheng J, Suzuki M, Fujita A, Fujimoto T. Lipid droplets are arrested in the ER membrane by tight binding of lipidated apolipoprotein B-100. *J Cell Sci* 2008;121:2415–2422.
13. Tokuyasu KT. A technique for ultracytometry of cell suspensions and tissues. *J Cell Biol* 1973;57:551–565.
14. Griffiths G, McDowall A, Back R, Dubochet J. On the preparation of cryosections for immunocytochemistry. *J Ultrastruct Res* 1984;89:65–78.
15. Slot JW, Geuze HJ. Cryosectioning and immunolabeling. *Nat Protoc* 2007;2:2480–2491.
16. Samson-Bouma M-E, Verthier N, Ginsel LA, Feldmann G, Fransen JA, Aggerbeck LP. Ultrastructural immunogold labeling of lipid-laden enterocytes from patients with genetic malabsorption syndromes. *Biol Cell* 1996;87:189–196.
17. Möbius W, Ohno-Iwashita Y, Donselaar EG van, Oorschot VMJ, Shimada Y, Fujimoto T, Heijnen HFG, Geuze HJ, Slot JW. Immunoelectron microscopic localization of cholesterol using biotinylated and non-cytolytic Perfringolysin O. *J Histochem Cytochem* 2002;50:43–55.
18. Roth J, Taatjes DJ, Warhol MJ. Prevention of non-specific interactions of gold-labeled reagents on tissue sections. *Histochemistry* 1989;92:47–56.
19. Bhattacharya AA, Grüne T, Curry S. Crystallographic analysis reveals common modes of binding of medium and long-chain fatty acids to human serum albumin. *J Mol Biol* 2000;303:721–732.
20. Moor H. Theory and practice of high pressure freezing. In: *Cryotechniques in Biological Electron Microscopy*. Springer; 1987. p.175–191.
21. Studer D, Michel M, Müller M. High pressure freezing comes of age. *Scanning Microsc Suppl* 1989;3:253–268; discussion 268–269.
22. Monaghan, Perusinghe, Müller. High-pressure freezing for immunocytochemistry. *J Microsc*

- 1998;192:248–258.
23. Kellenberger E, Dürrenberger M, Villiger W, Carlemalm E, Wurtz M. The efficiency of immunolabel on Lowicryl sections compared to theoretical predictions. *J Histochem Cytochem* 1987;35:959–969.
 24. Karreman MA, van Donselaar EG, Gerritsen HC, Verrips CT, Verkleij AJ. VIS2FIX: A High-Speed Fixation Method for Immuno-Electron Microscopy. *Traffic* 2011;12:806–814.
 25. Meex SJR, Andreo U, Sparks JD, Fisher EA. Huh-7 or HepG2 cells: which is the better model for studying human apolipoprotein-B100 assembly and secretion? *J Lipid Res* 2011;52:152–158.

Chapter 4

Tracing cellular lipid flows at the ultrastructural level using a clickable fatty acid

R.J. Mesman^{1,2,3,*}, E.G. van Donselaar², J.C.M. Holthuis^{1,2,4}

¹Membrane Enzymology, Department of Chemistry, Utrecht University, Padualaan 8, 3584 CH Utrecht, the Netherlands

²Biomolecular Imaging, Department of Biology, Utrecht University, Padualaan 8, 3584 CH Utrecht, the Netherlands

³Institute of Biomembranes, Utrecht University, Padualaan 8, 3584 CH Utrecht, the Netherlands

⁴Molecular Cell Biology, Fachbereich Biologie/Chemie, Universität Osnabrück, Barbarastraße 13, 49076 Osnabrück, Germany

*Corresponding author:

Abstract

Our current understanding of metabolic lipid flows in cells is primarily based on the analysis of lipid compositions of isolated subcellular organelles and imaging of fluorescent lipid analogues in cells. While these methods have their merits, they are ill suited to provide insight into lipid organization at the ultrastructural level. By combining click-chemistry with a recently developed sample preparation method for transmission electron microscopy, we here traced the localization of individual lipid molecules inside cells at the nanometer-scale. To this end, HepG2 cells were metabolically labeled with a clickable fatty acid and the subcellular distribution of this fatty acid, as it was incorporated into polar membrane lipids or stored as triacylglycerol in lipid droplets, was assessed using immuno-gold labeling. We show that pre-treatment of cells with various inhibitors of lipid metabolism causes substantial changes in localization patterns. Our results indicate that clickable fatty acids are valuable tools for analysing cellular lipid flows at the ultrastructural level.

Introduction

Cells contain hundreds of different lipid species that are implicated in a wide array of cellular processes, ranging from membrane organization, molecular sorting and energy metabolism to cell signalling [1]. Precise information on their subcellular distribution is crucial for a proper understanding of the function of individual lipid species. Fluorescent lipid analogs, such as lipids labeled with a fluorophore (see Maier 2002 [2] for a comprehensive review) or fluorescent polyene lipids [3], have been used to investigate the localization and trafficking of specific lipids. A disadvantage of fluorescent lipid analogs is that they sometimes behave differently from the molecules they are supposed to mimic [4–6]. Furthermore, the limited spatial resolution of fluorescence microscopy makes these probes unsuited for localization studies at the ultrastructural level.

Electron microscopy combined with conventional immuno-gold labeling would provide a better alternative. However, very few antibodies exist against individual lipid species whereas most of these antibodies are directed against glycolipids, such as Forssman glycolipid, and the gangliosides GM1 and GM3. The use of lipid-binding toxins such as cholera toxin (GM1), Shiga toxin (Gb3) or Theta toxin (cholesterol), on the other hand, can induce artificial clustering of their targets due to the presence of multiple lipid-binding sites.

Recently, Jao *et al.* [7] described an alternative method based on labeling of a bio-orthogonal chemical reporter, also known as Click-chemistry labeling [8]. Cells were metabolically labeled with propargylcholine as a clickable PC headgroup donor and subsequently covalently linked to a reporter molecule using azide alkyne Huisgen cycloaddition [9] with Cu(1) as catalyst. Using this technique Jao *et al.* were able to show the ultrastructural localization of phosphatidylcholine (PC) on Tokuyasu cryo-sections of aldehyde fixed cells. This provided a first demonstration of the potential of click chemistry for labeling of polar lipids. However, the method of labeling on thawed cryo-sections is not well suited for ultrastructural localization of lipids [10]. During thawing, membrane lipids undergo a redistribution to cover the hydrophobic area that becomes exposed following left after section through the membrane, resulting in lipid re-

distribution [10,11]. Also, since lipids are not efficiently fixed by aldehydes [12], lipids can re-localize in the plane of the membrane during the subsequent specimen preparation procedure. To acquire meaningful data on lipid localization, it is essential that both types of re-distribution do not take place [13]. This can be achieved if cells are cryo-immobilized and subsequently fixed from this frozen state. For optimal lipid preservation during sample preparation for transmission electron microscopy, we therefore decided to use cells immobilized by high pressure freezing. This was followed by either freeze-substitution and low temperature embedding in Lowycryl HM20 or processing according to the novel hydrated VIS2FIX method [14]. Both methods have a high level of lipid retention and in both procedures samples are treated with uranyl acetate, which stabilizes the distribution of phospholipids within the membrane [15–17]. Whereas for freeze-substituted samples the cells are embedded in resin before sectioning and labeling, in samples processed according to the hydrated VIS2FIX method labeling is carried out before embedding. This has been shown to allow for highly efficient immuno-labeling [14].

To allow a more comprehensive study of metabolic lipid flows in cells at nanometer scale, we labeled liver HepG2 cells with a clickable fatty acid (cFA) and monitored the localization of newly-synthesized lipids using click-chemistry and immune electron microscopy. As a model system we used the HepG2 hepatoma cell line. The liver plays a prominent role in lipid homeostasis. Fatty acid bound to albumin is rapidly taken up and metabolized by liver cells and used for the formation of polar lipids, or esterified to triacylglycerol. This is stored in lipid droplets or excreted in very low density lipoproteins (VLDL). A study by Pohl *et al.* [18] showed that after a 5 minute incubation with radio-labeled oleate bound to albumin $67.6 \pm 8.3\%$ of the incorporated $[3H]$ oleic acid was esterified to triglycerides (TAG) and other complex lipids. $15.7 \pm 6.8\%$ was recovered as acyl-CoA esters, while free oleic acid was virtually undetectable. According to Gibbons *et al.* [19] the capacity of HepG2 cells to synthesize TAG from extracellular oleate is about 30 fold higher than its capacity for phospholipid synthesis. We expect the cFA to behave in a similar fashion, being primarily incorporated in TAG, and, to a lesser extent, into polar lipids or used as energy substrate in the form of an acyl-CoA ester. Subsequently to modulate the lipid flow, we pre-incubated the cells with either the DGAT2 inhibitor Niacin to limit the synthesis of triacylglycerol or Brefeldin A to disrupt the secretory pathway and thereby VLDL formation.

Results and Discussion

Application of clickable fatty acid (cFA) to determine the subcellular distribution of newly synthesized lipids at the ultrastructural level

In this study, we used a bifunctional 15 carbon-long (C15) clickable fatty acid (cFA). This fatty acid also contains a photoactivatable diazirine ring, which can be used for UV-crosslinking [20], though this feature was not used in this study. To prevent accidental activation of the diazirine ring, the cFA was shielded from light at all times.

As proof of principle, HepG2 cells were metabolically loaded for 10 min with 100 μ M cFA complexed to BSA. Cells incubated with 100 μ M BSA-bound oleic acid (OA) served as negative control. After loading, the cells were gently trypsinized, high pressure frozen

and subsequently either freeze-substituted and embedded in lowicryl HM20 or processed via the hydrated VIS2FIX method [14]. We modified the labeling protocol from Jao *et al.*[7] using Phem buffer (pH6.9) without EGTA instead of Tris-HCl (pH 8). The click-reaction was performed on sections of lowicryl HM20 embedded HepG2 cells loaded with OA complexed to albumin, by incubating the sections for one hour on droplets containing biotin-azide, Cu(II) and ascorbic acid to reduce Cu(II) to Cu(I). Subsequently the biotin label was detected by immuno-gold labeling using rabbit anti-biotin and protein A gold. After labeling, background gold label could be observed on the resin and the cells. This background was dependent on the presence of Cu(I) (Figure 1A). In the presence of Cu(I) the biotin-azide appeared to react with one of the compounds in the HM20 resin, making this sample preparation method incompatible with click-chemistry. Instead, we decided to use these samples for analysis of possible ultrastructural changes caused by the various treatments.

On VIS2FIX sections, use of ascorbic acid for the reduction of Cu(II) considerably etched the sections. Replacing ascorbic acid by 100 μ M Tris[(1-benzyl-1H-1,2,3-triazol-4-yl)methyl]amine (TBTA), a stabilizing agent for Cu(I), was found to be adequate to obtain efficient labeling. Sections from HepG2 cells loaded with OA/albumin were essentially devoid of label (Figure 1B). Moreover, the low level of labeling observed in OA-loaded cells was entirely independent of TBTA or Cu(II), two essential cofactors in the click reaction that attaches biotin to the cFA. This shows that direct labeling of fatty acid molecules using click-chemistry is possible using samples processed according to the hydrated VIS2FIX method.

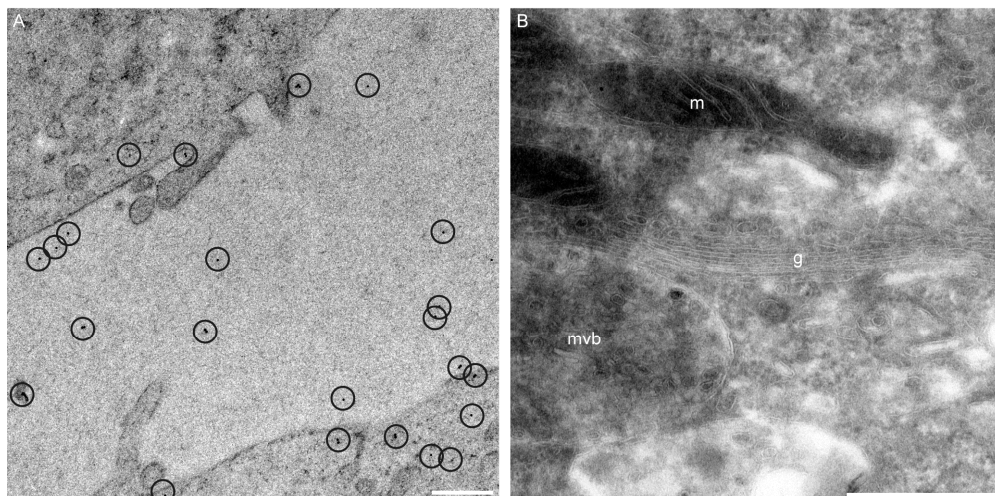


Figure 1 Validation of the optimal sample preparation method for click-labeling.

HepG2 cells, loaded with oleic acid/albumin for 10 min, were gently trypsinized and high-pressure frozen. Samples were either freeze-substituted and embedded in lowicryl HM20 at -50°C or processed according to the VIS2FIX_H method as described in Materials and Methods. Both Lowicryl and VIS2FIX sections were incubated for 1 h with biotin-azide in the presence of Cu(I), followed by immunodetection using Rabbit anti biotin and Protein-A gold. (A) Freeze-substituted samples embedded in Lowicryl HM20 showed background labeling on both the cells and the resin in the absence of cFA (circles). The background label depends on the presence of Cu(I) making this sample preparation method incompatible with click-labeling. (B) Hydrated VIS2FIX sections were devoid of label in the absence of cFA.

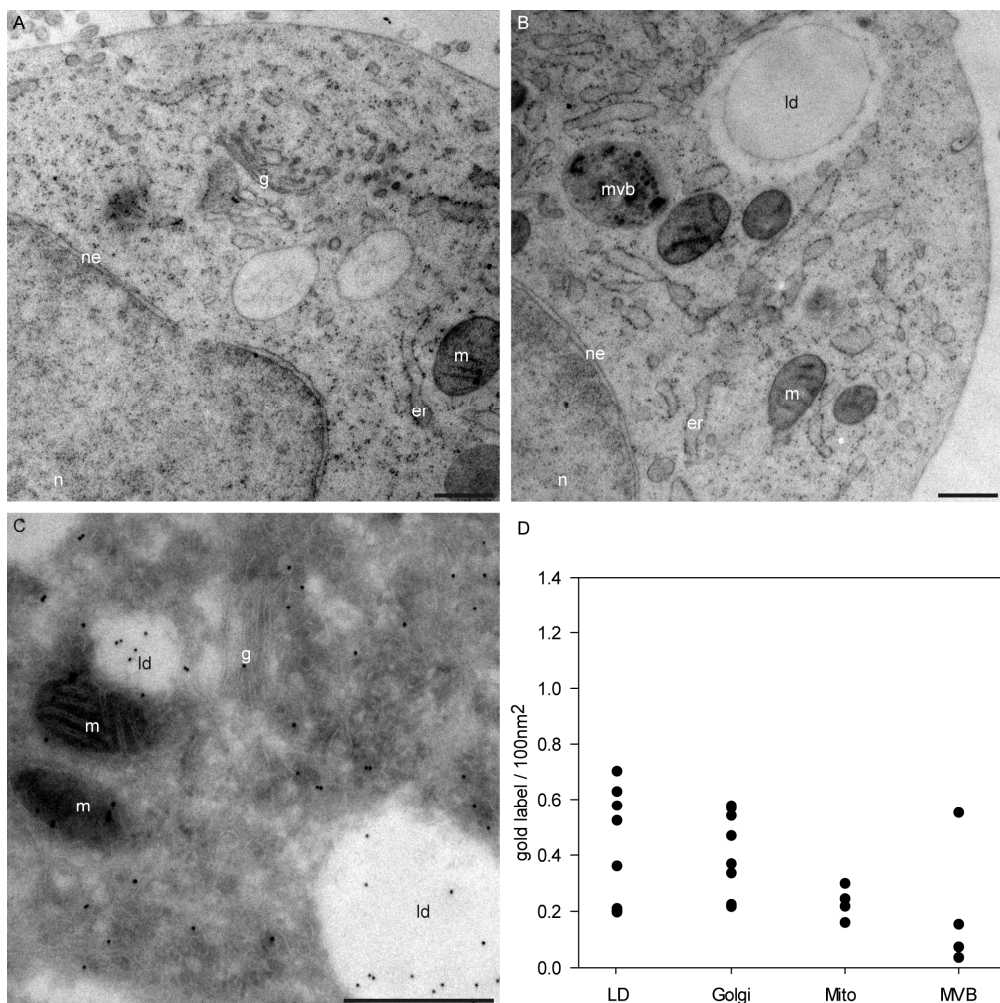


Figure 2 Cellular ultrastructure and localization of newly synthesized lipids using click-labeling.

HepG2 cells, loaded with cFA/albumin for 10 min, were gently trypsinized and high-pressure frozen. (A,B) Cells freeze-substituted and embedded in Lowicryl HM20 show a well preserved ultrastructure. The endoplasmic reticulum appeared to be slightly swollen, which is often associated with lipid loading. (C) Hydrated VIS2FIX sections of HepG2 cells loaded with cFA/albumin labeled for the presence of cFA using biotin-azide, Rabbit-anti biotin and protein-A gold. Cells loaded show gold label in ER, Golgi, LDs, MVBs and mitochondria. (D) Scatterplot of the amount of gold label for the different cellular compartments. All scale-bars represent 500 nm. er: endoplasmic reticulum, g: Golgi, ld: lipid droplet, m: mitochondria, mvb: multivesicular body, n: nucleus, ne: nuclear envelope.

Use of cFA as tool to monitor alterations in cellular lipid flows in response to DGAT inhibitor Niacin

Click-labeling on sections of HepG2 cells loaded with cFA showed gold label in the ER, Golgi complex, multi-vesicular bodies (MVB)s, mitochondrial outer membrane and lipid droplets (LDs) (Figure 2 C,D), indicating the presence of cFA or cFA-derived de novo-synthesized lipids in these compartments. Labeling of the mitochondria can be either due to an active uptake of cFA-CoA for β -oxidation or due to metabolic incorporation of cFA into polar lipids. Gold-label in the lipid droplets is most likely due to metabolic incorporation of cFA into TAG.

In mammalian cells, triacylglycerol (TAG) can be synthesized by 2 distinct enzymes, DGAT1 and DGAT2. The latter enzyme is mainly expressed in liver and adipose tissue [21,22]. In vivo studies showed that overexpression of DGAT1 in the liver resulted in increased very low-density lipoprotein (VLDL) secretion, whereas DGAT2 overexpression resulted in an increase of hepatic LD content [23]. This suggests that TAG synthesized by the two different enzymes also has a different cellular destination. To test if we could steer the direction of the lipid flow, we pre-incubated HepG2 cells for 50 min with the DGAT2 inhibitor [24]. Inhibition of DGAT2 should not only disrupt LD biogenesis, but may also enhance the formation of TAG by DGAT1 and thereby direct the lipid flux into the formation of VLDL.

After incubation with Niacin, the Golgi network appeared to be enlarged in most cells (Figure 3A). This could indicate hyper-activation of the secretory pathway. Compared to untreated cells, less LDs were present in the cells treated with Niacin (Figure 3B). Apart from these changes, the cellular morphology resembled that of untreated control cells. Results from the click labeling (Figure 3C,D) showed less gold label on the LDs present in the section, suggesting that LDs in Niacin-treated cells had incorporated less TAG synthesized from cFA. Overall, a slight increase in immuno-gold labeling of the Golgi complex in Niacin-treated cells could be observed. Furthermore, the amount of gold label on MVBs was increased compared to the untreated control cells. This could indicate an elevated incorporation of cFA into VLDL. An increase in labeling could also be observed for mitochondria, which could represent incorporation of cFA into acyl-CoA. These results show that cFA can be used to trace alterations in metabolic lipid flows at the ultrastructural level.

Impact of BFA on cellular ultrastructure and the localization of newly synthesized lipids

As inhibition of DGAT2 appears to increase the production of VLDL at the expense of LD formation, we reasoned that inhibition of VLDL assembly may redirect the lipid flow in favour of LD formation. Incubation of cells with Brefeldin A (BFA) inhibits the small GTPase Arf1p [25], which in turn destabilizes the Golgi complex and thereby disrupts VLDL secretion, which would reduce the amount of gold label in MVBs. Previously, BFA treatment has been shown to cause accumulation of TAG in LDs [26]. As shown in Figure 4A and -B, treatment of HepG2 cells with BFA destabilized the Golgi complex, caused a swelling of the ER and the nuclear envelope, and appeared to stimulate LD formation. Indeed, after performing click labeling to visualize the incorporation of cFA, the LDs in BFA-treated cells contained more gold-label in comparison to those of Niacin-treated cells. However the amount of gold-label on LDs

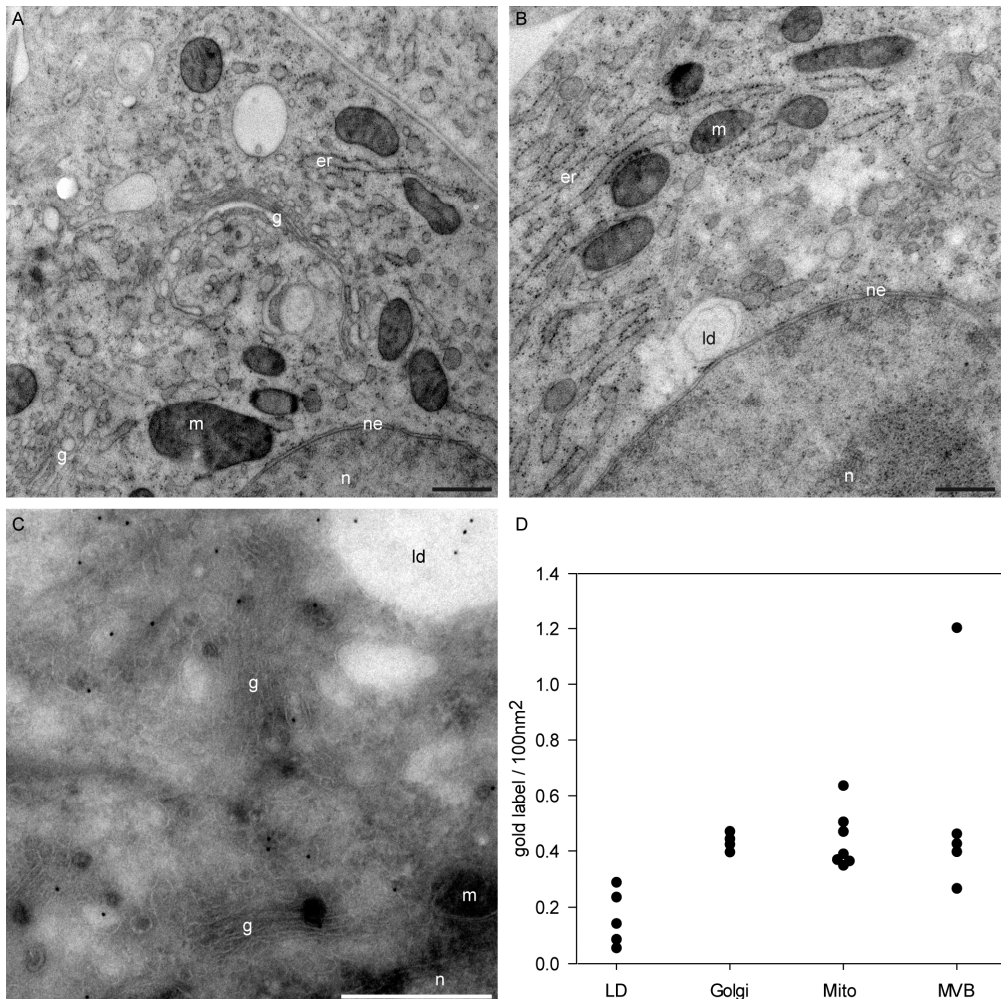


Figure 3 Impact of the DGAT2 inhibitor Niacin on cellular ultrastructure and the localization of newly synthesized clickable lipids. HepG2 cells were treated for 50 min with Niacin before being loaded with cFA and subsequently cryo-immobilized by high-pressure freezing. (A,B) Cells freeze-substituted and embedded in Lowicryl HM20 show a clear expansion of the Golgi system and less and smaller lipid droplets. (C) Click labeling on hydrated VIS2FIX sections reveals a decrease in label on LDs. The amount of gold-label on the Golgi appears to be slightly increased though this increase is more prominent on MVBs and mitochondria. (D) Scatterplot of the amount of gold label for the different cellular compartments. All scale-bars represent 500 nm. er: endoplasmic reticulum, g: Golgi, ld: lipid droplet, m: mitochondria, mvb: multivesicular body, n: nucleus, ne: nuclear envelope.

did not reach the level previously observed for untreated cells. This could indicate that BFA treatment also influences LD formation [27]. As expected, the amount of gold label on MVBs was much reduced, most likely due to the decrease in VLDL excretion. Once again there was a clear increase in gold label on mitochondria compared to untreated cells. This could indicate that the flow of cFA is shunted to the formation of acyl-CoA. Alternatively, DGAT2 has been shown to localize to the mitochondria associated ER

membranes [28], thus the increased labeling on mitochondria could be due to the formation of TAG in the mitochondria associated ER membranes.

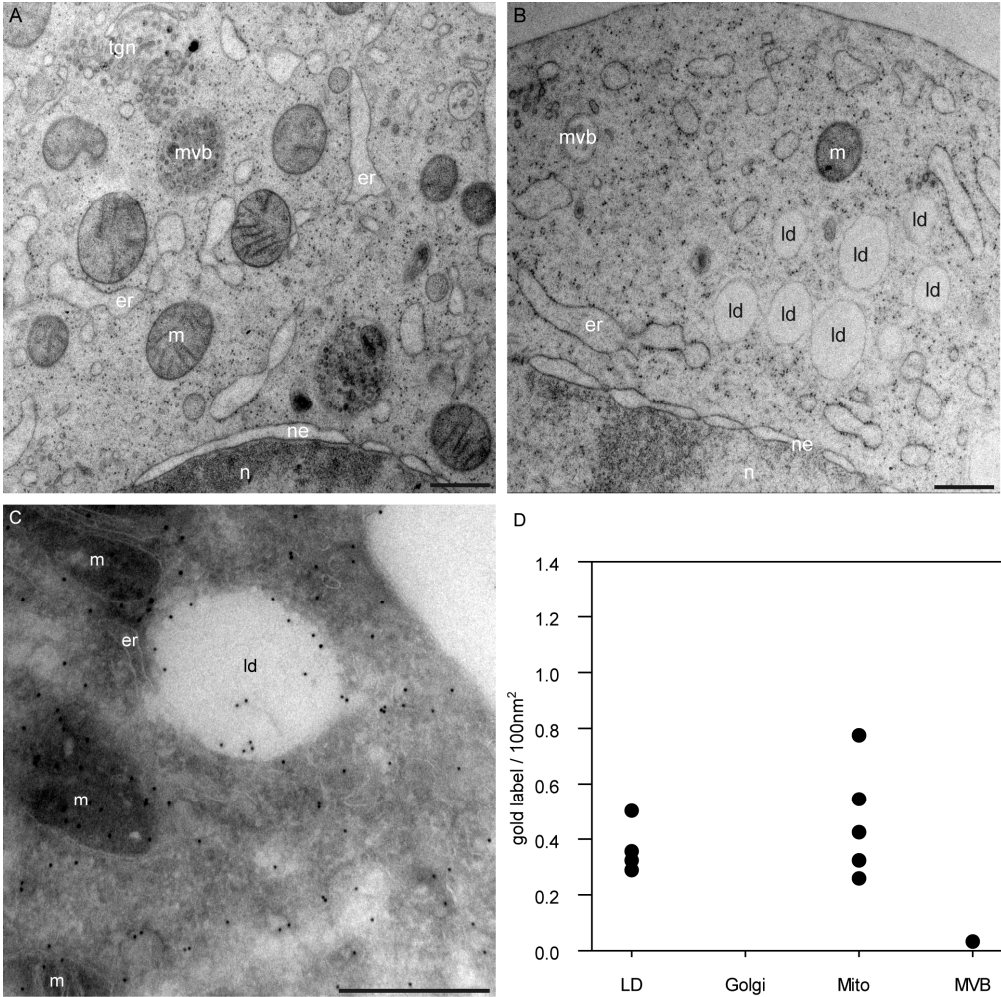


Figure 4 Impact of BFA on cellular ultrastructure and the localization of newly synthesized clickable lipids. HepG2 cells were treated for 50 min with Niacin before being loaded with cFA and subsequently cryo-immobilized by high-pressure freezing. (A,B) Cells freeze-substituted and embedded in Lowicryl HM20 show a disrupted Golgi system and characteristic swelling of the endoplasmic reticulum and nuclear envelope. Lipid droplets appear to be more abundant. (C) Click labeling on hydrated VIS2FIX sections shows an increase in gold label on LDs compared to cells treated with Niacin, also the label on mitochondria appears to be increased. (D) Scatterplot of the amount of gold label for the different cellular compartments. All scale-bars represent 500 nm. er: endoplasmic reticulum, g: Golgi, ld: lipid droplet, m: mitochondria, mvb: multivesicular body, n: nucleus, ne: nuclear envelope.

Effects of Niacin treatment on VLDL secretion

In HepG2 cells, fatty acids can be used for the synthesis of polar lipids or can be converted into TAG. TAG is either stored in LDs or excreted from the cell incorporated in VLDL. Inhibition of DGAT2 by Niacin partially inhibits the storage of cFA as TAG in lipid

droplets (see above). This, combined with the observed enlargement of the Golgi complex and increased labeling of MVBs suggests an increase in VLDL production. To verify this possibility, we performed immuno-labeling against ApoB, the main Apolipoprotein in VLDL, in Niacin-treated and control cells. The results however showed no increase in the amount of VLDL present in the secretory pathway compared to control cells (data not shown). However, it is known that HepG2 cells mostly produce VLDL with a low TAG content [29]. These results suggest that an increased incorporation of cFA into VLDL does not necessarily require an increase of VLDL particles.

Conclusion

Precise information on the localization of individual lipid molecules in cells is essential for a proper understanding of cellular lipid flows and function of the individual lipid species. Studies using fluorescent lipid analogs are limited by the spatial resolution of fluorescence microscopy. Furthermore, these fluorescent lipids do not always behave as their natural counterparts. The use of transmission electron microscopy would in principle allow localization of single lipid molecules at the ultrastructural level, but this technique is hampered by the lack of lipid-specific antibodies and the tendency of lipids to undergo redistribution during sample preparation. In the current study we have demonstrated that clickable fatty acids (cFAs) can be used in combination with optimized specimen preparation technique and immunogold labeling to localize individual lipid molecules at the nanometer scale. Importantly, our method also allows the visualization of cFA stored as TAG in lipid droplets. To our knowledge, this is the first study demonstrating the localization of individual lipid molecules in a LD at the ultrastructural level. Secondly we were able to visualize the changes in cellular lipid flows caused by inhibition of the triacylglycerol synthase DGAT2 or by disrupting the secretory pathway by incubation with Brefeldin A. Both treatments affected the amount of cFA incorporated as TAG into lipid droplets. The flow of lipid was re-directed to VLDL synthesis in case of DGAT2 inhibition. Treatment with Brefeldin A shunted the lipid flow to the mitochondria. This shows the possibilities of using clickable fatty acids combined with the VIS2FIX method to localize lipids at the ultrastructural level and visualize changes in lipid flow. Using this technique alongside more traditional biochemical methods may provide valuable data on the mechanisms involved in lipid metabolism and verify the cellular localization of these processes. Using shorter incubation times, for instance, would allow one to study the mechanism of lipid uptake. In addition, approaches based on this method could provide insight in the changes in lipid flow during the pathogenesis of disorders associated with changes in lipid metabolism.

With the current sample preparation method, though, there is always a lag of 5 minutes because cells need to be trypsinized into a cell suspension. If cells could be cultured on a substrate that is compatible with both high-pressure freezing and frozen hydrated sectioning this lag can be avoided.

Materials and methods

Preparation of FA/albumin stocks

Bi-functional C15 (cFA) was synthesized as described Haberkant *et al.* (submitted)[20].

Oleic acid (Sigma-Aldrich, St. Louis, MO) and cFA were bound to bovine albumin in a 6:1 molar ratio, as described in Van Greevenbroek *et al.* (1995)[30] Briefly, 20% w/v Bovine serum albumin (essentially fatty acid free, Sigma-Aldrich) was dissolved in culture medium at RT and subsequently cooled down to 4°C. Fatty acid in 96% ethanol was added to 100 mM NaOH in 96% Ethanol to a final concentration of 12mM FA. The ethanol was evaporated under N₂ flow, the resulting FA/NaOH pellet dissolved in 0.5ml AD at 55°C, followed by the addition of 0.5ml 20% BSA in culture medium. The FA/Albumin solution was stored at -20°C until used at a final concentration of 100µM FA, in FA free medium.

FA-free medium was prepared by supplementing low glucose DMEM with 10% FCS delipidated by chemical extraction with (2:1) di-Isopropylether (Sigma-Aldrich): 1-butanol (Sigma-Aldrich) as described by Cham & Knowles (1976)[31]. After extraction, FCS was subjected to nitrogen flow for 2 h before dialyzing three times overnight against PBS.

Inhibitors

Niacin (Sigma-Aldrich) was used in a final concentration of 3mM as described in Ganji *et al.* (2004)[24]. Brefeldin A (Sigma-Aldrich) was dissolved in ethanol to 1mg/ml, and used in a final concentration of 100 ng/ml.

Cell culture

HepG2 cells (ATCC, passage 3)(kind gift from CMC, UMCUtrecht, NL) were cultured in low glucose DMEM (PAA, Pasching, Austria) with 10% fetal bovine serum (PPA). All experiments were carried out between passage 5 to 7.

Lipid loading and high-pressure freezing

Cells were incubated with or without inhibitor for 50 min. Next, cFA/albumin or OA/albumin was added. Both were used at a final concentration of 100µM FA, in FA free medium. After 10 min incubation cells were gently trypsinized and spun down (150 rcf, 37°C).

Samples for VIS2FIX:

Supernatant was removed and the pellet was resuspended and mixed 1:1 with a solution of 30% dextran in culture medium. The resulting cell-suspension was loaded into copper tubes and frozen in a EMHPF operating at 2100 bar. Of each preparation 4 samples were frozen within 6 min after addition of the dextran, to prevent dextran endocytosis.

Samples for FS to Lowicryl (HM20):

Supernatant was removed and the pellet was resuspended and mixed 1:1 with a solution of 1% type IX agarose in culture medium. The resulting cell-suspension was loaded into 200 µm deep membrane carriers and frozen in a EMHPF (Leica

Microsystems, Vienna, Austria.) operating at 2100bar. Of each preparation 4 samples were frozen within 6 min after addition of the type IX agarose.

VIS2FIX

Hydrated VIS2FIX was performed as described in Karreman et al. (2010)[14]. Briefly; 80 nm frozen hydrated sections cut at -150°C using a cryo-ultramicrotome (UC6 FC6, Leica Microsystems) were adhered to copper grids with a carboncoated formvar support film by electro-static force using the Crion system (Leica Microsystems), transferred to an AFS2 (Leica Microsystems) at -90°C and placed on frozen fixative containing 0.2% Uranyl acetate, 0.2% Glutaraldehyde in 0.1M Phem. The fixative with the grids was thawed in 4.5 min on a stretching plate set to 40°C and subsequently incubated on ice for 10 min.

Freeze-substitution

Freeze-substitution was carried out in anhydrous acetone (SeccoSolv®, Merck, Darmstadt, Germany) containing 0.1% UA (Merck), from -90°C to -50°C, in an AFS2 (Leica Microsystems) Stepwise infiltration with HM20 (EMS, Hatfield, PA) at -50°C followed by polymerization by UV irradiation at -50°C for 5 days. After polymerization 50 nm sections were cut using a ultramicrotome (Ultracut E, Reichert-Jung now Leica Microsystems) and placed on copper grids with a carboncoated formvar support film. Sections were post-stained for 5 min with 4% aqueous uranyl acetate followed by 2 min Reynolds lead citrate.

Click-reaction and immuno-labeling

For immuno-localization of cFA, grids were placed on phem/glycin for 10 min and subsequently washed on 0.1 M phem -EGTA. Next the click reaction was performed by incubating the grids on droplets of 0.1 M Phem -EGTA, supplemented with 20µM Biotin-azide, 100 µM TBTA and 1 mM CuSO₄ for 1 h at room temperature. Grids were washed on drops of 0.1 M Phem, blocked for 20 min with 0.5% CFG (G7765, Sigma-Aldrich) in 0.1 M Phem and labeled using Rabbit anti-Biotin (100-4198, Rockland Immunochemicals, Gilbertsville, PA) followed by 10 nm Protein A gold (CMC, UMCUtrecht, NL). VIS2FIX_H sections were contrasted with uranyl oxalate (pH7) and stabilized in 1.8% methylcellulose / 0.4% uranyl acetate.

For immuno-localization of ApoB, sections were blocked for 20 min with 0.5% CFG 0.1 M Phem. Sections were subsequently labeled for ApoB using Goat anti-ApoB (#600.100.101, Rockland Immunochemicals, Gilbertsville, PA) followed by Rabbit anti-Goat IgG (Nordic Immunological Laboratories, Eindhoven, NL) followed by 10 nm protein-A gold (CMC UMCUtrecht). Antibodies were diluted in block buffer. Sections were contrasted with uranyl oxalate (pH7) and stabilized in 1.8% methylcellulose / 0.4% uranyl acetate.

Imaging

TEM micrographs were recorded on a Tecnai 12 120 kV transmission electron microscope (FEI Company) at 80 kV with a bottom mount TEMCam-F214 CCD camera (Tietz Video and Imageprocessing systems). In all figures, the TEM images are scaled for optimal contrast by employing linear adjustments of the levels of the entire image.

The number of gold particles per organelle surface area was counted (ten organelles for each experimental condition) using micrographs from three independent semi-blind labeling experiments in Fiji (ImageJ). The micrograph was overlaid with a 100 nm grid (using the Grid plugin) to assess the surface area for the various organelles.

Acknowledgments

We would like to thank Ruud Cox for the synthesis of the bi-functional fatty acid. Thanks to Joep van den Dikkenberg for his assistance during the HPF experiments.

References

1. Van Meer G, De Kroon AIPM. Lipid map of the mammalian cell. *J Cell Sci* 2011;124:5–8.
2. Maier O, Oberle V, Hoekstra D. Fluorescent lipid probes: some properties and applications (a review). *Chem Phys Lipids* 2002;116:3–18.
3. Kuerschner L, Ejsing CS, Ekroos K, Shevchenko A, Anderson KI, Thiele C. Polyene-lipids: A new tool to image lipids. *Nat Methods* 2004;2:39–45.
4. Kaiser RD, London E. Determination of the depth of BODIPY probes in model membranes by parallax analysis of fluorescence quenching. *Biochim Biophys Acta* 1998;1375:13–22.
5. Wang TY, Silvius JR. Different sphingolipids show differential partitioning into sphingolipid/cholesterol-rich domains in lipid bilayers. *Biophys J* 2000;79:1478–1489.
6. Halter D, Neumann S, Van Dijk SM, Wolthoorn J, De Mazière AM, Vieira OV, Mattjus P, Klumperman J, Van Meer G, Sprong H. Pre- and post-Golgi translocation of glucosylceramide in glycosphingolipid synthesis. *J Cell Biol* 2007;179:101–115.
7. Jao CY, Roth M, Welti R, Salic A. Metabolic labeling and direct imaging of choline phospholipids in vivo. *P Natl Acad Sci USA* 2009;106:15332–15337.
8. Salic A, Mitchison TJ. A chemical method for fast and sensitive detection of DNA synthesis in vivo. *P Natl Acad Sci USA* 2008;105:2415–2420.
9. Rostovtsev VV, Green LG, Fokin VV, Sharpless KB. A stepwise Huisgen cycloaddition process: copper(I)-catalyzed regioselective “ligation” of azides and terminal alkynes. *Angew Chem Int* 2002;41:2596–2599.
10. Van Genderen IL, Van Meer G, Slot JW, Geuze HJ, Voorhout WF. Subcellular localization of Forssman glycolipid in epithelial MDCK cells by immuno-electron microscopy after freeze-substitution. *J Cell Biol* 1991;115:1009–1019.
11. Möbius W, Ohno-Iwashita Y, Van Donselaar EG, Oorschot VMJ, Shimada Y, Fujimoto T, Heijnen HFG, Geuze HJ, Slot JW. Immunoelectron microscopic localization of cholesterol using biotinylated and non-cytolytic Perfringolysin O. *J Histochem Cytochem* 2002;50:43–55.
12. Roozmond RC. The effect of fixation with formaldehyde and glutaraldehyde on the composition of phospholipids extractable from rat hypothalamus. *J Histochem Cytochem* 1969;17:482–486.
13. Hoetzel S, Sprong H, Van Meer G. The way we view cellular (glyco)sphingolipids. *J Neurochem* 2007;103 Suppl 1:3–13.
14. Karreman MA, Van Donselaar EG, Gerritsen HC, Verrips CT, Verkleij AJ. VIS2FIX: a high-speed fixation method for immuno-electron microscopy. *Traffic* 2011;12:806–814.
15. Shah DO. Interaction of uranyl ions with phospholipid and cholesterol monolayers. *J Colloid Interface Sci* 1969;29:210–215.
16. Ginsburg H, Wolosin JM. Effects of uranyl ions on lipid bilayer membranes. *Chem Phys Lipids* 1979;23:125–131.
17. Huang TH, Blume A, Das Gupta SK, Griffin RG. Nuclear magnetic resonance and calorimetric study of the structure, dynamics, and phase behavior of uranyl ion / dipalmitoylphosphatidylcholine complexes. *Biophys J* 1988;54:173–179.
18. Pohl J, Ring A, Stremmel W. Uptake of long-chain fatty acids in HepG2 cells involves caveolae analysis of a novel pathway. *J Lipid Res* 2002;43:1390–1399.
19. Gibbons GF, Khurana R, Odwell A, Seelaender MC. Lipid balance in HepG2 cells: active synthesis and impaired mobilization. *J Lipid Res* 1994;35:1801–1808.
20. Haberkant P, Rajmakers R, Wildwater M, Sachsenheimer T, Brügger B, Houweling M, Van Meer G, Heck AJ., Holthuis JCM. In vivo profiling and visualization of cellular protein-lipid interactions using bifunctional fatty acids. Manuscript submitted
21. Oelkers P, Behari A, Cromley D, Billheimer JT, Sturley SL. Characterization of two human genes encoding acyl coenzyme A:cholesterol acyltransferase-related enzymes. *J Biol Chem* 1998;273:26765–26771.
22. Cases S, Stone SJ, Zhou P, Yen E, Tow B, Lardizabal KD, Voelker T, Farese RV. Cloning of DGAT2, a second mammalian diacylglycerol acyltransferase, and related family members. *J Biol Chem* 2001;276:38870–38876.

23. Yamazaki T, Sasaki E, Kakinuma C, Yano T, Miura S, Ezaki O. Increased very low density lipoprotein secretion and gonadal fat mass in mice overexpressing liver dgat1. *J Biol Chem* 2005;280:21506–21514.
24. Ganji SH, Tavintharan S, Zhu D, Xing Y, Kamanna VS, Kashyap ML. Niacin noncompetitively inhibits DGAT2 but not DGAT1 activity in HepG2 cells. *J Lipid Res* 2004;45:1835–1845.
25. Donaldson JG, Finazzi D, Klausner RD. Brefeldin A inhibits Golgi membrane-catalysed exchange of guanine nucleotide onto ARF protein. *Nature* 1992;360:350–352.
26. Ohsaki Y, Cheng J, Suzuki M, Fujita A, Fujimoto T. Lipid droplets are arrested in the ER membrane by tight binding of lipidated apolipoprotein B-100. *J Cell Sci* 2008;121:2415–2422.
27. Nakamura N, Banno Y, Tamiya-Koizumi K. Arf1-dependent PLD1 is localized to oleic acid-induced lipid droplets in NIH3T3 cells. *Biochem Biophys Res Commun* 2005;335:117–123.
28. Stone SJ, Levin MC, Zhou P, Han J, Walther TC, Farese RV Jr. The endoplasmic reticulum enzyme DGAT2 is found in mitochondria-associated membranes and has a mitochondrial targeting signal that promotes its association with mitochondria. *J Biol Chem* 2009;284:5352–5361.
29. Meex SJR, Andreo U, Sparks JD, Fisher EA. Huh-7 or HepG2 cells: which is the better model for studying human apolipoprotein-B100 assembly and secretion? *J Lipid Res* 2011;52:152–158.
30. Van Greevenbroek MM, Voorhout WF, Erkelens DW, Van Meer G, De Bruin TW. Palmitic acid and linoleic acid metabolism in Caco-2 cells: different triglyceride synthesis and lipoprotein secretion. *J Lipid Res* 1995;36:13–24.
31. Cham BE, Knowles BR. A solvent system for delipidation of plasma or serum without protein precipitation. *J Lipid Res* 1976;17:176–181.

Chapter 5

High-pressure freezing of adherent cells for frozen hydrated sectioning; a novel method

R.J. Mesman^{1,2,3,*}, J.A.Post^{2,3}

¹Membrane Enzymology, Department of Chemistry, Utrecht University, Padualaan 8, 3584 CH Utrecht, the Netherlands

²Biomolecular Imaging, Department of Biology, Utrecht University, Padualaan 8, 3584 CH Utrecht, the Netherlands

³Institute of Biomembranes, Utrecht University, Padualaan 8, 3584 CH Utrecht, the Netherlands

* Corresponding author

Abstract

With the development of Cryo Electron Microscopy Of Vitreous Sections (CEMOVIS), imaging cells in a close to native state has become a reality. However with the commonly used carriers for high-pressure freezing and cryo-sectioning, adherent grown cells need to be detached from their substrate or grown on dextran beads. Here a new method is presented for high-pressure freezing adherent growing cells for frozen-hydrated sectioning, CEMOVIS and VIS2FIX. Cells are cultured on golden grids, containing a carbon coated Formvar film, and frozen on a membrane carrier which provides the grids with the structural support needed to withstand the strain of trimming and cryo-sectioning. This method was successfully tested for the two different types of high-pressure freezers, those using a pressure chamber (HPM010, EMHPF, Wohlwend Compact 01/02, HPM100) and those directly pressurizing the sample (EMPact series).

Introduction

Cryo Electron Microscopy Of Vitreous Sections (CEMOVIS) allows the observation of samples in a frozen hydrated state, providing close to native ultrastructural details [1]. The main requirement for samples is that they can be frozen vitreous, usually by high pressure freezing, and can be sectioned in a cryo-ultramicrotome. This is done either by sectioning the sample within the carrier or by removing the carrier under liquid nitrogen and gluing the sample to a specimen pin [2] in the cryo-ultramicrotome at -145°C using cryo-glue [3]. The recently developed VIS2FIX method [4] also makes use of these frozen hydrated sections.

Currently there are three types of HPF carriers that can be sectioned without damaging the diamond knife; copper tubes, dome shaped gold plated carriers and the gold plated copper membrane carriers. Tubes are often used to freeze cell suspensions and they are relatively easy to mount and trim in a cryo-ultramicrotome. However in case of a sparse sample it is not possible to assess the location of the sample within the tube before sectioning. Previously we modified a specimen holder to allow the freezing of tubes in our HPF (Figure 1). Tube holders for the HPM010, EMHPF and Wohlwend Compact series, based on our design, are now commercially available directly from Engineering office M.Wohlwend (Sennwald, Switzerland) or distributed via Technotrade Inc.

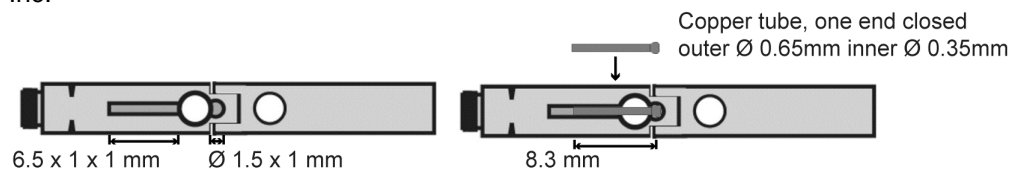


Figure 1 Modified EMHPF specimen holder for freezing copper tubes To allow the freezing of copper tubes in our HPF we modified a standard platelet specimen holder to fit a copper tube of 8.3 mm in length (half the length of a tube used in the EMPact). Tubes are frozen with one end closed. Specimen holders based on our design, are now commercially available for the HPM010, EMHPF and Wohlwend Compact series high-pressure freezers, either directly from Engineering office M.Wohlwend (Sennwald, Switzerland) or distributed via Technotrade Inc.

The dome shaped carriers were originally designed for freeze fracturing and can be used for freezing cell suspensions and tissues [5]. After high-pressure freezing these carriers are taken apart and the flat carrier containing the exposed sample is mounted in the cryo-ultramicrotome.

The membrane carriers are available in two depths, 100 and 200 μm , and can be used to freeze both cell suspensions and tissues, provided that they fit within the inner-dimensions of the carrier. With tissue, orientation of the sample within the membrane carriers is possible. Trimming of these carriers in the cryo-ultramicrotome however is a time consuming process due to the fact that membrane carriers have a 0.65 mm rim, which needs to be removed to expose the sample. Trimming should be done with care as not to damage the sample in the process.

The current carriers work well for cell suspensions and tissues but for adherent growing cells until now the most commonly used options for CEMOVIS specimen preparation are scraping [6] or trypsinizing [5] the cells to make a cell suspension. This of course can introduce artifacts or changes in the cellular ultrastructure. The best approach would be to grow the cells on a support that can be frozen and sectioned. This is not possible with the supports commonly used for freeze substitution, such as sapphire discs [7,8], Aclar [9,10], filter membranes [11]. The one exception to this are dextran spheres (Cytodex)[12] which can be used as a support for adhered cells for CEMOVIS, as shown by Hagen & Grünwald [13]. However these spheres were reported to have a low surface to volume ratio which resulted in a low cell density per section. Trials with a different geometry dextran carrier, which had a closer packing within the tube did not freeze well. This is most likely due to the high thermal capacity of these carriers.

In theory adhering cells can be cultured inside membrane carriers. In practice this met with two main problems: First, the level of confluence could only be assessed by looking at the cells growing around the carrier, since the carriers are not translucent. Secondly, although membrane carriers are gold plated, a small area of copper is exposed when the carriers are cut from the strip they are supplied in. This exposed area provides enough free copper to be incompatible with cell growth.

Here a different approach is used, by growing cells on golden grids with a carbon-coated formvar film. These grids are frozen on top of 100 or 200 μm deep membrane carriers, providing the fragile grids with a sturdy support to withstand the forces generated during trimming.

To test this method HepG2 cells were grown on golden grids on the bottom of Petridishes. Grids were placed, cells down, on a membrane carrier filled with 20% dextran in culture medium and high-pressure frozen in an EMHPF. Spacer rings were used to ensure the sandwich fitted in the standard platelet holder (Figure 2A, B). Since the standard platelet holder of our HPF was used, the method can directly be used in all other HPFs which are able to freeze platelets. To test the compatibility of this method with the EMPact series of high pressure freezers, I also tried freezing of the grid / membrane carrier sandwich in an EM-Pact1 using the flat specimen pod (Figure 2C).

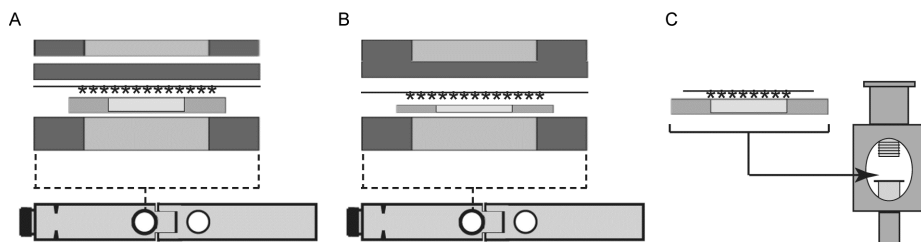


Figure 2 Freezing the grid / MC sandwiches in the EMHPF and EMPact

Specimen stacks for freezing the grid / MC sandwiches in the platelet holder (A,B) or the EMPact (C). (A) Specimen stack for the 200 µm deep MC consists of a 400 µm thick ring, followed by the MC. After filling the MC the grid is placed cells(*) down on the MC. The sandwich is closed with a lecithin coated 200 µm thick plate followed by a 200 µm thick ring to ensure a total height of 1 mm. (B) Specimen stack for the 100 µm deep MC, here the stack is closed off with a lecithin coated 0/300 (Type B) platelet to ensure a total height of 1 mm. (C) For freezing the grid/MC sandwich in the EMPact, the grid should lie in the center of the MC. The sandwich is carefully loaded into the pod and the pod is tightened with a force of 30Ncm.

Results / Discussion

Cryo-electron microscopy on sections from grids frozen in the EMHPF

Dipping the grids in medium containing dextran before freezing ensures that the ice on each side of the grid has the same viscosity. If this is not the case the sectioning properties of the ice will differ on either side of the grid. Figure 3a shows a section from a grid which has dextran only on the cell-side of the grid. As can be observed, there are more crevasses in the ice below the formvar film. This can also lead to curling of the ribbon during sectioning. In the section the formvar film can be easily identified (Figure 3A, B, arrows) and traced throughout the section. This facilitates finding the cells within the section. Since cells were frozen at 80% confluence, cell-cell contacts could be readily identified (Figure 3C). All samples analyzed appeared vitreous in the diffraction image (Figure 3A, D).

Applicability of the method in the EMPact

For this method to be compatible with the EMPact, it is essential that the diamond in the pod makes a proper seal on the grid / membrane carrier sandwich. This is only the case if the rim of the grid falls within the diameter of the diamond. Therefore we used formvar coated aperture grids with an outer diameter of 2.3 mm and an inner diameter of 1 mm (Veco). As described in Vanhecke et al.[14] overfilling the membrane carrier can lead to bulging out during freezing. Therefore excess medium was blotted from the grid before placing it on the pre-filled membrane carrier. Out of the 6 samples frozen in the EMPact two were bulged out, most likely due to over-filling of the sample carrier. Upon trimming of the carrier the ice appeared to be uniformly black. Again the formvar film could be easily identified within the section (Figure 4A). All analyzed samples appeared vitreous in the diffraction image (Figure 4B).

Choice of carrier thickness

Membrane carriers are available in two depths, 100 and 200 µm. Initially we tested this method using the 200 µm deep membrane carriers, to have the sturdiest support for the grid during trimming and sectioning. Using this carrier thickness both freezing and

trimming were successful. Later trials with the 100 μm carriers showed that also these carriers can be used without the risk of bending during trimming, if the feed of the cryo-ultramicrotome is kept below 100 nm while trimming away the sides of the carrier.

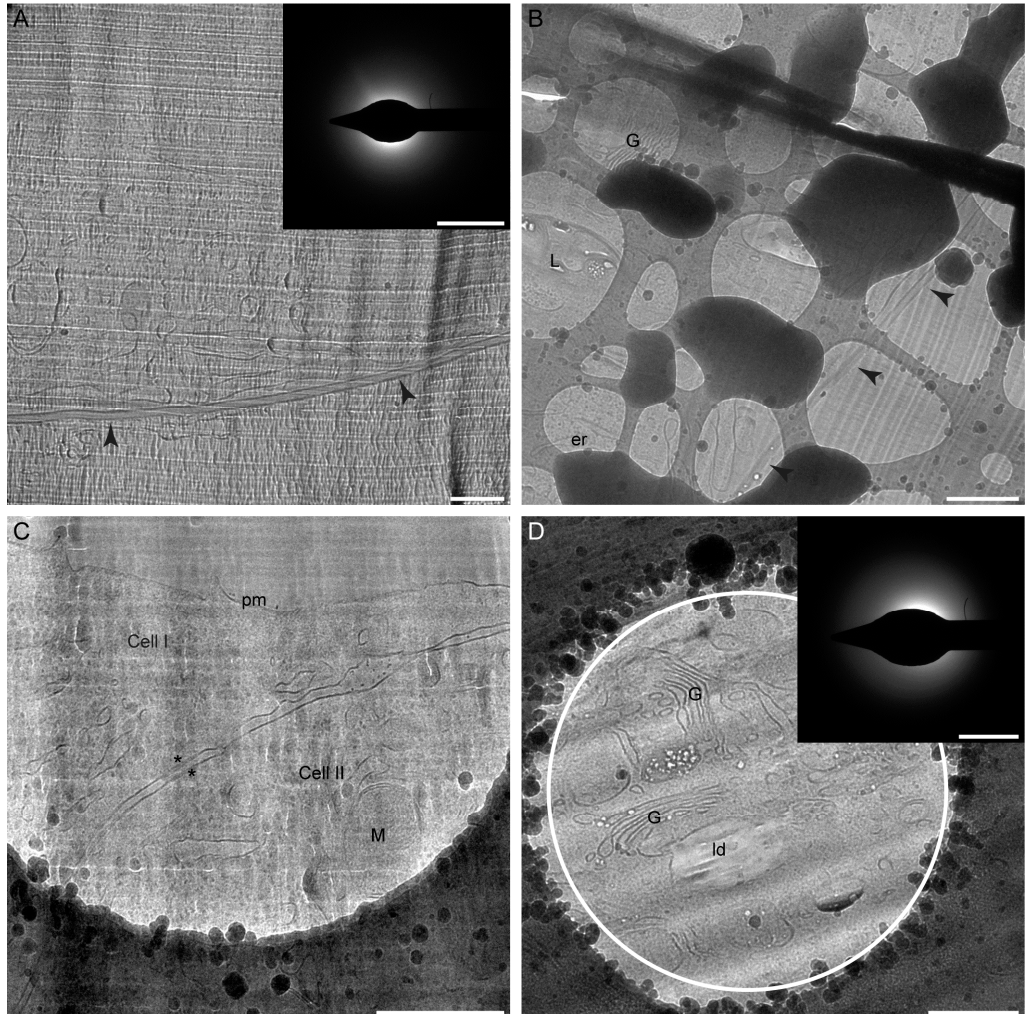


Figure 3 Frozen hydrated sections of cells grown on golden grids and high-pressure frozen in an EMHPF. The formvar film can be easily identified within the sections (arrowheads) which facilitates finding cells within the section. (A) Section from a sample where culture medium containing dextran was only applied to the cell-side of the grid. Crevasses appear more prominent below the Formvar film, likely due to the different sectioning properties. The sample appeared to be vitreous in the diffraction pattern (inset). (B-D) Sections from a sample with dextran on both sides of the grid. (B) Since sections were cut without the use of a cryosphere, some suffered from ice contamination though cells could still be identified between the ice crystals. (C) As cells were at 80% confluence, cell-cell contacts were frequently observed. (D) Cellular components could be readily identified, again the sample appeared to be vitreous in the diffraction pattern (inset). Diffraction pattern taken before the image in panel D, white ring indicates the selected area aperture. All micrograph scalebars indicate 500 nm, scalebars for diffractograms indicate 5nm. er: endoplasmic reticulum, G: Golgi, L: lysosome, Id: lipid droplet, M: mitochondria, pm: plasma membrane, *: desmosome.

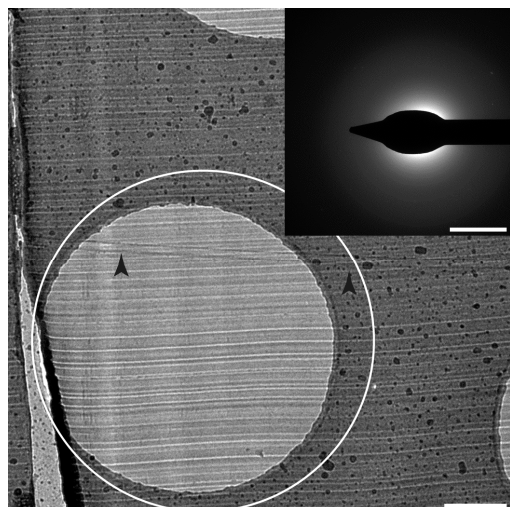


Figure 4 Frozen hydrated sections of grid / MC sandwiches frozen in an EMPact1 Freezing the grid / MC sandwich in the EMPact was tested without cells. 2.3 mm Ø aperture style grids provided the best seal with the diamond in the carrier pod. Again the Formvar film (arrowheads) could be traced throughout the section and sections appeared vitreous in the diffraction image (Inset). White ring indicates the selected area aperture. Micrograph scalebar indicates 500 nm, diffractogram scalebar indicates 5 nm.

Conclusion

Here a novel method was demonstrated for high pressure freezing adherent cells for frozen hydrated sectioning, applicable in all currently used high pressure freezers. These sections can be either directly viewed in the cryo-TEM (CEMOVIS) or processed via the VIS2FIX method. Cells grown on golden grids are high pressure frozen on a membrane carrier, which provides the fragile grids with the support needed during trimming and sectioning. This allows cells to be imaged in the cryo-electron microscope without the need of detaching them from the surface they were grown on, thereby preventing possible changes in the ultrastructure caused by the detachment process. Furthermore the orientation of the cells is retained which facilitates the study of polarized cells. This brings CEMOVIS one step closer to imaging adhered cells in their native state.

Although there is still only one layer of cells within the section, the Formvar film can be easily identified and traced throughout the section, this facilitates finding the cells within the section. Another advantage is that the time required to prepare a specimen for freezing is much reduced. This enables the use of short incubation times in pulse-chase studies or when using inhibitors or stimulants. Since the cells are cultured on a flat translucent surface, cells can be imaged by fluorescence microscopy before freezing, making this method readily compatible with correlative microscopy.

Materials and methods

Preparation of golden grids for cellculture

Gold plated grids (Athens broad rim (100# Hexagonal) or Veco 2.3 mm Ø aperture style, Agar scientific, Essex, UK) were washed three times in acetone p.a. and dried under nitrogen gas flow. Grids were placed dull side down on freshly prepared formvar films floating on water. Films with grids were picked up using cleaned 50 µm thick Alcar® strips and dried over-night. The next day a thin layer of carbon was evaporated on top of the formvar film and the Alcar strips with grids were adhered to the bottom of 6cm Petridishes using matrigel[10]. After solidifying at 37°C dishes were sterilized by UV irradiation for 1 hour in a lamellar flow cabinet.

Cellculture

HepG2 cells (ATCC, P3) (kind gift from CMC UMC-Utrecht) were cultured in low glucose DMEM (#E15-891, PAA, Pasching, Austria) supplemented with 10% fetal bovine serum (#A15-151, PAA). All experiments were carried out at passage 5 to 7. Cells were seeded in 6 cm Petridishes, with grids, and allowed to grow for four days. One day before freezing culture medium was changed for pre-equilibrated low glucose DMEM supplemented with 10% FBS and 25mM Hepes for buffering of the pH during sample preparation.

High-pressure freezing

Cells and media were kept at 37°C up until the very moment of high-pressure freezing, using a small incubator and a stretching plate as work table. On average samples were loaded and frozen within one minute. We were able to freeze 10 samples within 14 minutes, taking into account the regeneration time of 1.5 minutes for our HPF.

Freezing of cells grown on golden grids in the EMHPF

The sandwich was partially assembled in the standard specimen holder (spacer ring, membrane carrier) and the membrane carrier was filled with medium containing 20% dextran (40kD, #31389, Fluka, Buchs, Germany). Next a grid containing HepG2 cells at 80% confluence was taken out of the petridish, dipped in a drop of medium containing 20% dextran and placed, cells down, on the membrane carrier. The sandwich was closed either by adding a lecithin coated 200 µm thick aluminium plate and a 200 µm thick spacer ring when using 200 µm deep carriers (Figure 2A) or a lecithin coated 300/0 platelet when using 100 µm deep carriers (Figure 2B) ensuring a specimen stack of 1 mm thick. After closing the specimen holder, the sample was high-pressure frozen in an EMHPF operating at 2100 bar.

Freezing of the grid / membrane carrier sandwich in the EMPact

In the EM-Pact membrane carriers are frozen in specialized pods in which the sample cavity is closed off by a diamond. In order for the sample to be frozen properly it is essential that the sample cavity is completely sealed. Therefore 2.3 mm Ø aperture grids with an inner diameter of 1mm were used, which are closed off efficiently by the diamond in the carrier pod. For freezing the grid /membrane carrier sandwich with medium containing 20% dextran, the guidelines for filling membrane carriers given in Vanhecke *et al.*[14] were followed. Grids were dipped in a drop of medium containing 20% dextran and excess medium was blotted off by touching the rim of the grid with wetted filter paper. Next the grids were placed, cells down, on the membrane carrier. The sandwich was loaded into the pod and sealed by the screw and diamond with a torque force of 30Ncm (supplementary figure 1c). The pod was loaded into the EM-Pact1 and frozen. After freezing, pods were opened under liquid nitrogen and the carrier was inspected visually. Bulged out carriers were discarded.

Cryo-ultramicrotomy

When present, spacer rings and cover-plates were removed under liquid nitrogen and the grid-membrane carrier sandwich was transferred to the cryo-ultramicrotome, pre-cooled at -150°C . The membrane carrier was mounted horizontally, grid facing up, into a smooth beaked flat specimen holder. Here a holder based on the model described in Michel *et al.* [15] was used, as an alternative a cryo-AFM holder can be used. Both allow the sample to be stored liquid nitrogen after trimming or sectioning while mounted in the holder. The holder was rotated 91° clockwise and the front surface was trimmed at 100 mm/s with 100 nm feed to expose the ice using a cryo-trim 20 diamond knife (Diatome, Biel/Bienne, Switzerland). The 1° degree angle made sure that the grid would not be pushed out of the sandwich while trimming. Next the holder was turned 90° clockwise to the horizontal position, grid facing down, and the sides were trimmed down stepwise from the side of the carrier at 80 mm/s with 100 nm feed to form a stepped pyramid. After trimming the sides, the holder was turned clockwise and the bottom of the carrier was trimmed away, stepwise at 80 mm/s with 100 nm feed, to form a 60 nm wide blockface with the grid almost in the center. This prevented the ribbon from curling during sectioning. 50 nm sections were cut on a 35° cryo-immuno knife (Diatome) and statically adhered to a glow-discharged (200# hex) grid (lacy carbon or holey carbon) using the Cryon system (Leica microsystems). Grids were collected in a small grid box and stored in filtered liquid nitrogen.

Cryo-electron microscopy and imaging

Grids were loaded in a pre-cooled cryo-holder (Gatan Inc., Pleasanton, CA) and imaged in a Tecnai T12 (FEI Company) operating at 120kV. TEM micrographs were recorded on a bottom mount 4k Eagle CCD camera (FEI Company). When needed, the TEM images were scaled for optimal contrast by employing linear adjustments of the levels for the entire image.

Acknowledgments

I would like to extend my gratitude to Elly van Donselaar for her assistance during the high-pressure freezing and for critically reading the manuscript. Thanks to Daniel Studer for the useful discussions. Lastly I would like to thank the CMC, UMCUtrecht for allowing me to use their EMPact1.

References

1. Al-Amoudi A, Chang J-J, Leforestier A, McDowall A, Salamin LM, Norlén LPO, Richter K, Blanc NS, Studer D, Dubochet J. Cryo-electron microscopy of vitreous sections. *EMBO J* 2004;23:3583–3588.
2. Sartori N, Richter K, Dubochet J. Vitrification depth can be increased more than 10-fold by high-pressure freezing. *J Microsc* 1993;172:55–61.
3. Richter K. A cryoglue to mount vitreous biological specimens for cryoultramicrotomy at 110K. *J Microsc* 1994;173:143–147.
4. Karreman MA, van Donselaar EG, Gerritsen HC, Verrips CT, Verkleij AJ. VIS2FIX: a high-speed fixation method for immuno-electron microscopy. *Traffic* 2011;12:806–814.
5. Bouchet-Marquis C, Hoenger A. Cryo-electron tomography on vitrified sections: A critical analysis of benefits and limitations for structural cell biology. *Histochem Cell Biol* 2011;42:152–162.
6. Bouchet-Marquis C, Dubochet J, Fakan S. Cryoelectron microscopy of vitrified sections: a new challenge for the analysis of functional nuclear architecture. *Histochemistry and Cell Biology* 2006;125:43–51.
7. Hess MW, Müller M, Debbage PL, Vetterlein M, Pavelka M. Cryopreparation provides new insight into the effects of brefeldin A on the structure of the HepG2 Golgi apparatus. *J Struct Biol* 2000;130:63–72.
8. Reipert S, Fischer I, Wiche G. High-pressure freezing of epithelial cells on sapphire coverslips. *J Microsc* 2004;213:81–85.
9. Jiménez N, Humbel BM, van Donselaar E, Verkleij AJ, Burger KNJ. Aclar discs: a versatile substrate for routine high-pressure freezing of mammalian cell monolayers. *J Microsc* 2006;221:216–223.
10. Jiménez N, Van Donselaar EG, De Winter DAM, Vocking K, Verkleij AJ, Post JA. Gridded Aclar: preparation methods and use for correlative light and electron microscopy of cell monolayers, by TEM and FIB–SEM. *J Microsc* 2010;237:208–220.
11. Morphew MK, McIntosh JR. The use of filter membranes for high-pressure freezing of cell monolayers. *J Microsc* 2003;212:21–25.
12. Zeuschner D, Geerts WJC, van Donselaar E, Humbel BM, Slot JW, Koster AJ, Klumperman J. Immuno-electron tomography of ER exit sites reveals the existence of free COPII-coated transport carriers. *Nat Cell Biol* 2006;8:377–383.
13. Hagen C, Grünewald K. Microcarriers for high-pressure freezing and cryosectioning of adherent cells. *J Microsc* 2008;230:288–296.
14. Vanhecke D, Zuber B, Brugger SD, Studer D. Safe high-pressure freezing of infectious microorganisms. *J Microsc* 2012;246:124–128.
15. Michel M, Hillmann T, Müller M. Cryosectioning of plant material frozen at high pressure. *J Microsc* 1991;163:3–18.

Chapter 6:

Summarizing Discussion

Electron microscopy as a tool to study lipid organization at the ultrastructural level

Lipids are essential for cellular life, functioning either organized as bilayer membranes to compartmentalize cellular processes, as signaling molecules or as metabolic energy storage. Our current knowledge on lipid organization and processes involved in cellular lipid homeostasis is mainly based on biochemical data. However, the resolving power of the most commonly used biochemical methods (molecular analysis of cellular fractions and the use of fluorescent lipid analogs) is limited. To gain further insight in the subcellular lipid distribution and processes involved in cellular lipid homeostasis would require a high resolution method which allows the study of lipids within the cellular context. Here, we explored the use of one such approach, transmission electron microscopy, to study cellular lipids, lipid droplets and lipoproteins at the ultrastructural level.

Sample preparation

Since the introduction of transmission electron microscopy in 1931 by Ruska and Knoll and its first use on biological specimens [1] the transmission electron microscope has been used to study samples at an ever increasing magnification. With a spatial resolution well below the 200 nm limit of conventional light and fluorescence microscopes, the transmission electron microscope provides a tool to study cellular components at a magnification that allows the visualization of large molecules (proteins, etc). In theory a spatial resolution down to 1-2 Ångström can be reached. In practice, the effective spatial resolution is limited by the thickness of the sample and the way it has been prepared. As discussed in Chapter 1, electron microscopes operate at a high vacuum. Therefore specialized sample preparation is required to protect specimens against this high vacuum by either immobilizing or replacing the water within the specimen. Furthermore the specimen can be stained with heavy metals to provide additional contrast. However, the preparation steps can also alter the ultrastructure of the specimen. The retention of cellular lipids depends heavily on the sample preparation procedure. Organic solvents used for dehydration of the sample can readily extract the lipids we wish to image. During conventional dehydration using ethanol up to 70% of all cellular lipids are extracted. The extraction of lipids depends on the polarity of the solvent: solvents with low polarity extract less polar lipids compared to more polar solvents. For neutral lipids this is the other way around. Solvent polarity increases with lower temperatures. Therefore, lipid extraction is reduced at low temperatures. Based on data from the literature, the extraction of polar lipids during freeze substitution appears to depend on the amount of water molecules bound to the polar lipid head-group. This leads us to hypothesize that this hydration shell needs to be substituted before the solvent can

interact with the lipid head-groups. This reduces the time in which lipids are exposed to the solvent, thereby diminishing the lipid extraction. In samples freeze-substituted in acetone containing uranyl acetate and embedded in Lowicryl HM20 at -50°C, the outer layer of neutral lipid in lipid droplets (LDs) appeared to be extracted (Chapter 2). This layer reportedly contains more saturated neutral lipids, which have a higher polarity than the unsaturated lipids in the core of the LD. Using a lowicryl resin that can be polymerized at even lower temperatures (Lowicryl HM23) may prevent this extraction. However, at such low infiltration temperatures there is a risk that the acetone in the substitution medium might not have dissolved all the water within the sample. An alternative can be substitution with methanol at -90°C and switching to acetone before the temperature is raised. Preliminary experiments with this method show promising results (unpublished data).

Lipid preservation is the highest in those preparation procedures which do not require dehydration; Cryo-electron microscopy of vitreous sections (CEMOVIS) [2], hydrated VIS2FIX [3]. An alternative is dehydration at sub-zero temperatures; freeze-substitution combined with low temperature embedding. Reduction of lipid extraction does not necessarily imply that the spatial organization of the polar lipids within the cellular membranes is retained. Only when using CEMOVIS, in which the sample is observed at liquid nitrogen temperatures, this can be assured. In all other sample preparation procedures, the use of uranyl acetate is essential to maintain the spatial organization of phospholipids since it is able to bind up to four lipid phosphorus groups [4,5]. Equipped with this knowledge, we were able to label individual lipid molecules within the cell by click-labeling (Chapter 4). Using this method we were even able, for the first time, to visualize the incorporation of a clickable fatty acid as neutral lipids into lipid droplets (LDs). We showed that clickable fatty acids provide a promising new tool for studying the distribution of de-novo synthesized lipids and changes in the lipid flow. Using the novel method for high-pressure freezing adherent cells (Chapter 5) the time between stimulating the cells with fatty acid (FA) and freezing can be much reduced. This facilitates the use of clickable fatty acids to elucidate the FA uptake route. Additionally, in a model-system which allows for more intervention in lipid biosynthetic pathways, such as yeast or *C. elegans*, the use of clickable fatty acids could provide additional insights in lipid biosynthesis.

Lipid droplet biogenesis

Cellular lipids can be stored in an esterified form as neutral lipids (triglycerides or sterol-esters) in lipid droplets. One of the main functions of these LDs is that of a buffer in lipid homeostasis, by storing excess lipids in an esterified form. FA bound to albumin is rapidly taken up by the cell and used in the synthesis of, for instance, phosphatidic acid (PA), the precursor for most polar lipids and diacylglycerol (DAG). DAG functions as a signaling

molecule involved in insulin signaling and the PI3K-signaling pathway. Furthermore DAG is essentially a polar lipid without a head-group, which influences membrane curvature. Therefore, an excess of DAG could seriously disturb cellular function. DAG is rapidly converted to the inert triacylglycerol (TAG) by addition of an extra acyl chain by members of the diacylglycerol-acyl-transferase (DGAT) protein family. LDs have been implicated in the pathogenesis of several diseases ranging from insulin resistance [6,7] to muscle dystrophy [8]. However it is quite straight-forward that in any situation in which cellular lipid homeostasis and metabolism is disturbed, lipid droplets will be formed to store the excess of lipid in the safest possible way. In Chapter 2 we showed direct membrane contacts between LDs and the endoplasmic reticulum (ER) membrane using electron tomography on sections of high-pressure frozen - freeze-substituted and Epon embedded samples. For other cellular organelles these interactions were mainly close apposition to the LD. In a VIS2FIX_H processed section of THP-1 cells labeled for LAMP2, a LAMP2 positive lysosome was found in close association with a LD. Tomographic reconstruction of this section showed a possible hemi-fusion between the outer membrane of the lysosome and the phospholipid monolayer of the LD. This suggests a role for micro-autophagy in LD metabolism.

The early stages of lipid droplet formation remain elusive. However, we were able to detect the PAT protein TIP47 in oleic acid stimulated TIP47 knock-down Hela cells by immuno-labeling on hydrated VIS2FIX sections. The gold label indicated the presence of TIP47 on small electron translucent structures in the mitochondria-associated ER membrane, where the triacylglycerol synthase DGAT2 reportedly resides [9]. These structures may very well be early lipid droplets. One other result pointing in this direction was obtained in the experiments with clickable fatty acids (Chapter 5) in brefeldin A-treated cells. In a preliminary experiment, we tried the click labeling on hydrated VIS2FIX sections fixed with glutaraldehyde, uranyl acetate and osmium tetroxide. The click labeling itself did not work (likely due to the reaction of osmium with the alkyne bond) but we observed a pattern of round osmophilic structures on the mitochondria-associated ER membranes (Figure 1). These data combined strengthen the theory that LD biogenesis takes place in the mitochondria-associated ER. To fully elucidate the mechanism of LD formation will require a more detailed and quantitative analysis. If mitochondria-associated ER membranes are indeed the site of LD biogenesis, TIP47 should no longer be present on these membranes when TIP47kd HeLa cells are grown in delipidated medium. In addition, electron tomography on oleic acid stimulated TIP47kd HeLa cells labeled for TIP47 could be used to determine the nature of the observed electron translucent structures in these ER subdomains. Ultimately, in control HeLa cells, TIP47 should also localize to the mitochondria-associated ER membranes shortly after oleic acid treatment.

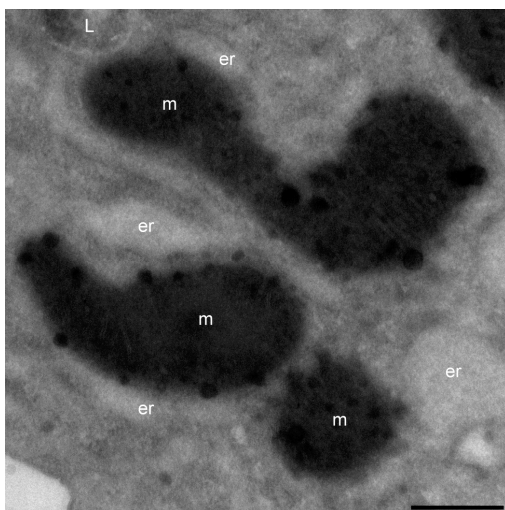


Figure 1 Osmophilic structures on the mitochondria-associated ER membrane Frozen hydrated sections of HepG2 cells, treated with brefeldin A and incubated with clickable fatty acid, were processed via the hydrated VIS2FIX method using 0.2% glutaraldehyde, 0.2% uranyl acetate and 0.1% osmium tetroxide in 0.1 M Phem as fixative. Round osmophilic structures could be detected in the mitochondria-associated ER membranes. er: endoplasmic reticulum, L: lysosome, m: mitochondria. Scale bar represents 500 nm.

VLDL assembly

For transport from the intestine to the liver and from the liver to the adipose tissue, in the blood circulation lipids are esterified to neutral lipids and packed in lipoproteins (chylomicrons and very low density lipoprotein (VLDL)). VLDL is synthesized postprandially by the liver and transports triacylglycerol from the liver to the peripheral tissues. VLDL can be identified by its main apo-protein ApoB100. Being a precursor for the low density lipoprotein (LDL), a high level of VLDL is considered to be a risk factor for atherosclerosis and cardiovascular disease [10–12]. The mechanism of VLDL assembly is largely unknown and immuno-gold labeling for ApoB could provide valuable insights. In the literature however, low labeling efficiency and loss of antigenicity of ApoB have been reported [13]. In Chapter 3 we found that this reported low labeling efficiency for ApoB on Tokuyasu cryo-sections [13] is due to the delipidating action of the lipid free bovine serum albumin (BSA) used in the blocking step. By changing the blocking solution to either acetylated bovine serum albumin (BSA-c) or cold water fish skin gelatin (CFG) we were able to retain the antigenicity of ApoB. The loss of antigenicity by delipidation, as reported here, may very well occur in other proteins that depend on the binding of lipids for their proper 3d conformation. Furthermore, we developed an alternative section pickup by statically adhering the sections to a grid using the Crion system and thawing the grids on buffer. This gave a clear reduction in the loss of cellular content in sections from cells fixed in 4% formaldehyde, thereby increasing the level of ultrastructural preservation. This method can readily be applied when a high degree of structural preservation is needed and fixation with 2% formaldehyde and 0.5% glutaraldehyde is impossible due to glutaraldehyde sensitive antigens. Where the second lipidation step of ApoB takes place is

still unknown; it has been suggested that the VLDL2 particles fuse with each other to form VLDL1. Another theory is that there are TAG rich 'luminal lipid droplets' [14] which fuse with VLDL2 to form a fully lipidated VLDL1 particle. It could be that these 'luminal lipid droplets' are actually Apo-protein E (ApoE) or Apo-protein C (ApoC) positive lipoproteins, since both ApoE and ApoC have been shown to be dynamically associated with VLDL.

Open questions and outlook

The results from the experiments discussed in the previous chapters also gave rise to new questions. Some of these may be readily addressed using the technical advances presented in this thesis.

Does the TAG in VLDL originate from LDs or from de-novo synthesis by DGAT1? Work on animal models supports the latter view. Ohsaki *et al.*[15] reported the formation of ApoB crescents around lipid droplets, which increased in number upon Brefeldin A (BFA) treatment. It was suggested that lipid droplets fused with the ER membrane to stabilize ApoB. However these structures could be formed in a number of ways. In the normal situation ApoB is co-translationally lipidated by the microsomal transfer protein (MTP) (Figure 2A). Upon BFA treatment the inhibition of VLDL maturation could cause partially lipidated ApoB to fuse back with the membrane (Figure 2B). These small lipid inclusions could aggregate and thereby form an ApoB crescent (Figure 2D). Another possible mechanism could be that BFA treatment stops the maturation of ApoB, while the synthesis of triacylglycerol by DGAT1 continues, thereby forming an ApoB crescent. We did not observe ApoB crescents in FA stimulated HepG2 cells when immuno-labeling for ApoB (Chapter 4). Even after BFA treatment these structures were not observed (Chapter 5). One possible explanation is that in the study of Ohsaki *et al.*[15] cells were incubated for 2 hours with FA before fixation, whereas we used much shorter incubation times. This suggests that the ApoB crescents are formed between 1 and 2 hours incubation with FA. By immuno-labeling cells, cryo-immobilized at specific time points between 1 and 2 hours FA incubation, it should be possible to elucidate the mechanism of ApoB crescent formation. If existing LDs truly fuse back, this could be shown by first treating the cells with oleic acid to increase the number of LDs, after which cells should be treated with both BFA and Niacin. Next cells should be challenged with clickable fatty acids for 2 hours before cryo immobilization. After click-labeling to localize the clickable FA and immuno-labeling for ApoB, LDs in ApoB crescents should contain almost no clickable lipid if existing lipid droplets were used to form the ApoB crescent.

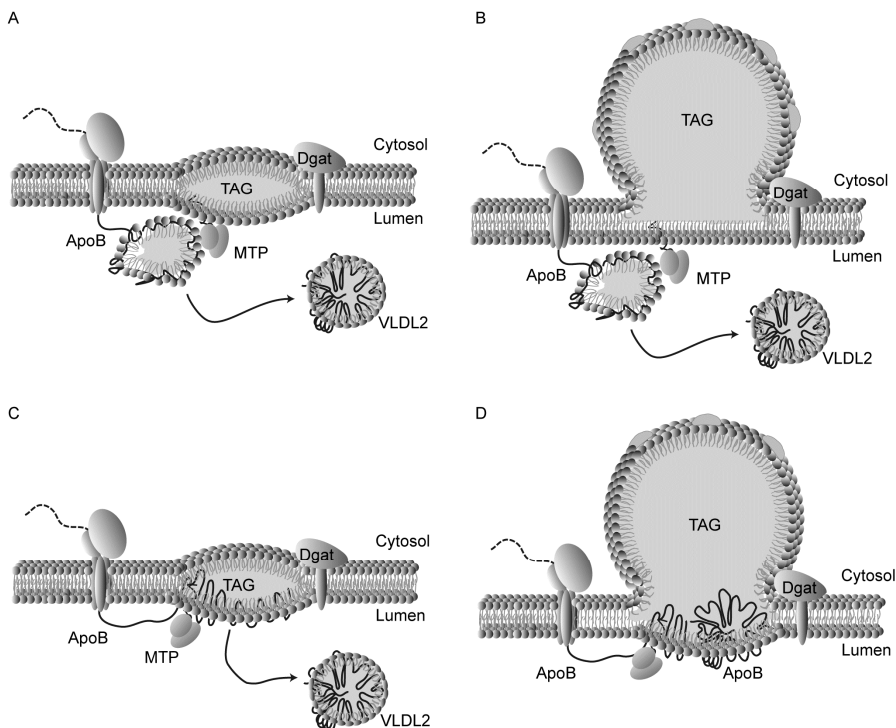


Figure 2 Possible alternative mechanisms for the formation of ApoB crescents around LDs (A) In the normal situation ApoB is co-translationally lipidated by MTP to form VLDL2, most likely using triacylglycerol synthesized by DGAT1. During incubation with Brefeldin A, maturation of the lipidated ApoB is inhibited. This could cause the following situations: (B) While the maturation of ApoB is inhibited, the synthesis of triacylglycerol continues, forming an LD. (C) Partially lipidated ApoB associates with the luminal leaflet of the ER and starts to aggregate, (D) causing the local TAG inclusions to fuse to form an LD.

Are there parallels between LD and VLDL formation? Based on the structural homology between lipoproteins and LDs, a comparable model for lipoprotein and LD formation has been suggested. VLDL and chylomicrons contain the most TAG of all lipoproteins. Both are formed by co-translational lipidation of ApoB (ApoB100 for hepatic VLDL and ApoB48 for chylomicrons) by MTP in the lumen of the ER. While the presence of MTP is necessary for the formation of lipidated ApoB, there are reports that the initial binding of phospholipids to ApoB is not dependent on MTP [16–18]. For LDs, there are two lipid droplet-associated proteins that stay associated with the LD: perilipin (perilipin1) and adipose differentiation related protein (ADFP / perilipin2). Knockdown of perilipin in animal models does not inhibit lipid droplet formation, but rather enhances lipolysis in adipose tissue [19]. Knockdown of ADFP in mice reduces hepatic LD content by 60% without affecting adipogenesis [20]. The VLDL production was reported to be

comparable to wild-type. However, in another study loss of ADFP function was almost fully compensated for by an increased expression of TIP47 [21]. TIP47 knockdown markedly reduced LD formation while the level of TAG remained comparable to wild-type cells [22]. Upon oleic-acid stimulation of TIP47-depleted cells, the levels of ADFP increased two- to three-fold [22]. TIP47 has been reported to bind to phospholipid packing defects in the membrane, which can be caused by increased curvature or increased levels of DAG [23]. These results suggest that the role which PAT proteins play in LD formation is markedly different from the role of ApoB in VLDL biogenesis.

How and where are lipid droplets formed? While we obtained initial evidence pointing to the mitochondria- associated ER membrane as the site of LD biogenesis, we were unable to convincingly show inclusion of neutral lipid at this site. Using a combination of electron microscopy techniques on TIP47 knockdown cells stimulated with oleic acid, it may be possible to verify the inclusion of neutral lipid. One approach would be combining CEMOVIS with fluorescence microscopy. Cells incubated with oleic acid and the recently developed, more specific, neutral lipid dye LD540 [24] could be frozen with the method presented in Chapter 5 to freeze adherent cells for frozen hydrated sectioning. After sectioning, the fluorescent signal corresponding to the neutral lipid inclusions may be detected by fluorescence microscopy, thereby identifying the regions of interest before analyzing the sections in the Cryo-electron microscope. This approach requires the use of a fluorescence microscope with a cryo-stage or the integrated fluorescence - electron microscope (ILEM) [25] equipped with a cryo-holder to keep the sections in a vitreous state while imaging. However, the dye will have to be functional at liquid nitrogen temperatures and provide enough fluorescent signal to be detectable when it is incorporated in the small neutral lipid inclusions within the section. Another approach would be combining CEMOVIS with VIS2FIX. Since both techniques use frozen hydrated sections it would be possible to process one section via the hydrated VIS2FIX method and use the next for CEMOVIS. By labeling the VIS2FIX section for TIP47 the regions of LD formation could then be identified and the corresponding regions imaged in the section intended for CEMOVIS. Both methods might also be combined, it would be interesting to see whether vitreous sections imaged in the Cryo-TEM could still be successfully processed via the hydrated VIS2FIX method. This would allow verification of the identity of cellular components found using cryo-transmission electron microscopy by immuno-labeling.

In conclusion, we have shown that, with the right sample preparation procedures, electron microscopy is a potentially powerful tool to study the various aspects of cellular lipid metabolism at the ultrastructural level. In the future, combining the information provided by electron microscopy with biochemical data may further advance our knowledge on the life of lipids, lipid droplets and lipoproteins.

References

1. Marton L. Electron microscopy of biological objects. *Nature* 1934;133:911.
2. Al-Amoudi A, Chang J-J, Leforestier A, McDowall A, Salamin LM, Norlén LPO, Richter K, Blanc NS, Studer D, Dubochet J. Cryo-electron microscopy of vitreous sections. *EMBO J* 2004;23:3583–3588.
3. Karreman MA, Van Donselaar EG, Gerritsen HC, Verrips CT, Verkleij AJ. VIS2FIX: a high-speed fixation method for immuno-electron microscopy. *Traffic* 2011;12:806–814.
4. Shah DO. Interaction of uranyl ions with phospholipid and cholesterol monolayers. *J Colloid Interface Sci* 1969;29:210–215.
5. Ginsburg H, Wolosin JM. Effects of uranyl ions on lipid bilayer membranes. *Chem Phys Lipids* 1979;23:125–131.
6. Meex RCR, Schrauwen P, Hesselink MKC. The modulation of myocellular fat stores; lipid droplet dynamics in health and disease. *Am J Physiol Regul Integr Comp Physiol* 2009;
7. Le Lay S, Dugail I. Connecting lipid droplet biology and the metabolic syndrome. *Prog Lipid Res* 2009;48:191–195.
8. Vantyghem MC, Pigny P, Maurage CA, Rouaix-Emery N, Stojkovic T, Cuisset JM, Millaire A, Lascols O, Vermersch P, Wemeau JL, Capeau J, Vigouroux C. Patients with familial partial lipodystrophy of the Dunnigan type due to a LMNA R482W mutation show muscular and cardiac abnormalities. *J Clin Endocrinol Metab* 2004;89:5337–5346.
9. Stone SJ, Levin MC, Zhou P, Han J, Walther TC, Farese RV Jr. The endoplasmic reticulum enzyme DGAT2 is found in mitochondria-associated membranes and has a mitochondrial targeting signal that promotes its association with mitochondria. *J Biol Chem* 2009;284:5352–5361.
10. Olson RE. Discovery of the Lipoproteins, Their Role in Fat Transport and Their Significance as Risk Factors. *J Nutr* 1998;128:439S–443S.
11. Walldius G, Jungner I. The apoB/apoA-I ratio: a strong, new risk factor for cardiovascular disease and a target for lipid-lowering therapy--a review of the evidence. *J Intern Med* 2006;259:493–519.
12. Olofsson S-O, Wiklund O, Borén J. Apolipoproteins A-I and B: biosynthesis, role in the development of atherosclerosis and targets for intervention against cardiovascular disease. *Vasc Health Risk Manag* 2007;3:491–502.
13. Samson-Bouma M-E, Verthier N, Ginsel LA, Feldmann G, Fransen JA, Aggerbeck LP. Ultrastructural immunogold labeling of lipid-laden enterocytes from patients with genetic malabsorption syndromes. *Biol Cell* 1996;87:189–196.
14. Kulinski A, Rustaeus S, Vance JE. Microsomal triacylglycerol transfer protein is required for luminal accretion of triacylglycerol not associated with ApoB, as well as for ApoB lipidation. *J Biol Chem* 2002;277:31516–31525.
15. Ohsaki O, Jinglei C, Fujita A, Fujimoto T. Lipid droplets are a site of ubiquitin-dependent degradation of apolipoprotein B. *Cell Struct Funct* 2005;30:74–74.
16. Manchekar M, Richardson PE, Forte TM, Datta G, Segrest JP, Dashti N. Apolipoprotein b-containing lipoprotein particle assembly lipid capacity of the nascent lipoprotein particle. *J Biol Chem* 2004;279:39757–39766.
17. Dashti N, Manchekar M, Liu Y, Sun Z, Segrest JP. Microsomal triglyceride transfer protein activity is not required for the initiation of apolipoprotein B-containing lipoprotein assembly in McA-RH7777 cells. *J Biol Chem* 2007;282:28597–28608.

18. Liu Y, Manchekar M, Sun Z, Richardson PE, Dashti N. Apolipoprotein B-containing lipoprotein assembly in microsomal triglyceride transfer protein-deficient McA-RH7777 cells. *J Lipid Res* 2010;51:2253–2264.
19. Tansey JT, Sztalryd C, Gruia-Gray J, Roush DL, Zee JV, Gavrilova O, Reitman ML, Deng CX, Li C, Kimmel AR, Londos C. Perilipin ablation results in a lean mouse with aberrant adipocyte lipolysis, enhanced leptin production, and resistance to diet-induced obesity. *Proc Natl Acad Sci USA* 2001;98:6494–6499.
20. Chang BH-J, Li L, Paul A, Taniguchi S, Nannegari V, Heird WC, Chan L. Protection against fatty liver but normal adipogenesis in mice lacking adipose differentiation-related protein. *Mol Cell Biol* 2006;26:1063–1076.
21. Sztalryd C, Bell M, Lu X, Mertz P, Hickenbottom S, Chang BH-J, Chan L, Kimmel AR, Londos C. Functional compensation for adipose differentiation-related protein (ADFP) by Tip47 in an ADFP null embryonic cell line. *J Biol Chem* 2006;281:34341–34348.
22. Bulankina AV, Deggerich A, Wenzel D, Mutenda K, Wittmann JG, Rudolph MG, Burger KNJ, Höning S. TIP47 functions in the biogenesis of lipid droplets. *J Cell Biol* 2009;185:641–655.
23. Skinner JR, Shew TM, Schwartz DM, Tzekov A, Lepus CM, Abumrad NA, Wolins NE. Diacylglycerol enrichment of endoplasmic reticulum or lipid droplets recruits perilipin 3/TIP47 during lipid storage and mobilization. *J Biol Chem* 2009;284:30941–30948.
24. Spandl J, White DJ, Peychl J, Thiele C. Live cell multicolor imaging of lipid droplets with a new dye, LD540. *Traffic* 2009;10:1579–1584.
25. Agronskaia AV, Valentijn JA, Van Driel LF, Schneijdenberg CTWM, Humbel BM, Van Bergen en Henegouwen PMP, Verkleij AJ, Koster AJ, Gerritsen HC. Integrated fluorescence and transmission electron microscopy. *J Struct Biol* 2008;164:183–189.

Samenvatting

Lipiden, lipid druppels en lipoproteïnen in hun cellulaire context; een ultrastructurele aanpak

Lipiden zijn essentiële bouwstenen voor de cel, de kleinste eenheid van het leven. Georganiseerd als dubbellaag membranen dienen ze om cellulaire processen te compartimentaliseren, ze kunnen functioneren als signaalmoleculen of als opslag voor metabole energie. Onze huidige kennis over de organisatie en cellulaire homeostase van lipiden is voornamelijk gebaseerd op biochemische data. Deze biochemische methoden kunnen niet alle vragen beantwoorden. Om verder inzicht te krijgen en de studie van lipiden in binnen de cel mogelijk te maken is een andere techniek nodig. In dit proefschrift onderzoeken we mogelijkheid om met transmissie-elektronen microscopie, cellulaire lipiden, lipide druppels en lipoproteïnen te bestuderen op ultrastructureel niveau. Door de preparatie technieken te optimaliseren zijn we in staat lipiden in de cel te behouden. Dit maakt het mogelijk om meer inzicht te krijgen in de vorming van lipide druppels en lipoproteïnen. Ook kunnen we nieuw gevormde lipiden aantonen binnen de cel op ultrastructureel niveau, met behulp van een gemodificeerd vetzuur. Een nieuwe techniek voor het invriezen van cellen maakt het mogelijk om deze met nog mindere externe invloeden te bestuderen. Transmissie-electronen microscopie blijkt een krachtig instrument voor het bestuderen van lipiden binnen de cel. In toekomstig onderzoek kan het combineren van de informatie die door elektronen microscopie verkregen is, met biochemische data onze kennis over de rol van lipiden in cellulair leven sterk vergroten.

Acknowledgements / Dankwoord

With these paragraphs this thesis, describing the result of four years of research, setbacks and small victories, comes to a close. Though I find it difficult to express something as complex as gratitude in mere words, I would like to take the opportunity here to thank all those who have, in one way or the other, contributed to the completion of this work:

THANKS!

..however, I feel some more details are required, as to whom this thanks should go:

To Dick, Koert, Kees, Jan, Rüdiger, Joke, Jana, Wytske, Henk, Hugo, Fernanda, Antionette and all other members of the former division of Endocrinology and Metabolism; Thanks for making me feel at home and helping me along during the first year of my PhD. Koert, bedankt dat je het aandurfde om met mij dit project te beginnen. Ik vind het nog steeds jammer dat we niet langer samen hebben kunnen werken, de beslissing daarover was helaas niet aan ons om te nemen,

To Gerrit, Maarten, Joost, Toon, Joep, Ruud, Antionette (again!), Cecile, Seléne, Suzanne, Hanka, Tine and all other members of the former division of Membrane Enzymology. Gerrit en Joost, bedankt voor jullie begeleiding in de laatste drie jaar van mijn promotie onderzoek. Joep en Ruud, bedankt voor alle hulp, koffie pauses vrijdagmiddag borrels en goede gesprekken! Hanka und Tine, Ich würde dir beiden danken für ein schöne zeit. Es war wirklich großartig das Evil Office mit ihnen zu teilen, besonders den secret cake parties und den besten gossip. Sie beiden fehlen mir noch immer!

To Jan Andries, Willie, Wallie, Elly, Karin, Theo, Chris, Hans, Cor, Nuria, Matthia, Emine, Matthijs and all other members of the former division of Biomolecular Imaging. Jan Andries, bedankt voor je hulp bij het schrijven van deze thesis. Elly, de afgelopen vier jaar was jij de meest constante factor. Ik wil je graag bedanken voor al je steun en advies. Ik voel me bevoorrecht dat je jouw kennis en kunde met me hebt willen delen en me hebt ingewijd in de kunst van EM sample preparatie. Ik hoop in de toekomst nog vaak met je samen te kunnen werken! Nuria, bedankt dat je, in een voor jou hectische periode, de tijd wilde nemen om me te helpen met mijn eerste manuscript, ik heb er veel van geleerd. Matthia, bedankt dat je mijn schrijf-maatje en stok-achter-de-deur wilde zijn! Ik hoop dat je het naar je zin gaat hebben in Heidelberg, al ga ik je vrolijke lach wel missen.. Emine, I really enjoyed our talks, discussing with you gave me a chance to reflect upon issues of my own.

To Laura, Ming, Sarah, Muriel and all members of Microbiology in Nijmegen, were I hope to spend at least the coming three years. Laura, bedankt voor al je hulp tijdens het schrijven van mijn thesis en voor je vertrouwen in mij als postdoc.

Last but not least, to my parents and my own family. Karin, Elin Kyra en June, ik zou niet weten waar ik zonder jullie steun en liefde zou zijn.

Curriculum Vitae

Rob Mesman was born on January 2nd, 1982 in Gouda, the Netherlands. After graduating from secondary school in 1999 he started studying Biomedical Technology at the Technical University of Eindhoven. In 2001 he decided to change course and enrolled at Utrecht University to study Biology, for which he obtained his bachelor degree in 2004. Continuing his studies in the master program Biology of Disease at the same university, he obtained his master degree in BioMedical Sciences in August 2008. In September of that year he started his PhD project on the morpho-functional characterization of lipid droplets in the division of Endocrinology and Metabolism, supervised by Dr. K.N.J. Burger and Prof. Dr. D.J. van der Horst, until the group fell victim to reorganization in the spring of 2009.

Having lost his supervisor and promotor, but being allowed to keep his PhD project, he continued his research at the division of Membrane Enzymology; supervised by Prof. Dr. G.F.B.P. van Meer and Prof. Dr. J.C.M. Holthuis respectively, with technical support from the division of BioMolecular Imaging. The results of which have been presented here in this thesis.

Currently, Rob is employed as a postdoc in the department of Microbiology at the Radboud University Nijmegen conducting ultrastructural analysis of microbiological specimens using advanced electron microscopy techniques.

Publications:

R.J. Mesman, E.G. van Donselaar, J.A. Post

Improving immuno-gold labeling of Apolipoprotein B by maintaining its lipidation state.

Manuscript submitted

R.J. Mesman, E.G. van Donselaar, J.C.M. Holthuis

Tracing cellular lipid flows at the ultrastructural level using a clickable fatty acid

Manuscript in preparation

R.J. Mesman

A novel method for high-pressure freezing of adherent cells for frozen hydrated sectioning and CEMOVIS

Manuscript submitted

D.A.M. de Winter, **R.J. Mesman**, M.F. Hayles, C.T.W.M. Schneijdenberg, C. Mathisen
J.A. Post

In-situ Integrity Control of frozen-hydrated, vitreous lamellas prepared by the cryo-Focused Ion Beam-Scanning Electron Microscope

Manuscript submitted

